DC# 113-022-002

JAYCOR

SPENT FUEL POOL

THERMAL-HYDRAULIC ANALYSIS

FOR BIG ROCK POINT

By:

Dr. David A. Sargis
Mr. Ralph E. Ferguson

Fluid Dynamics Group

JAYCOR Report J82-5285F

October 26, 1982

Checked By Dr. James H. Stuhmiller

11011 Torreyana Road - Post Office Box 85154 · San Diego, California 92138 · (714) 453-6380

CONTENTS

1. SUMMARY

The objective of this thermal-hydraulic analysis is an accurate prediction of maximum wall temperatures in the Big Rock Point spent fuel pool during a period of time when the regular fuel pool cooling system pumps are not operating.

Pool cooling is assumed to be due solely to the natural circulation of 100°F water entering at 30 gallons per minute from a pipe located at the top northeast corner of the fuel storage pool. Heating is due to 441 assemblies generating a total of 216,783 watts with 62% of the total coming from 21 assemblies located in the bottom northwest corner.

The EITACC-SFP code is used to solve the three-dimensional, Navier-Stokes equations with buoyancy and thermal convection. A finite difference mesh is chosen to resolve each rack and the major flow paths around the racks. Friction due to cross flow and flows through the fuel assemblies is modeled.

The calculated results show that the largest temperature occurs just above the hot assembly in the northwest corner and is less than 3°F warmer than the average pool temperature. This result is also confirmed by a simpler, one-dimensional thermal-hydraulic analysis. The calculated flow paths of the cooling water are analyzed to assist in visualizing the results.

2. TECHNICAL APPROACH

The Navier-Stokes partial differential equations for conservation of mass and momentum and the transport equation for the liquid temperature are solved in a three dimensional cartesian mesh. In Appendix A, the governing partial differential equations are shown. The fluid dynamics equations are solved using finite difference expressions of the differential equations with an explicit time step treatment to advance the time dependent variables. The pressure matrix is solved using direct matrix inversion algorithm which ensures accurate pressure solutions even in the high aspect ratio computational mesh cells in the spent fuel pool geometry. Steady state is approached through the natural transient of the system.

The entire three-dimensional pool is solved in these calculations, including the two existing A-racks and the B-rack, as well as the new F, D, and E racks. Cross flows in the new racks are restricted due to the horizontal plates which prevent upward flow except through the fuel assembly regions. The older A and B racks are open to cross flows and also allow upwards flows between and through the heated assemblies. Friction factors are used to model frictional pressure losses through the assemblies as well as in the rectangular ducts and openings between assemblies. Flow blockages due to structural material and geometry are treated using area and volume porosity factors.

Heat sources in these calculations are based on 441 assemblies with 121 rods in each assembly. The total heat rate is assumed to be 210,783 watts (see Table 1) with the hottest 21 assemblies placed in the northwest corner of the pool in the F rack. The next hottest 83 assemblies are also assumed to be in the F-rack so that approximately 82% of the total heat source is placed in the northwest corner of the pool. The hottest remaining sources are placed in rack B, followed by racks A, D, and E in that order.

The calculations described below use the three-dimensional EITACC-SFP (Equation Independent Time-Average Conformal Coordinates-Spent Fuel Pool) code. The EITACC system of codes consists of computer programs for calculating fluid dynamics effects using a variety of equation sets and finite difference

Table 1. Heat Sources for EITACC Calculations[6]

Cooling Time (Days/Years)	Number of Assemblies	Best Estimate* Watts/Assy	Normalization Factor	Final Estimate Watts/Assy
30 days	21	3,785	1.68	6,359
365 days	21	754	1.68	1,267
2 years	21	398	1.1	438
3 years	21	251	1.1	276
4 years	21	180	1.1	198
5 years	21	143	1.1	157
6 years	21	123	1.1	135
7 years	21	110	1.1	121
8 years	21	102	1.1	112
9 years	252	96	1.1	105
Total	441			216,783 watts

*EPRICELL computer code - explicit summation of fission product decay heats.

equations. The EITACC techniques have been used to solve many categories of fluid flows including incompressible, compressible, stratified, two-phase, turbulent, and one-, two- and three-dimensional flows. The heart of the EITACC method is a modular set of FORTRAN subroutines for solving the fluid transport equations and resulting elliptic pressure equations and a standard set of diagnostic and plotting routines.

Reference 1 describes the basic EITACC computational methodology while Refs. 2 and 3 describe two applications of the method to calculations of stratified flow in the damaged Three Mile Island core and to numerical simulation of swirling flow in a centrifugal steam separator.

The EITACC-SFP computer program is presently an unverified code and its status may be considered experimental.

3. MAJOR ASSUMPTIONS

BOUSSINESQ APPROXIMATION

The temperature variations within the flow result in variations in fluid properties such as the viscosity and density. When pressure variations are small, it is sufficient to treat all fluid properties as constant with the exception of the variation of density in the buoyancy force. See Reference 7. When the ambient hydrostatic pressure is subtracted, the Boussinesq approximation results in a buoyancy term, $\Delta\rho g$, in the vertical momentum equation (Equation A-3 in Appendix A). For small temperature differences, the dependence of ρ can be linearized to $\Delta\rho \equiv -\alpha\rho_o\Delta T$, where α is the volumetric coefficient of thermal expansion of the fluid, ρ_o is the constant, reference fluid density, and ΔT is the temperature difference from the reference value.

ADIABATIC WALL BOUNDARY CONDITIONS

The walls are assumed to be at the same temperature as the adjoining fluid. This approximation is judged to lead to a conservative (hotter than actual) wall temperature, since any net heat conducted out of the pool would lower the pool temperatures.

NO SURFACE COOLING

This, again, is judged to be a conservative approximation.

SMALL GAPS MODELED WITH POROSITY

The 3-1/2" spaces between the fuel racks and the walls and the spaces between individual racks are included in the area and volume porosities of the computational cells and are not resolved separately. Other open flow areas are resolved. Because the walls are adiabatic there will be no thermal boundary layer and the absence of an unheated gap near the wall should result in a conservative (warm) temperature field.

CROSS FLOW RESTRICTIONS IN CLOSED RACKS

Hydraulically, there are two types of heated fuel racks in the spent fuel pool, closed and open. The newer, closed racks (F, D, and E) have horizontal plates which prevent upward flow outside of the heated assemblies. The older, open racks (A and B) do not. To prevent the incorrect mixing of liquid inside and outside the assemblies in the closed racks, cross flow has been restricted through large horizontal friction factors.

UNIFORM SPILLOVER TREATMENT

Water leaving the spent fuel pool is assumed to spill over the top of the east pool wall uniformly. Computationally this is approximated by removing water vertically from the top row of cells along the east wall at a rate that corresponds to the inflow.

4. PROBLEM INPUT

COMPUTATIONAL MESH

Figures 1 and 2 show a plan view of the actual pool rack configuration and the computational approximation used in EITACC-SFP for this analysis. Index I numbers cells from west to east, K from south to north, and J from bottom to top. The outer layer of cells (I = 1,14; J = 1,12; K = 1,11) are outside the physical domain and are used to keep track of boundary conditions.

Table 2 gives the cell dimensions in inches. The fuel racks are assumed to be 4" off the pool floor and 84-1/2" in height. The channel racks (C) are assumed to be 151.8" in height. A side view of typical rack arrangements is shown below in Figure 3 in an x-y plane.

FRICTION FACTORS

The friction factors used to model the flow through the heated assemblies are derived in Appendix B. Cross-flows in the newer, closed racks (F, D, and E) are suppressed with large friction factors. For vertical flows through assemblies, frictional pressure losses of the form $-f'_y \rho v^2/2$ are used where the f's are derived from Idel'Chik[4] and the Handbook of Heat Transfer.[5] Lateral flows between assemblies are modeled with frictional pressure losses of the form $-k_x \rho u$ and $-k_z \rho w$. The lateral friction factors are treated implicitly in the momentum equations. Both the C-rack and fuel equipment areas in Figures 1 and 2 are assumed to be open flow areas in these calculations. A summary of the friction factors used in the heated racks is shown in Table 3.

HEAT DISTRIBUTION

The total heat source and inlet cooling flow used in these calculations result in an average well stirred pool temperature of ~ 149.2°F. Table 1 lists the decay heats for all 441 assemblies. The hottest assemblies are assumed to be loaded into the F rack at the northwest corner of the pool. Rack F contains 21 assemblies of 6359 watts/assembly, 21 assemblies of 1267 watts/assembly, 21 assemblies of 438 watts/assembly, 21 assemblies of 276 watts/assembly, and 20

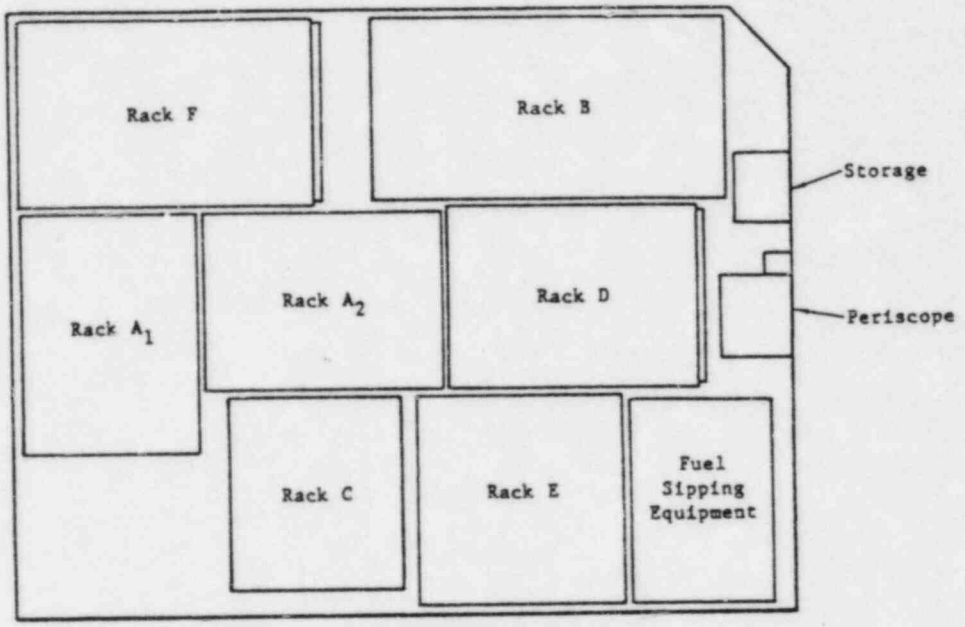

Figure 1. Actual Spent Fuel Pool Geometry

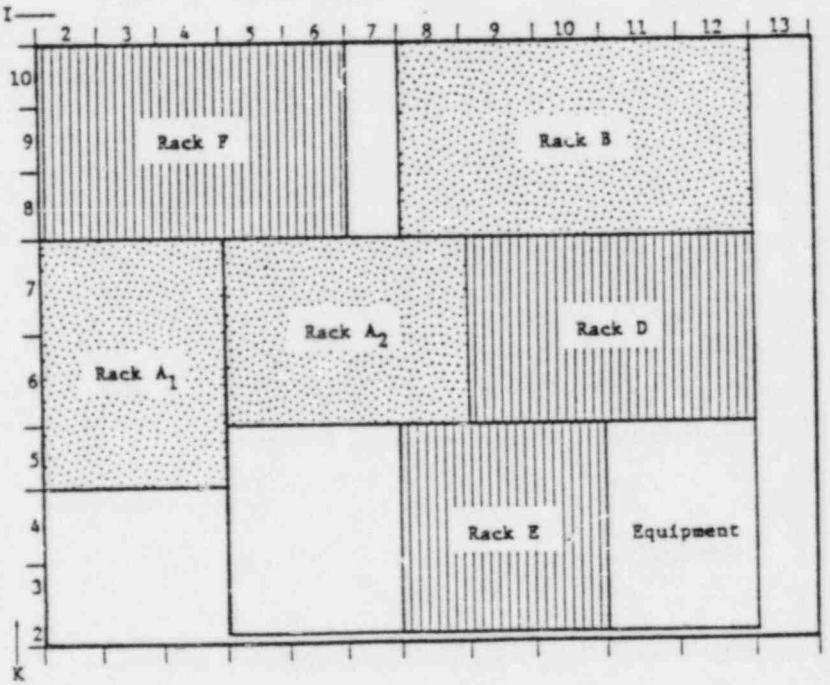

Figure 2. Computational Pool Geometry

Table 2. Computational Mesh Spacings

I	Δx (in.)	J	Δy (in.)	K	Δz (in.)
2	25.0	2	4.0	2	6.25
3	25.0	3	26.167	3	29.0
4	24.75	4	28.167	4	29.0
5	25.0	5	28.167	5	24.25
6	24.0	6	33.65	6	36.875
7	20.0	7	33.65	7	36.875
8	27.42	8	48.05	8	25.58
9	27.42	9	48.05	9	25.58
10	27.42	10	48.05	10	25.58
11	29.5	11	48.05		
12	29.5				
13	26.5				

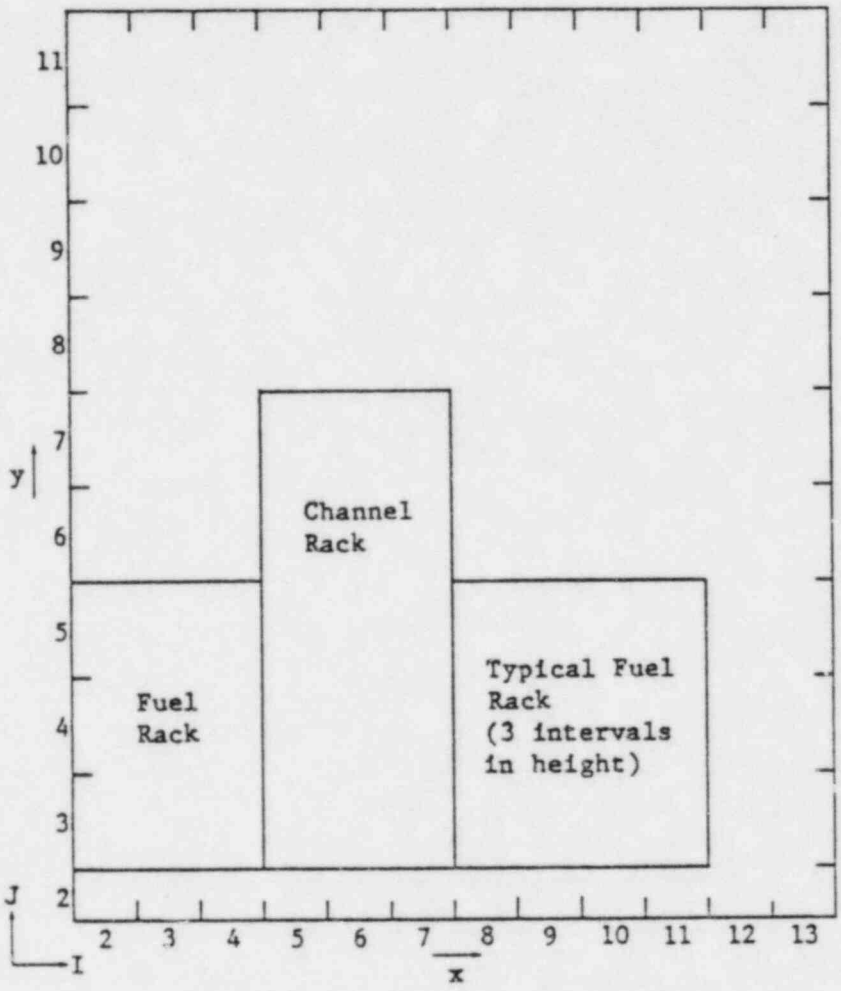

Figure 3. Typical Vertical Rack Arrangements

Table 3. Summary of Friction Factors

Rack	k_x (1/s)	f'_y (1/m)	k_z (1/s)
A	0.00273	2.56	0.00273
B	0.00273	2.56	0.00273
C	0.	0.	0.
D	50.	2.56	50.0
E	50.	2.56	50.
F	50.	2.56	50.

assemblies of 198 watts/assembly for a total of 104 assemblies and a total of 179,1000 watts. 82% of the total heat source is located in the F-rack and the rest of the assemblies are placed uniformly in racks B, A, D, and E in decreasing order of heat generation rate. The number of assemblies in each rack is presented in Table 4.

POROSITY DISTRIBUTION

A porosity (beta) method is used to account for flow obstructions and stagnant regions. The area betas are defined in all three directions as ratios of the flow areas to the computational cell areas. The volume betas for each cell are defined to be the ratios of the fluid volumes to the computational cell volumes. In Appendix A, the β_x, β_y, β_z and volume beta, β, are shown as they appear in the partial differential equations. In Appendix C, the numerical values for these blockage factors are computed in detail. A summary of the beta values used in the EITACC-SFP calculations is presented in Table 5.

BOUNDARY CONDITIONS

The pool walls, floor, and free surface are treated as frictionless planes with zero normal velocities. The cold 100°F inlet water, injected at 30 gallons per minute, has a specified inlet downward velocity of 0.0388 m/sec at the cell at the northeast corner of the pool, I = 12, J = 11, K = 10. Water is also allowed to leave the pool in an upwards direction along the east wall of the pool, I = 13, J = 11, K = 2 to 10, with a uniform velocity, 0.000463 m/sec.

PHYSICAL CONSTANTS

$\rho = 1000$ (kg/m^3)	water density
$\alpha = 5 \times 10^{-4}$ $(°C^{-1})$	coefficient of thermal expansion
$g = 9.8$ (m/sec^2)	acceleration due to gravity
k_x, f_y, k_z	friction factors - see Table 3
β_x, β_y, β_z, β	beta blockage factors - see Table 5
$\mu = 0.03$ (kg/m-sec)	first coefficient of viscosity
$\lambda = 0$	second coefficient of viscosity

Table 4. Fuel Assembly Rack Capacities

Type of Rack	Number of Racks	Nominal Capacity	Rack Status	Actual Spaces	Type of Storage
A	2	6 × 8	Existing	96	Fuel and Incores
B	1	6 × 12	Existing	72	Fuel and Cont. Blades
C	1	9 × 10	Existing	90	Fuel Channels Only
D	1	8 × 11	New	88	Spent Fuel
E	1	9 × 9	New	81	Spent Fuel
F	1	8 × 13	New	104	Spent Fuel

Table 5. Summary of BETA Calculations

I	J	K	Rack	β_x	β_y	β_z	$BETA_{vol}$
2-6	3-5	8-10	F	0.114	0.257	0.121	0.712
8-12	3-5	8-10	B	0.433	0.807	0.384	0.825
2-4	3-5	5-7	A_1	0.408	0.656	0.418	0.828
5-8	3-5	6-7	A_2	0.410	0.645	0.398	0.822
9-12	3-5	6-7	D	0.119	0.246	0.110	0.724
8-10	3-5	3-5	E	0.122	0.281	0.122	0.685

5. DISCUSSION OF RESULTS

5.1 SIMPLIFIED FLOW ANALYSIS

In order to provide physical insight into the spent fuel pool heating calculations, the simplified analytical model described below was developed to make first order predictions.

At equilibrium, the vertical temperature gradient in a heated assembly region will be given by

$$\beta_y v \frac{dT}{dy} = \left(\frac{dT}{dt}\right)_s \quad . \tag{1}$$

Across an assembly of length L the temperature difference is

$$\Delta T = \frac{L}{\beta_y v} \left(\frac{dT}{dt}\right)_s \quad . \tag{2}$$

If we assume that the frictional pressure loss in the assembly is given by

$$\Delta p_f = f'_y \frac{\rho v^2}{2} L \tag{3}$$

and is just balanced by the upward pressure due to buoyancy, Δp_B, then

$$\Delta p_B = f'_y \frac{\rho v^2}{2} L \quad . \tag{4}$$

But Δp_f is given by $\Delta \rho L g = \rho \alpha \Delta T L$ so that Equation (4) becomes

$$\rho \alpha \Delta T L g = f'_y \frac{\rho v^2}{2} L \quad . \tag{5}$$

Using Equation (2) in (4), we find

$$\boxed{v^3 = \frac{2\alpha}{\beta_y f'_y} Lg \left(\frac{dT}{dt}\right)_s \quad .} \tag{6}$$

Equation (6) is a simple relationship between fluid velocity and the heated assembly frictional, geometry, and heating parameters. For the hottest assembly in rack F we have

$$\alpha \equiv 5 \times 10^{-4} \ (^{\circ}C^{-1})$$

$$\left(\frac{dT}{dt}\right)_s \equiv 0.012 \ (^{\circ}/sec)$$

$$g = 9.8 \ m/sec^2$$

$$L = 2.14 \ m$$

$$\beta_y = 0.257$$

$$f_y' = 2.56 \ m^{-1}$$

so that Equation (6) yields

$$\boxed{v_{est} \equiv 0.0726 \ m/sec \ .} \qquad (7)$$

Using Eq. (7) in Eq. (1) gives

$$\Delta T \equiv \frac{\left(\frac{dT}{dt}\right)_s \cdot L}{\beta_y v_{est}} = \frac{(0.012)(2.14)}{(0.257)(0.0726)} = 1.38^{\circ}C = 2.48^{\circ}F \ . \qquad (7)$$

The estimated temperature rise and vertical velocity are within ~ 20% of maximum values found from the detailed EITACC-SFP calculation.

5.2 THREE DIMENSIONAL EITACC-SFP RESULTS

Appendix D presents computer plots of fluid velocity vector fields and temperature contour plots for the Big Rock Point spent fuel pool at approximately 1550 seconds after natural circulation cooling has been initiated. After 1550 seconds, cold water particles injected into the system will have had time to make several transits through the heated assemblies and allowed the system to reach steady state. The calculated average pool temperature is less than 0.1°F of the final equilibrium value and is essentially not changing with time. Energy conservation calculations relating the injection cooling

rate, assembly heating rates, and outflow heat losses, indicate extremely small changes with time so that maximum wall and pool temperatures appear to have been reached at about 500 seconds. A sensible steady state has been reached.

In Appendix D detailed graphical output from EITACC-SFP is shown for each K-plane (x-y vertical plane) at 1550 seconds. The results along with tabulated output indicate a maximum wall temperature of about 66.6°C = 151.9°F in the NW corner along the F rack. This represents a temperature difference from the mean pool temperature of approximately 2.7°F. The velocities through the hottest channel are approximately 0.057 m/sec which are about 80% of the velocities predicted by the simple model in Section 5.1. Therefore, the EITACC-SFP temperature calculations through the hottest assembly will also be about 25% higher than in the simple model. The differences are due to the exact flow pattern caused by the blockages within the pool.

Temperature contour plots of the four spent fuel pool walls, I = 2, I = 13, K = 2, and K = 10, as well as the floor, J = 2, are also included to better demonstrate the heating patterns.

The EITACC-SFP calculations also show that the hottest rack, the F-rack, also has the highest water flow rates. For the closed racks, the F-rack has about 569 gallons/minute of flow rate, while the cooler D and E racks have flow rates of 156 and 149 gallons/minute, respectively.

The fluid velocity vector plots also illustrate typical flow patterns through the various racks. In Figure 4 a typical cold fluid path from injection to several transits through the pool is shown. The cold water falls from the inlet to the pool floor, moves diagonally to a position below the F-rack and then flows upwards through the assembly. The heated water rises to near the surface, mixes with colder water, moves diagonally across the pool and then falls again. Heating causes the particle to rise and mix again and begin another swirling loop through the pool. A typical particle may have several hundred transits through the pool before being ejected at the top of the east wall.

The next six figures (Figs. 5 to 10) show typical initial cold fluid flow paths through the six hottest computational cells in the F-rack. The first

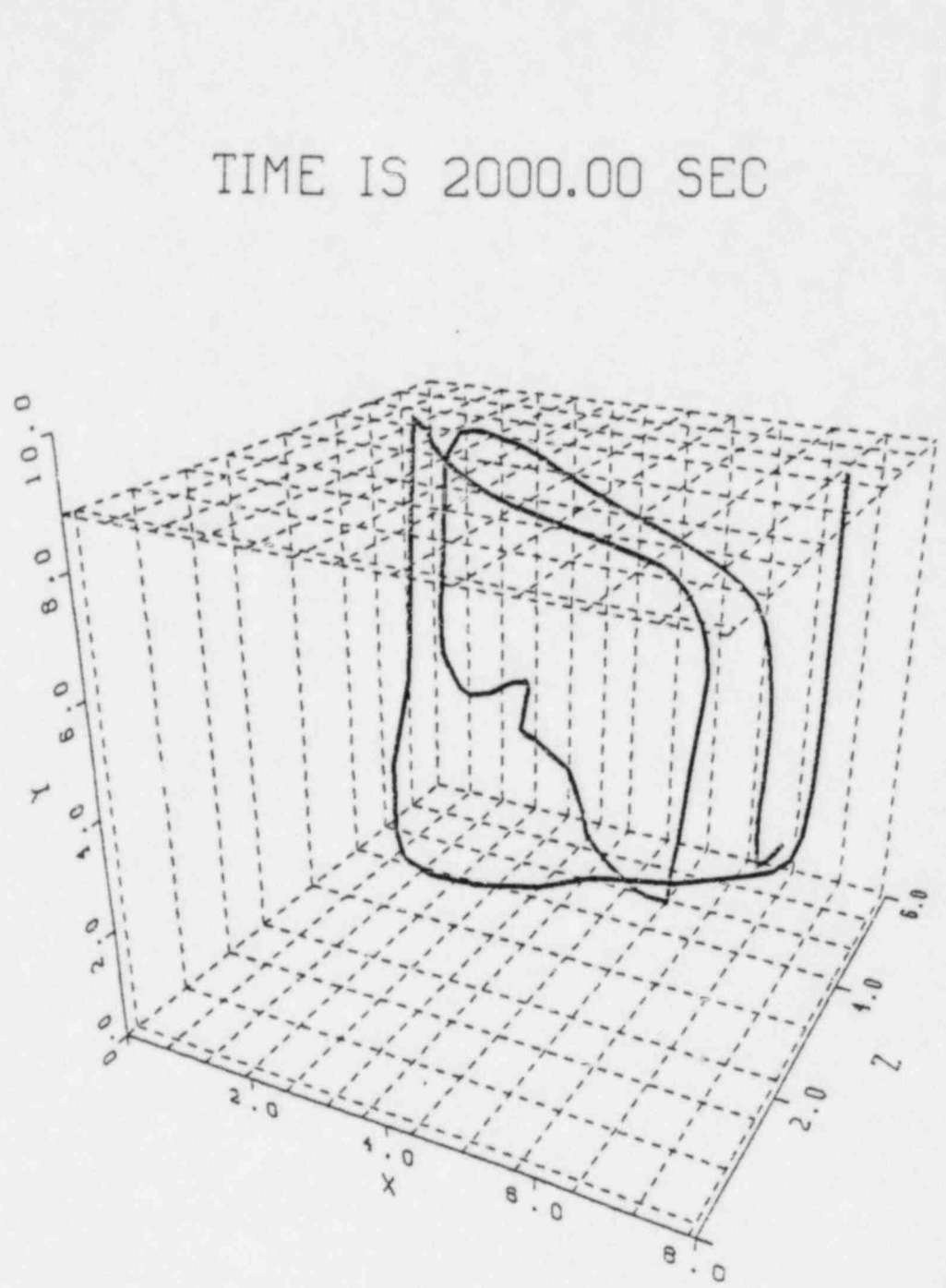

Figure 4.

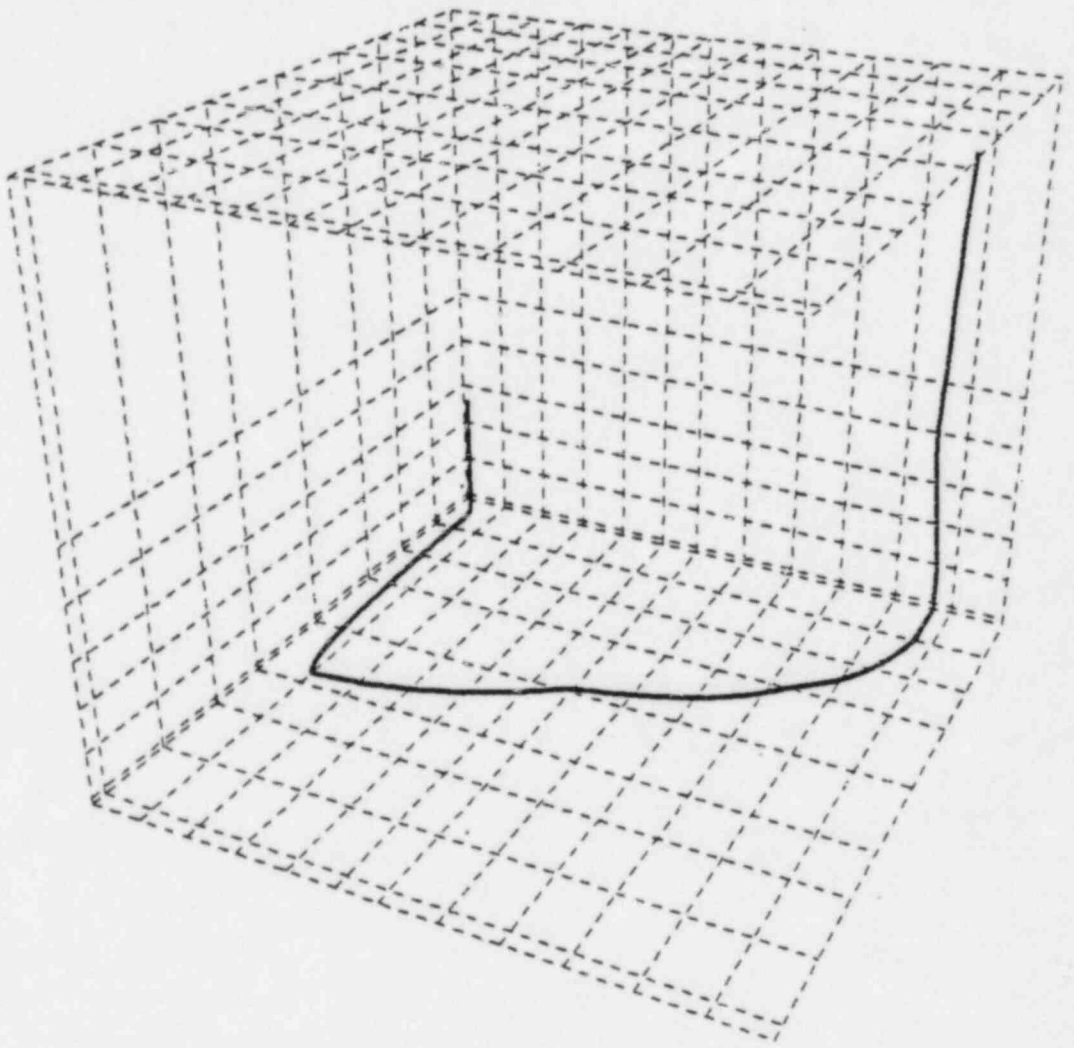

Figure 5.

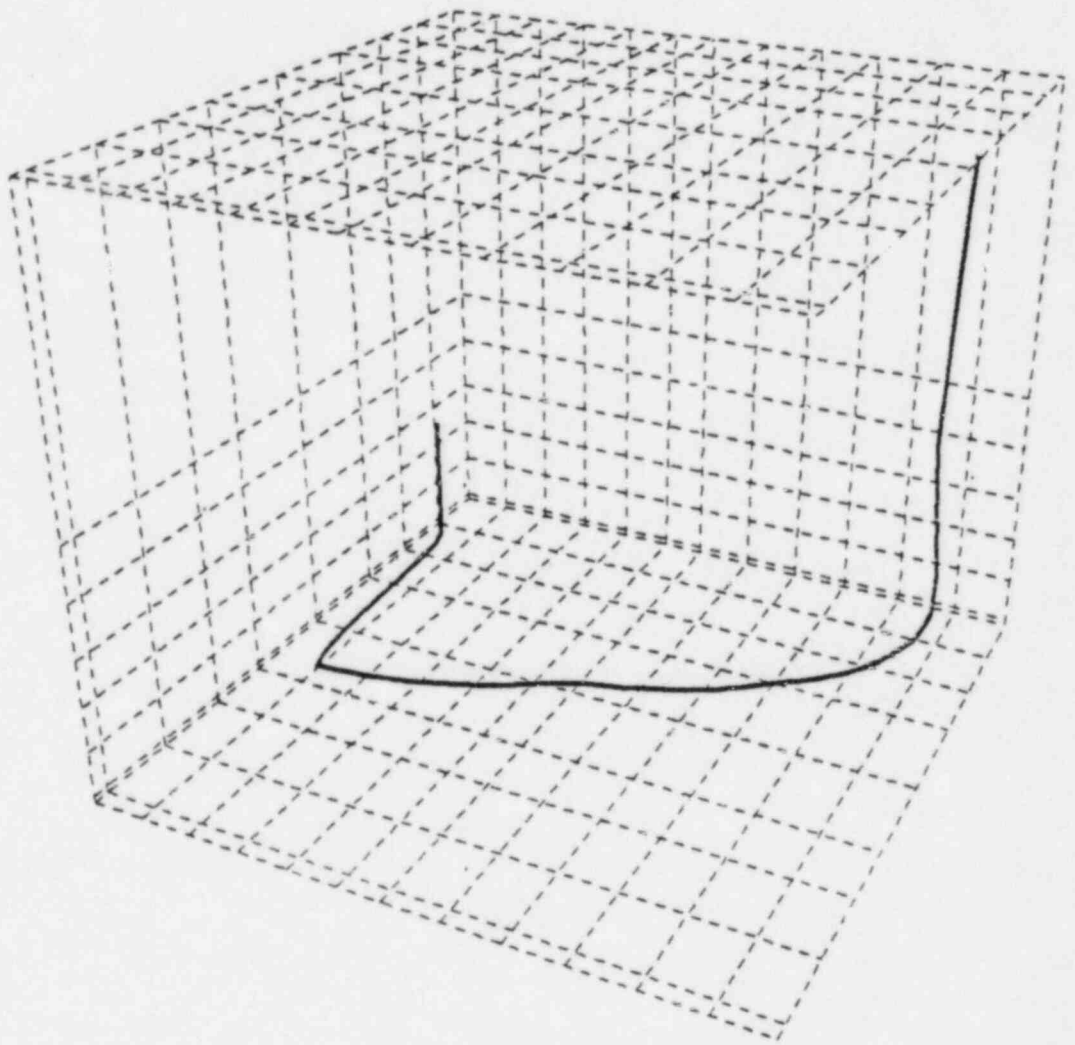

Figure 6.

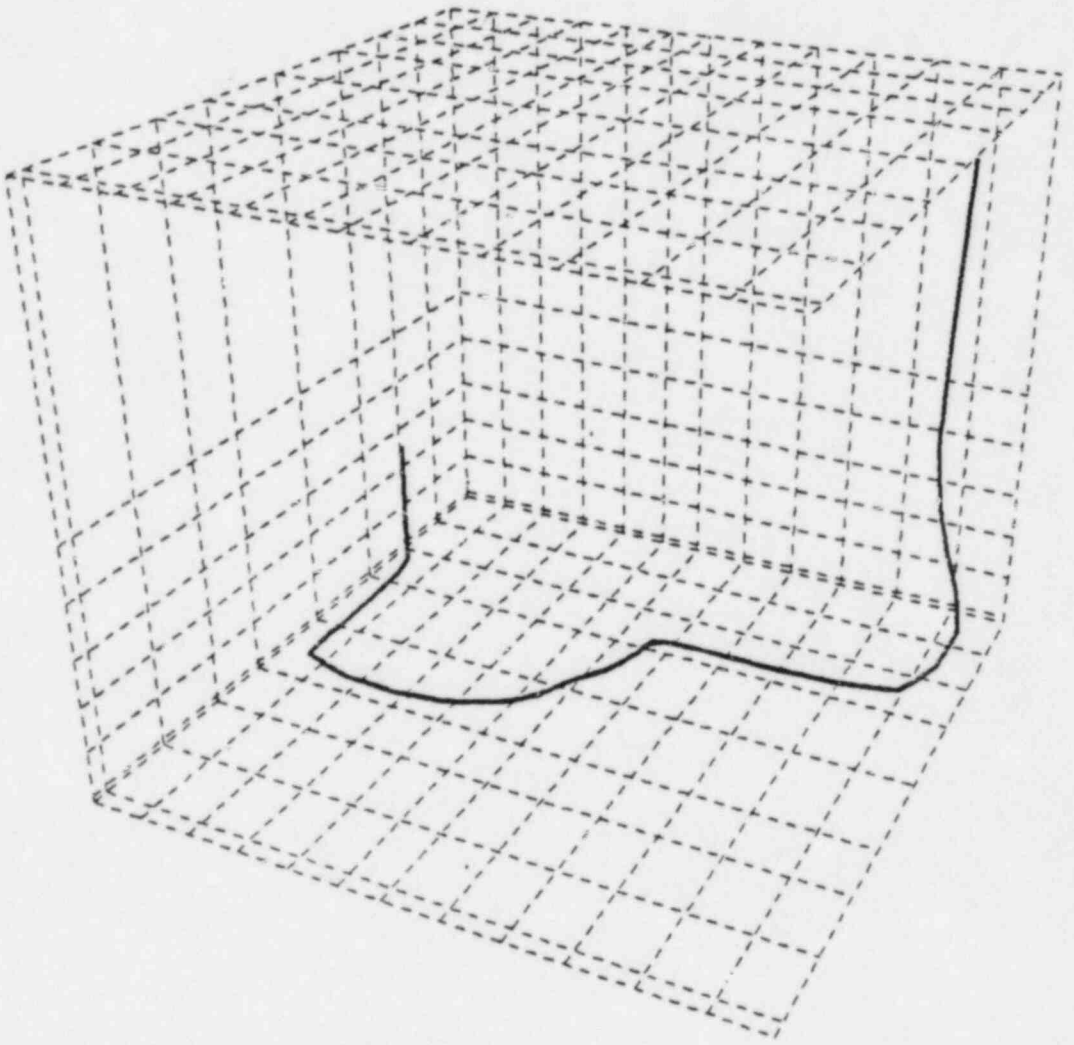

Figure 7.

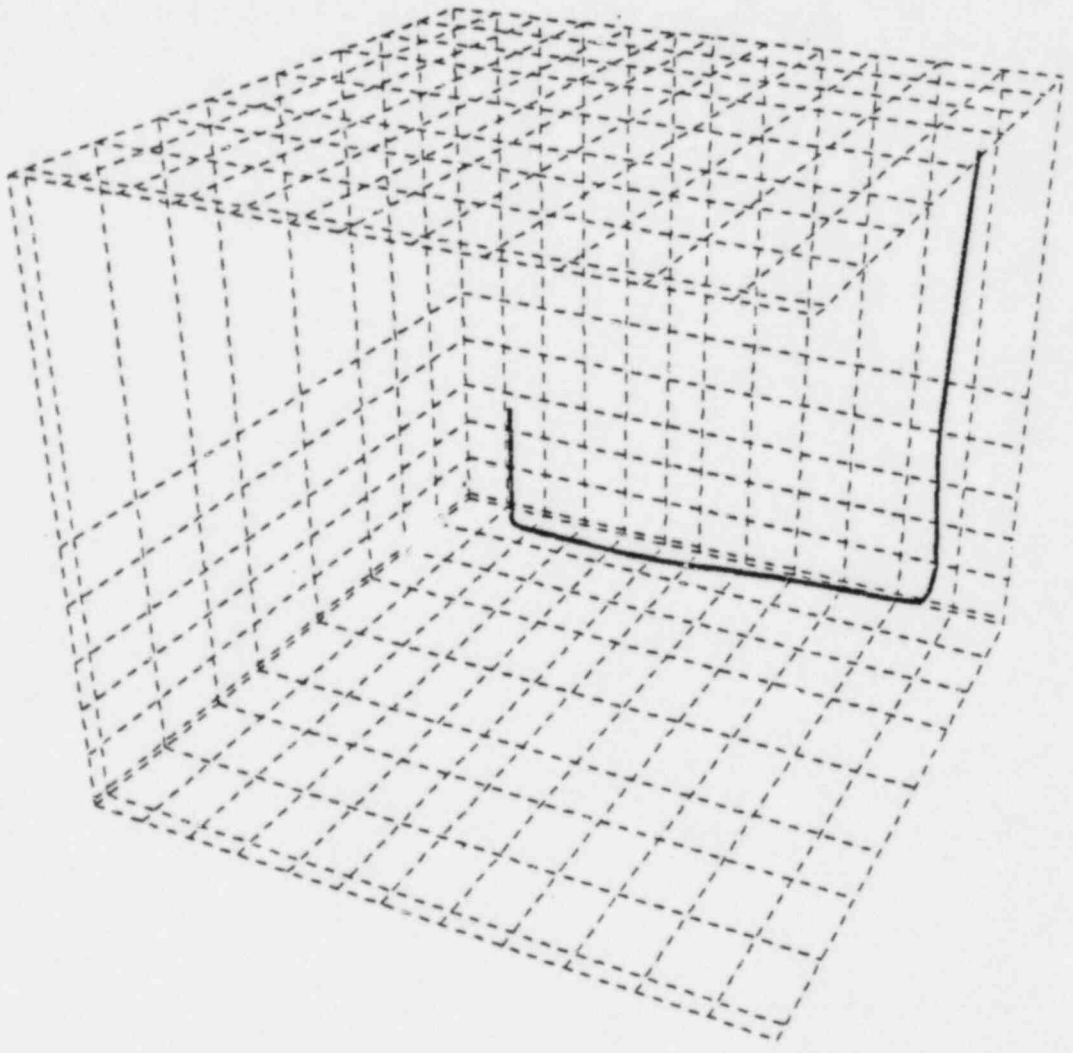

Figure 8.

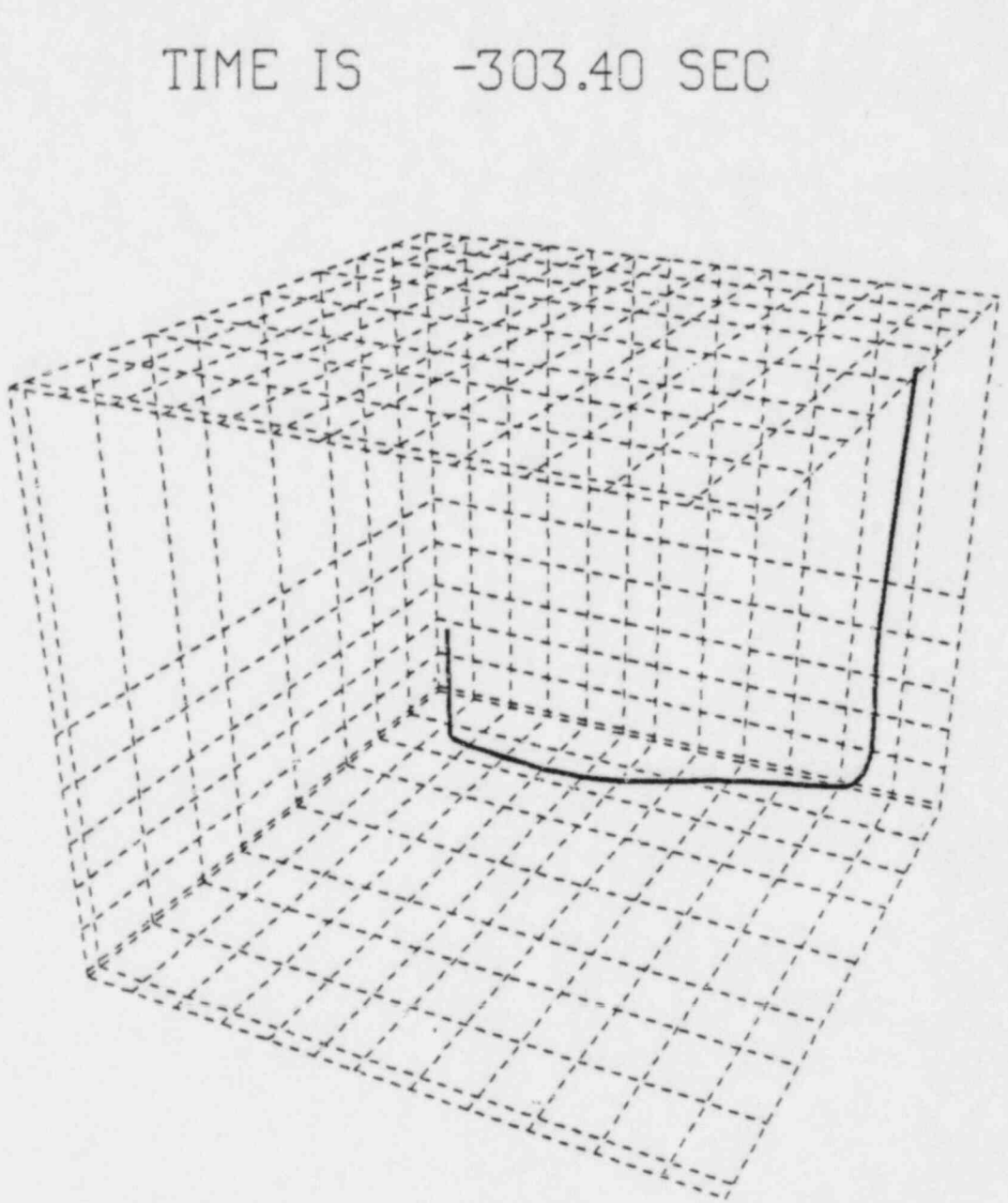

Figure 9.

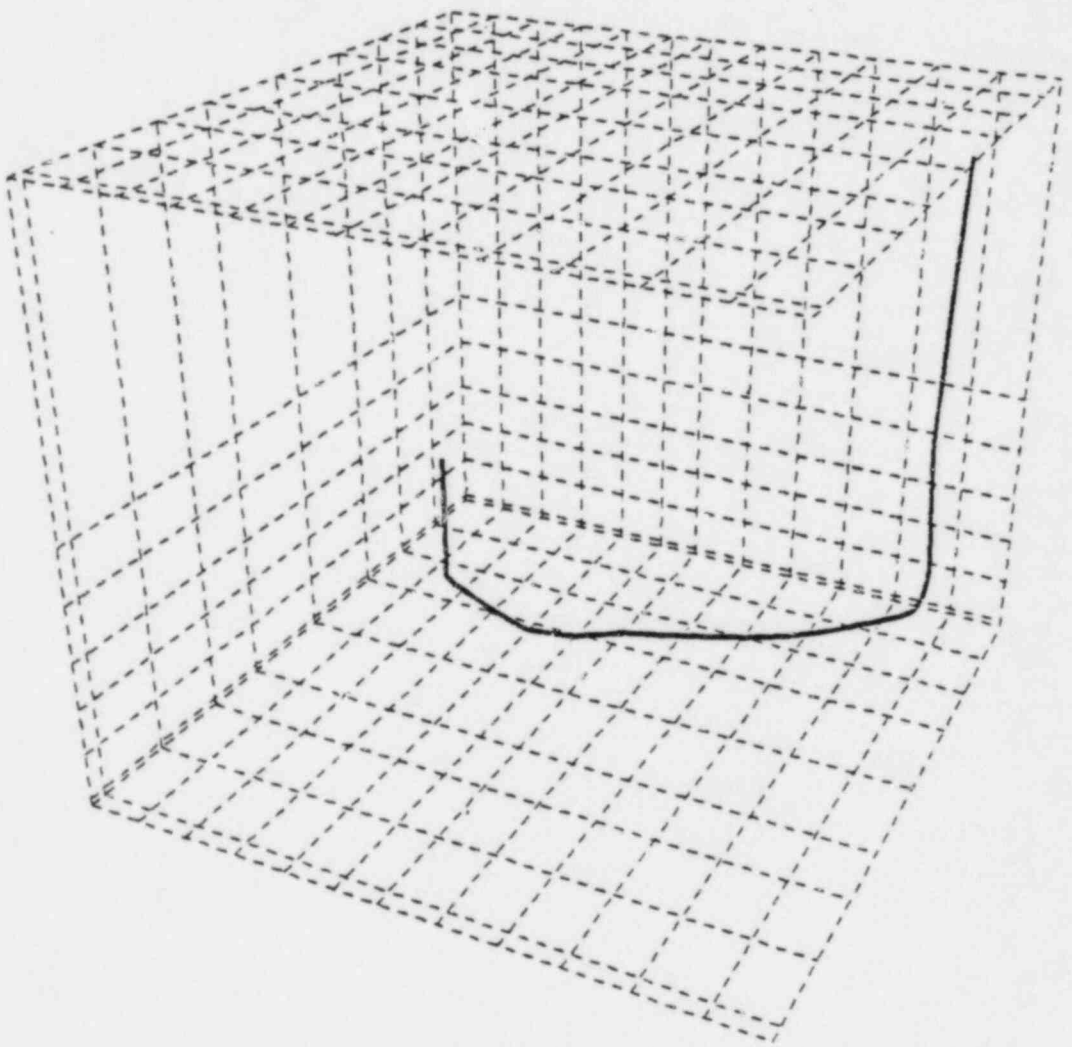

Figure 10.

figure shows that for the hottest element, in the extreme northwest corner of the pool, a typical cold water path starts with injection, followed by water dropping to the pool floor, diagonal flow across the floor, then flows along the west wall to the heated cell, and upwards. The time required for this typical cold water path is approximately 500 seconds. The next two figures show similar flow paths for the next two hottest elements along the east wall. The next three figures, Figures 8 to 10, show different shorter typical cold water paths from injection to other cooler locations in the heated F-rack. Figure 8 in particular shows cold injected water falling to the floor, moving under the B-rack to a position below the F-rack before passing upwards through the hot assembly.

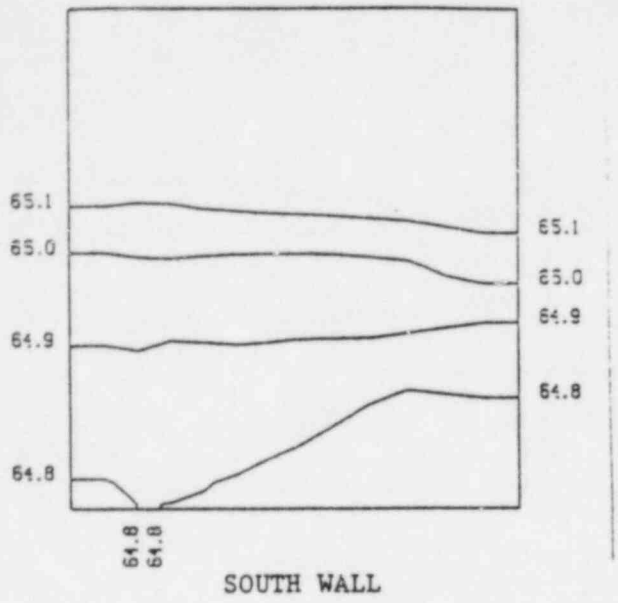

SOUTH WALL

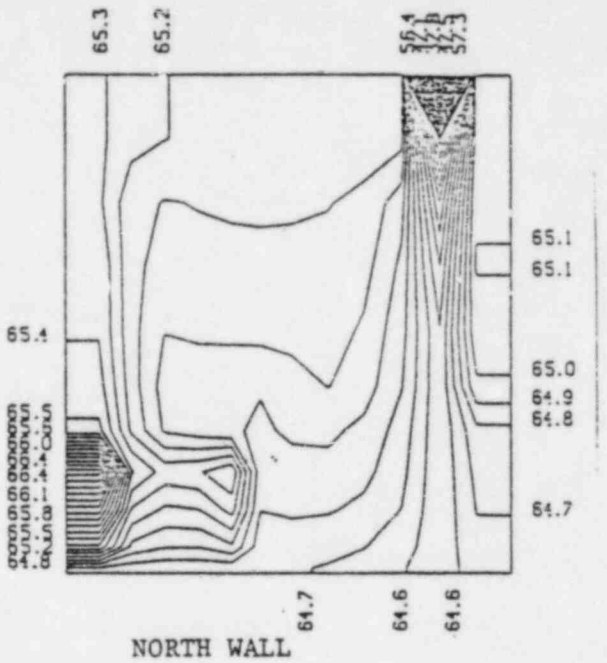

NORTH WALL

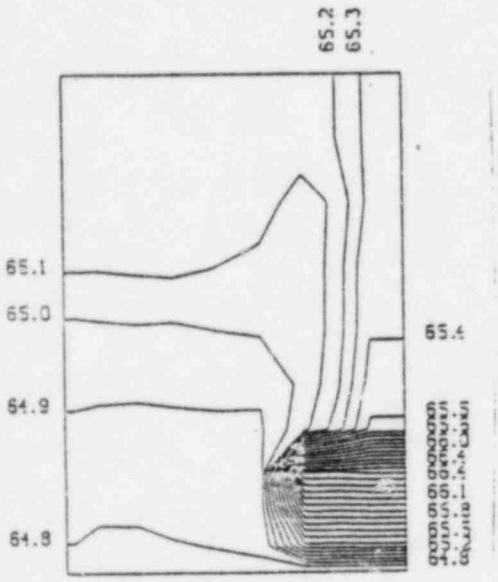

WEST WALL

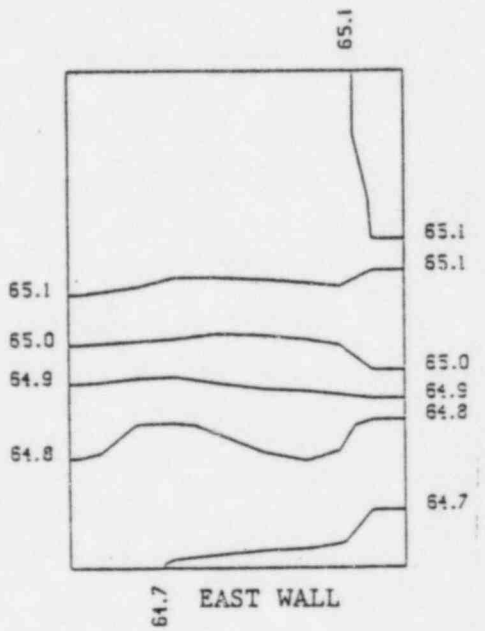

EAST WALL

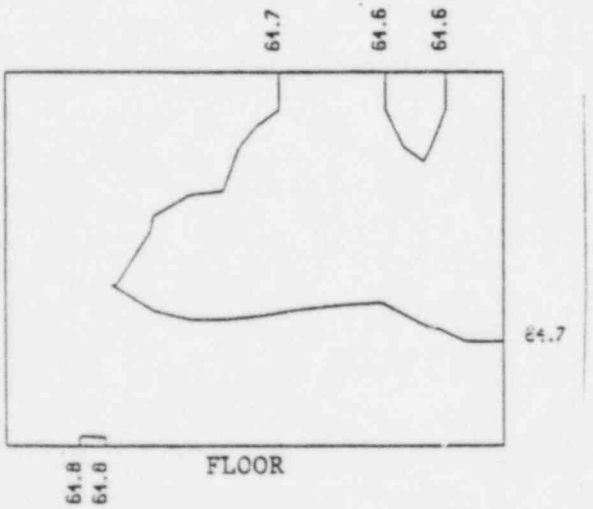

FLOOR

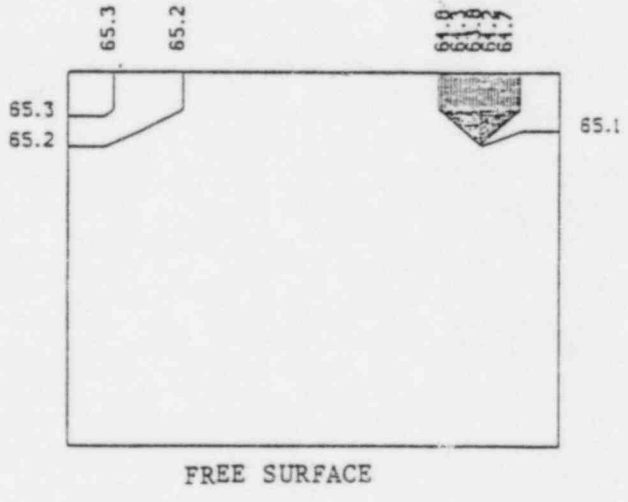

FREE SURFACE

TEMPERATURE CONTOURS ON THE SIX SIDES OF THE SPENT FUEL POOL

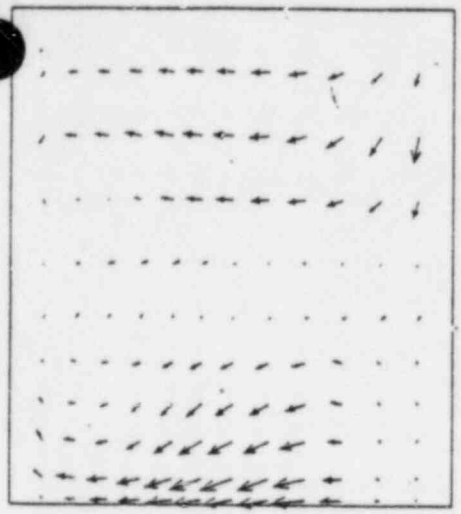

K = 2 (SOUTH WALL)

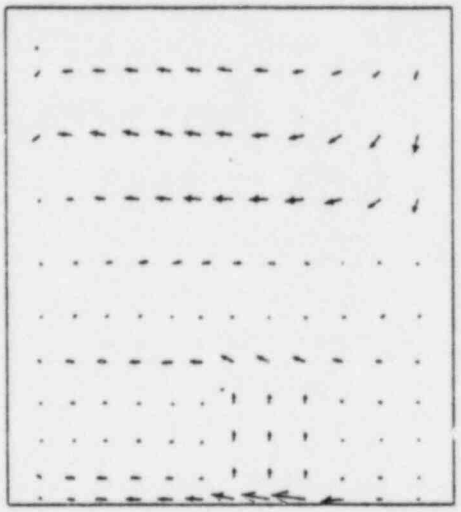

K = 3

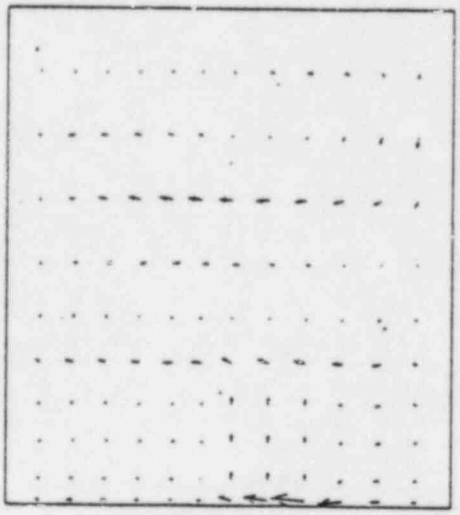

K = 4

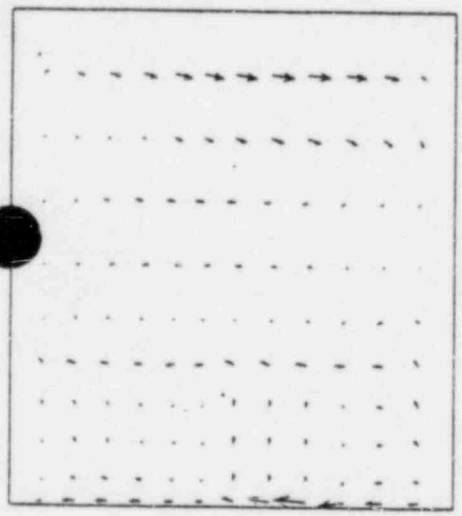

K = 5

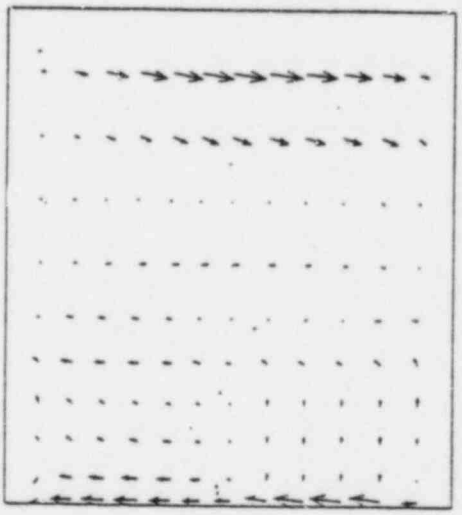

K = 6

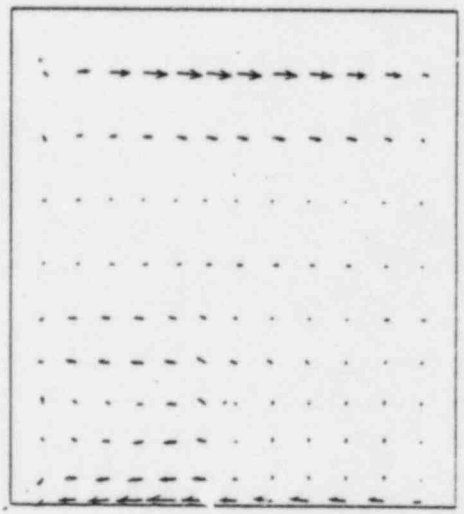

K = 7

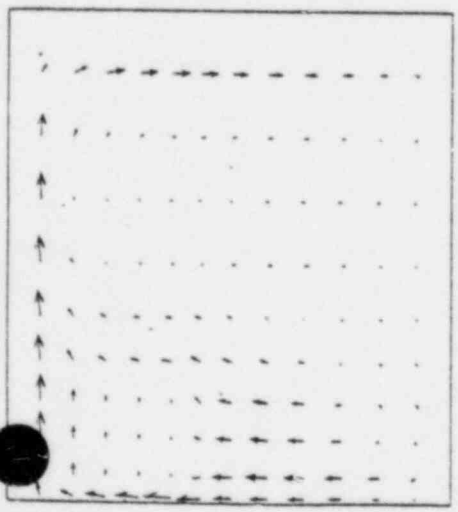

K = 8

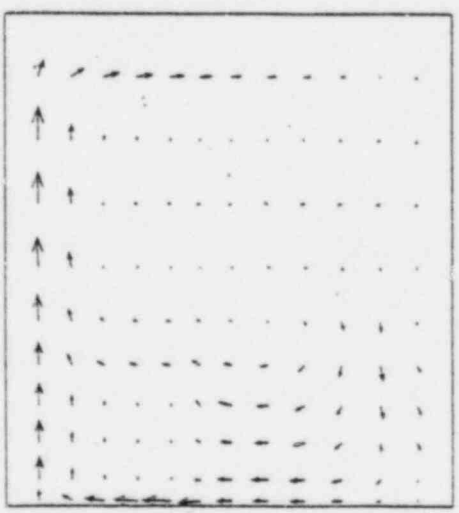

K = 9

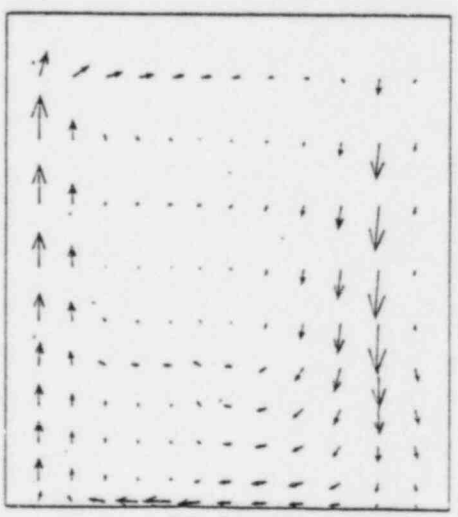

K = 10 (NORTH WALL)

FLOW IN VARIOUS EAST-WEST PLANES

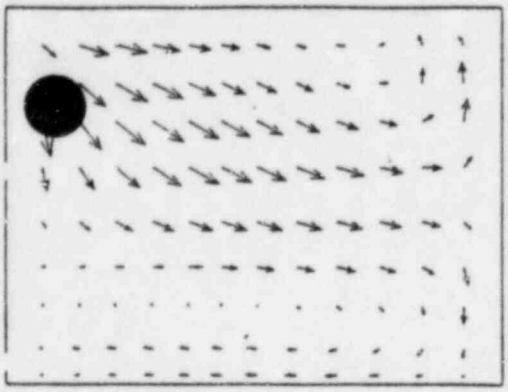

J = 11 (FREE SURFACE)

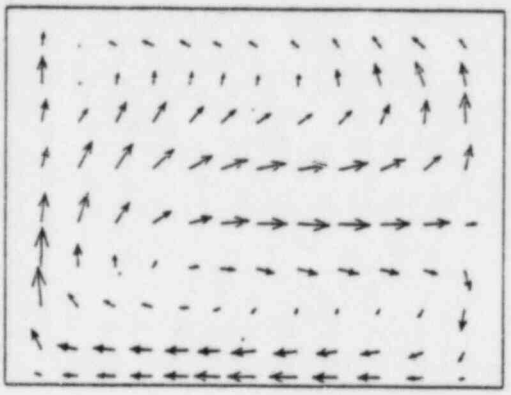

J = 10

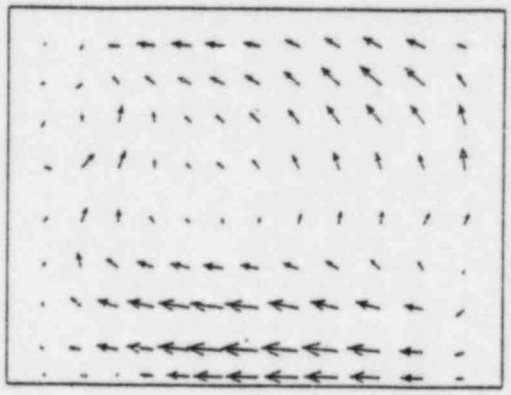

J = 9

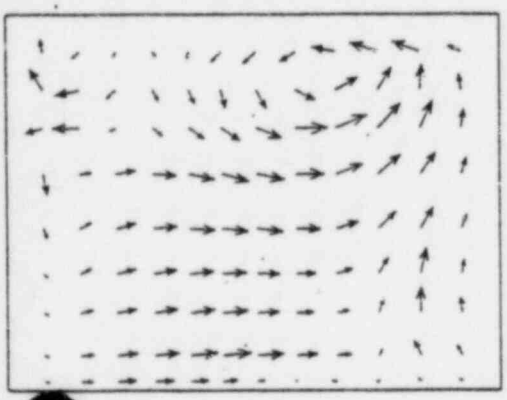

J = 8

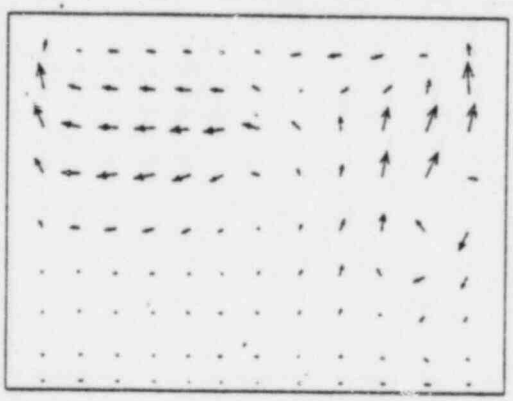

J = 7

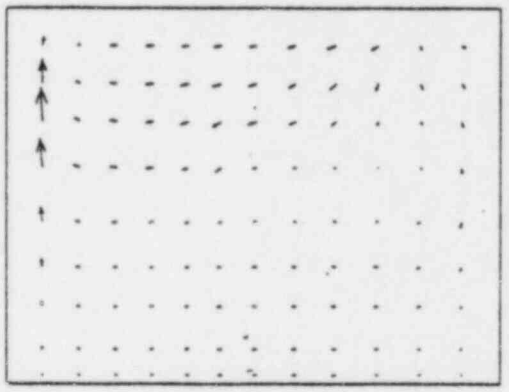

J = 6

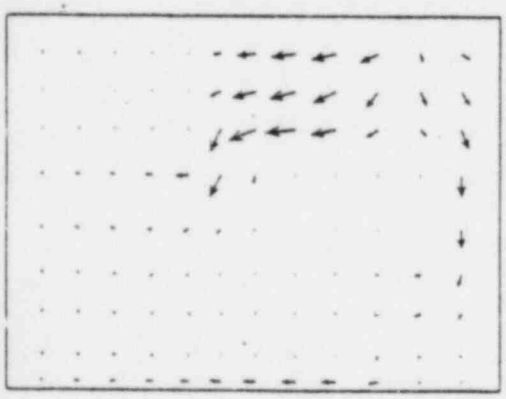

J = 5

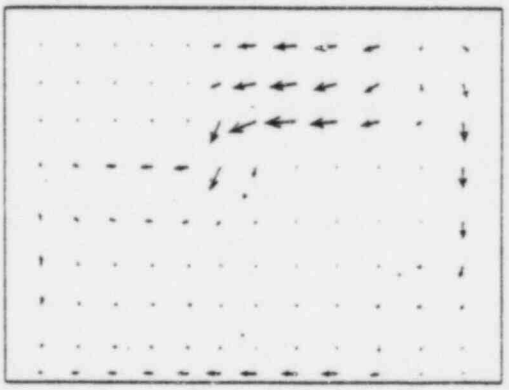

J = 4

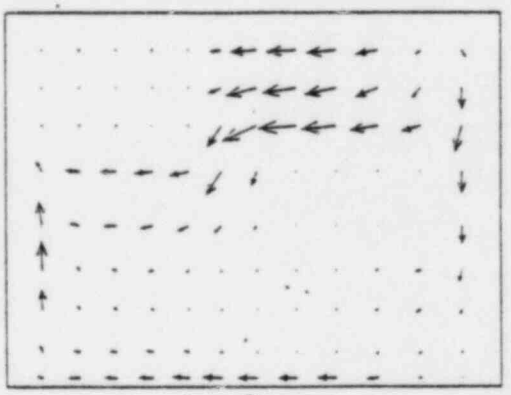

J = 3

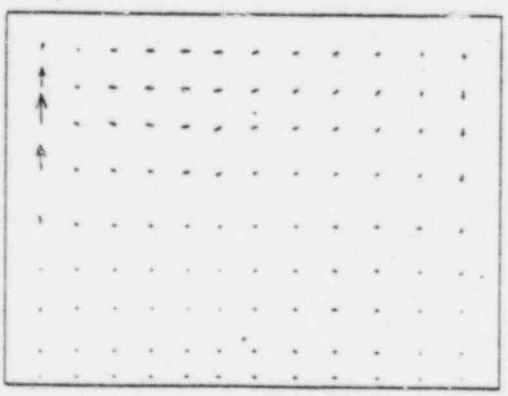

J = 2 (FLOOR)

FLOW IN VARIOUS HORIZONTAL PLANES

APPENDIX A

PARTIAL DIFFERENTIAL EQUATIONS SOLVED

APPENDIX A

PARTIAL DIFFERENTIAL EQUATIONS SOLVED

The partial differential equations solved include a mass conservation equation, (A-1), three momentum equations, (A-2) to (A-4), and a temperature equation, (A-5). In cartesian, x-y-z, coordinates these equations may be written as:

$$\frac{\partial \rho}{\partial t} + \frac{1}{\beta}\frac{\partial}{\partial x}\left\{(\beta_x \rho u) + \frac{\partial}{\partial y}(\beta_y \rho v) + \frac{\partial}{\partial z}(\beta_z \rho w)\right\} = 0 \quad \text{(mass conservation)} \qquad \text{(A-1)}$$

$$\frac{\partial \rho u}{\partial t} + \frac{1}{\beta}\frac{\partial}{\partial x}\left\{\beta_x \rho u^2\right\} + \frac{1}{\beta}\frac{\partial}{\partial y}\left\{\beta_y \rho uv\right\} + \frac{1}{\beta}\frac{\partial}{\partial z}\left\{\beta_z \rho uw\right\}$$
$$= -\frac{\partial p}{\partial x} + 2\frac{\partial}{\partial x}\mu\left(\frac{\partial u}{\partial x}\right) + \frac{\partial}{\partial y}\left\{\mu\left(\frac{\partial v}{\partial x} + \frac{\partial u}{\partial y}\right)\right\} + \frac{\partial}{\partial z}\left\{\mu\left(\frac{\partial w}{\partial x} + \frac{\partial u}{\partial z}\right)\right\}$$
$$+ \frac{\partial}{\partial x}(\lambda\Delta) - k_x \rho u \qquad \text{(x-momentum conservation)} \qquad \text{(A-2)}$$

$$\frac{\partial \rho v}{\partial t} + \frac{1}{\beta}\frac{\partial}{\partial x}(\beta_x \rho uv) + \frac{1}{\beta}\frac{\partial}{\partial y}(\beta_y \rho v^2) + \frac{1}{\beta}\frac{\partial}{\partial z}(\beta_z \rho vw)$$
$$= -\frac{\partial p}{\partial y} + \frac{\partial}{\partial x}\left\{\mu\left(\frac{\partial u}{\partial y} + \frac{\partial v}{\partial x}\right)\right\} + 2\frac{\partial}{\partial y}\mu\left(\frac{\partial v}{\partial y}\right) + \frac{\partial}{\partial z}\left\{\mu\left(\frac{\partial v}{\partial z} + \frac{\partial w}{\partial y}\right)\right\} + \frac{\partial}{\partial y}(\lambda\Delta)$$
$$- f_y' \frac{\rho v^2}{2} + \Delta\rho \cdot g \qquad \text{(y-momentum conservation)} \qquad \text{(A-3)}$$

$$\frac{\partial \rho w}{\partial t} + \frac{1}{\beta}\frac{\partial}{\partial x}(\beta_x \rho uw) + \frac{1}{\beta}\frac{\partial}{\partial y}(\beta_y \rho vw) + \frac{1}{\beta}\frac{\partial}{\partial z}(\beta_z \rho w^2)$$
$$= -\frac{\partial p}{\partial z} + \frac{\partial}{\partial x}\left\{\mu\left(\frac{\partial u}{\partial z} + \frac{\partial w}{\partial x}\right)\right\} + \frac{\partial}{\partial y}\left\{\mu\left(\frac{\partial w}{\partial y} + \frac{\partial v}{\partial z}\right)\right\} + 2\frac{\partial}{\partial z}\left(\mu\frac{\partial w}{\partial z}\right)$$
$$+ \frac{\partial}{\partial z}(\lambda\Delta) - k_z \rho w \qquad \text{(z-momentum conservation)} \qquad \text{(A-4)}$$

$$\frac{\partial T}{\partial t} + \frac{1}{\beta}\left\{\frac{\partial}{\partial x}\left(\beta_x u T\right) + \frac{\partial}{\partial y}\left(\beta_y v T\right) + \frac{\partial}{\partial z}\left(\beta_z w T\right)\right\} = \frac{\partial}{\partial x}\left(\frac{\mu}{\rho}\frac{\partial T}{\partial x}\right) + \frac{\partial}{\partial y}\left(\frac{\mu}{\rho}\frac{\partial T}{\partial y}\right) + \frac{\partial}{\partial z}\left(\frac{\mu}{\rho}\frac{\partial T}{\partial z}\right) + \frac{1}{\beta}\left(\frac{dT}{dt}\right)_s$$

(temperature equation) (A-5)

In Eqs. (A-1) to (A-5) the following notation is used:

f'_y friction factor in the y-direction (m^{-1})

g acceleration due to gravity (m/sec^2)

k_x friction factor in the x-direction (sec^{-1})

k_z friction factor in the z-direction (sec^{-1})

$\left(\frac{dT}{dt}\right)_s$ heat source for fueled assemblies (°C/sec)

p pressure ($newtons/m^2$)

t time (sec)

T fluid temperature (°C)

u x-component of the fluid velocity (m/sec)

v y-component of the fluid velocity (m/sec)

w z-component of the fluid velocity (m/sec)

α volumetric coefficient of thermal expansion ($°C^{-1}$)

β_x fractional fluid area in x-direction

β_y fractional fluid area in y-direction

β_z fractional fluid area in z-direction

β fractional fluid volume

$\Delta \equiv \frac{\partial}{\partial x}(u) + \frac{\partial}{\partial y}(v) + \frac{\partial}{\partial z}(w)$

$\Delta\rho \equiv \rho\alpha(\Delta T)$ = change in fluid density due to temperature changes (kg/m^3)

ρ fluid density (kg/m^3)

λ second coefficient of viscosity (kg/m-sec)

μ first coefficient of viscosity (kg/m-sec)

APPENDIX B

FRICTION FACTOR CALCULATIONS

For fueled assemblies, the following flow areas are used:

$$A_{RODS} = 23.44\ in^2$$

$$A_{SPACERS\ MINIMUM} = 19.74\ in^2$$

$$A_{TP1} = 18.12\ in^2$$

$$A_{TP2} = 19.46\ in^2$$

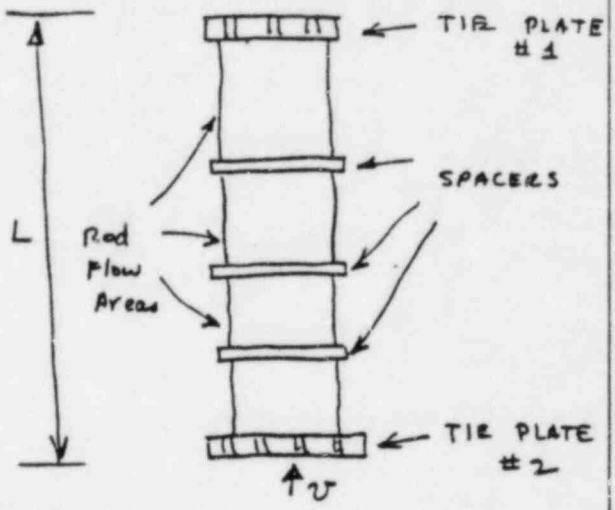

For conservative results, assume all 3 spacer regions have the minimum flow area of $19.74\ in^2$.

The total pressure loss through the assembly may be written as

$$\Delta P_{ASM} \cdot A_{FLOW} \cong \left\{ \Delta P_{RODS} \cdot A_{SHEAR} + 3 \cdot \Delta P_{SPACERS} \cdot A_{FLOW} + (\Delta P_{TP1} + \Delta P_{TP2}) A_{FLOW} \right\}$$

or

$$\Delta P_{ASM} \cong \left\{ \Delta P_{RODS} \frac{A_{SHEAR}}{A_{FLOW}} + 3 \cdot \Delta P_{SPACERS} + \Delta P_{TP1} + \Delta P_{TP2} \right\} \qquad (B\text{-}1)$$

For Reynolds numbers $\sim 10^4$, Fig 114 from Reference 5, for longitudinal flow over a square array of tubes, (see Fig 114 below), gives

$$\Delta P_{RODS} = f_{RODS} * \frac{\rho V^2}{2} \cong .007 * \frac{\rho V^2}{2} \qquad (B\text{-}2)$$

Similarly for the spacers and the plates we may write

$$\left.\begin{aligned} \Delta P_{SPACERS} &\cong f_{SPACER} * \rho V^2/2 \\ \Delta P_{TP_1} &\cong f_{TR1} * \rho V^2/2 \\ \Delta P_{TP2} &\cong f_{TP2} * \rho V^2/2 \end{aligned}\right\} \qquad (B\text{-}3)$$

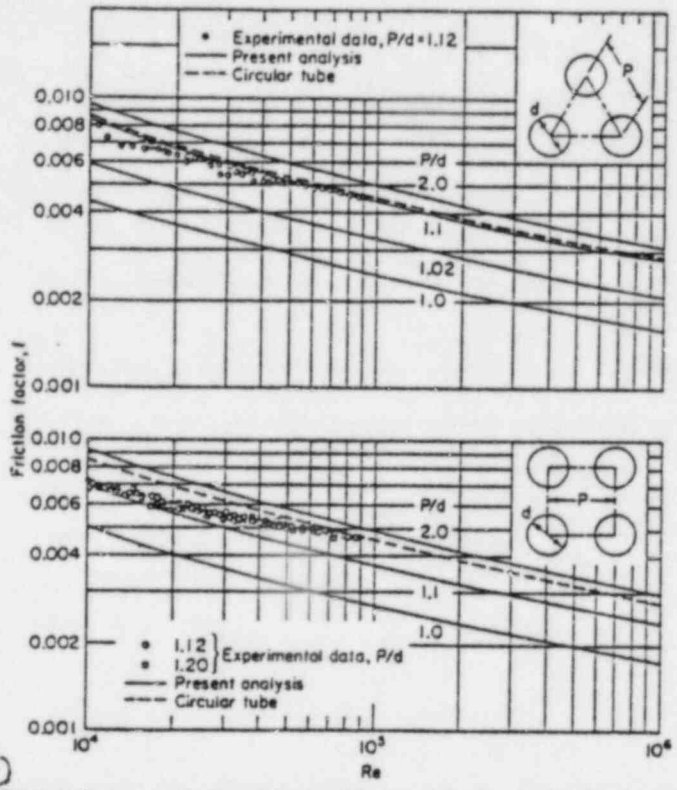

(5)

Fig. 114. Friction factor versus Reynolds number for turbulent flow through triangular and rectangular array. Reynolds number based on D_e.

$$f \equiv \Delta P / \rho v^2/2$$

or

$$\Delta P_{ASH} \cong \left\{ f_{RODS} \frac{A_{shear}}{A_{flow}} + 3 f_{SPACERS} + f_{TP1} + f_{TP2} \right\} \frac{\rho v^2}{2} . \qquad (B\text{-}4)$$

For the frictional losses due to spacers and tie plates, we use curves from Pag. 32 of Idel'chuk [4] for plane grids or perforated sheets (see curves on next page).

We define Fo to be the constricted flow area through spacer and tie plate regions, and F_1 to be

Plane grid (perforated sheet) with sharp-edged orifices

$\left(\frac{l}{d_h} = 0 \div 0.015\right)$. $\left(\mathrm{Re} = \frac{w_0 d_h}{\nu} < 10^5\right)$

Section VIII

Diagram 8-2

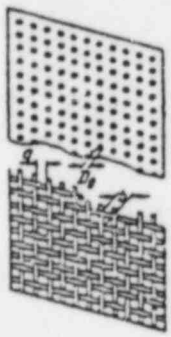

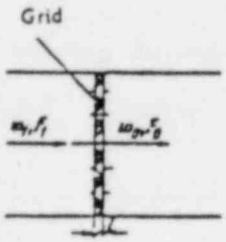

$$\zeta = \frac{\Delta H}{\frac{\gamma w_1^2}{2g}} \cong \left[\zeta_\varphi + \bar{\varepsilon}_0^{\mathrm{Re}}(\zeta_0 - \bar{f})^2\right]\frac{1}{\bar{f}^2}$$ (approximately

where ζ_φ is determined from the curves $\zeta_\varphi = f_3(\mathrm{Re})$ for different $\bar{f}$ on graph a;

$\bar{\varepsilon}_0^{\mathrm{Re}}$ is determined from $\bar{\varepsilon}_0^{\mathrm{Re}} = f_2(\mathrm{Re})$ on graph a;

$\zeta_0 = 1 + 0.707\sqrt{1-\bar{f}}$ is determinated from the curve $\zeta_0 = f(\bar{f})$ on graph b.

Re	2.5·10	4·10	6·10	10^5	$2\cdot10^5$	$4\cdot10^5$	10^6	$2\cdot10^6$	$4\cdot10^6$	10^7	$2\cdot10^7$	10^8	$2\cdot10^8$	$>10^8$
$\bar{\varepsilon}_0^{\mathrm{Re}}$	0.34	0.36	0.37	0.40	0.43	0.46	0.53	0.59	0.64	0.74	0.81	0.94	0.96	0.98

$\frac{F_0}{F_1}$	Values of ζ_φ													
0	1.94	1.38	1.14	0.89	0.69	0.54	0.39	0.30	0.22	0.15	0.11	0.04	0.01	0
0.2	1.78	1.36	1.05	0.85	0.67	0.57	0.36	0.26	0.20	0.13	0.09	0.03	0.01	0
0.3	1.57	1.16	0.88	0.75	0.57	0.43	0.30	0.22	0.17	0.10	0.07	0.02	0.01	0
0.4	1.35	0.99	0.79	0.57	0.40	0.28	0.19	0.14	0.10	0.06	0.04	0.02	0.01	0
0.5	1.10	0.75	0.55	0.34	0.19	0.12	0.07	0.05	0.03	0.02	0.01	0.01	0.01	0
0.6	0.85	0.56	0.30	0.19	0.10	0.06	0.03	0.02	0.01	0.01	0	0	0	0
0.7	0.58	0.37	0.23	0.11	0.06	0.03	0.02	0.01	0	0	0	0	0	0
0.8	0.40	0.24	0.13	0.06	0.03	0.02	0.01	0	0	0	0	0	0	0
0.9	0.20	0.13	0.08	0.03	0.01	0	0	0	0	0	0	0	0	0
0.95	0.03	0.03	0.02	0	0	0	0	0	0	0	0	0	0	0

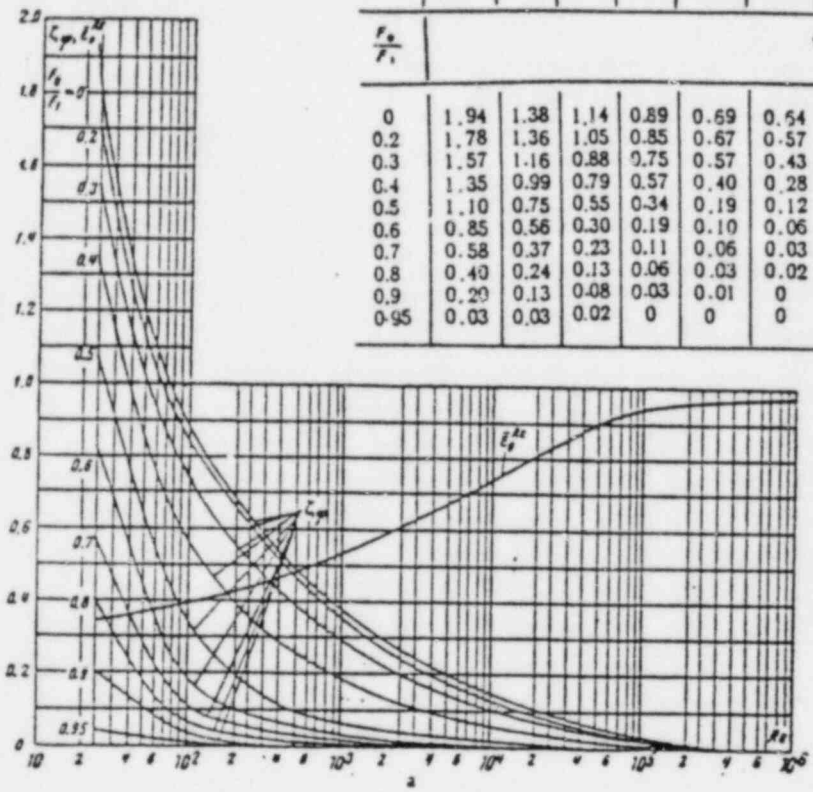

$d_h = \frac{4f_0}{\Pi_0}$; Π_0 – perimeters;

$\bar{f} = \frac{F_0}{F_1}$;

ν = is taken from § 1-3, b.

$\bar{f}$	0	0.1	0.2	0.3	0.4	0.5	0.6	0.7	0.8	0.9	1.0
ζ_0	1.71	1.67	1.63	1.59	1.55	1.50	1.45	1.39	1.32	1.22	1.0

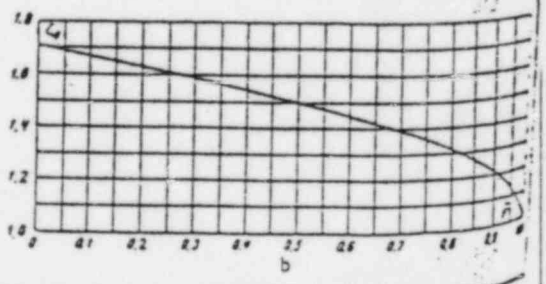

Reference #4. 322

the unrestricted fluid flow area.

Then
$$\left.\begin{aligned} \bar{f}_{SPACERS} &\cong F_0/F_1 = \frac{19.74}{23.44} = .842 \\ \bar{f}_{TP1} &\cong \frac{19.46}{23.44} = .830 \\ \bar{f}_{TP2} &\cong 18.37/23.44 = .773 \end{aligned}\right\} \quad (B\text{-}5)$$

Then from Idelchik,
$$\zeta \equiv \frac{\Delta p}{\rho v^2/2} \cong \left\{ \zeta_\phi + \varepsilon_\theta^{2E} (\zeta_0 - \bar{f})^2 \right\} 1/f^2 \qquad (B\text{-}6)$$

for the spacers and tie plates. For $Re \sim 10^4$, the curves on previous page allow construction of the following table:

	$\bar{f}$	ζ_ϕ	ε_θ	ζ_0	$\zeta = f$	
SPACERS	.842	0.0	0.74	1.28	.200	$= f_{SPACER}$
TP1	.830	0.0	0.74	1.29	.227	$= f_{TP1}$
TP2	.773	0.0	0.74	1.32	.370	$= f_{TP2}$

Using these f factors in Eq. (B-4) we find

$$\Delta P_{ASH} \cong \left\{ \underbrace{.007}_{f_{SPACERS}} + \frac{\pi \overbrace{D_{rods}}^{.444"} \times 121 \times \overbrace{L}^{84.5"}}{\underbrace{23.44}_{A_{FLOW}}} + \left(3(.2) + .227 + .370\right) \right\} \frac{\rho v^2}{2}$$

or

$$\boxed{\frac{\Delta P_{ASH}}{L_{ASH}} \cong \underbrace{\left(.0509\ in^{-1} + .01417\ in^{-1}\right)}_{f_{TOTAL}} \frac{\rho v^2}{2} = \left(\frac{2.56}{m}\right) \frac{\rho v^2}{2}} \qquad (B\text{-}7)$$

m^{-1} units for f_{TOTAL}

Friction Factors For Flow Thru Rectangular Ducts

We can use either a turbulent tube formula with hydraulic diameter chosen to represent the ducts, or Fig. 94 of Ref 5, shown on next page.

We $Re = \frac{D_H v}{\nu}$ $\quad \nu \simeq .445 \times 10^{-3}$ cm²/sec $\quad$ and $D_H = 4 * \frac{\text{Flow Area}}{\text{Wetted Perimeter}}$.

$\therefore Re \sim 5133 * V(\text{cm/sec})$

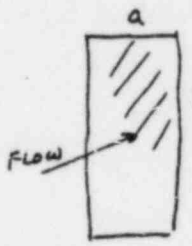

$D_H = \frac{4 * a * b}{2(a+b)}$

$\simeq \frac{4(4.75)(84.5)}{2(4.75+84.5)}$

for $a = 4.75"$, $b = 84.5"$ $\quad D_H \simeq 8.99"$

If $v \simeq 5$ cm/sec, $Re \Rightarrow 2.6 \times 10^4$

and from Fig. 94 below we have

for turbulent flow $4f \simeq .025$

or $f \simeq .00625$.

In terms of the pressure loss through a typical duct, we have

$$\frac{\Delta P}{L} \sim \frac{4}{D_H} f \frac{\rho v^2}{2} = f' \frac{\rho v^2}{2} \qquad \text{where } \boxed{f' = .1095 \equiv \frac{4}{D_H} f} \quad (\text{ft}^{-1})$$

In EITACC, in the x and z directions, (cross-flows), we use k_x and k_z friction factors where $k_x \rho u$ replaces $\frac{1}{2} f_x \rho u^2$

for example.

Therefore, we find for $u \simeq w \simeq .05$ m/sec.

$$\boxed{k_x = k_z \simeq \frac{f' \frac{1}{2} \rho u^2}{\rho u} = \frac{f' u}{2} \simeq .00273 \quad \text{sec}^{-1}}$$

↑ for Racks A + B (open)

For Racks D, E, and F, (closed) Set $k_x = k_z = 50$ sec^{-1} to prevent cross flows.

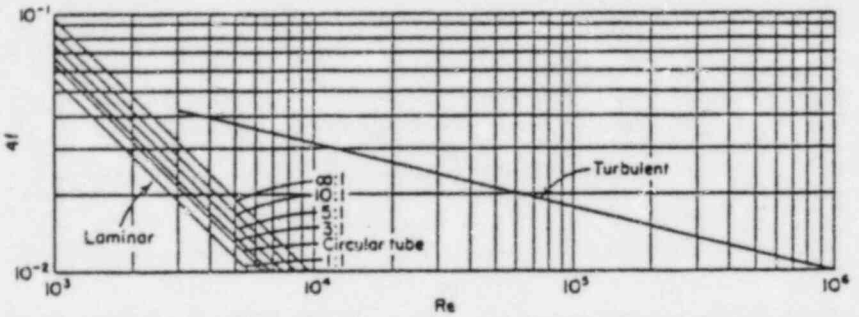

Fig. 94. Correlation of available data for rectangular duct friction coefficients using D_e, solid line for Re > 10^4 is the circular tube correlation. (Ref. 5).

APPENDIX C

CALCULATE AREA AND VOLUME BETAS

Calculate Area and Volume Beta Blockage Factors.

Define area betas to be = Fluid Flow Areas / Computational cell areas

$= \beta_x, \beta_y, \beta_z$

Define volume betas to = Fluid volumes / computational cell volumes.

Closed Racks -(F, D, E)

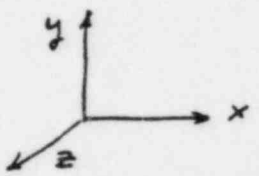

Allow flow in x and z directions between assemblies.
Assume flow in y direction only thru the 121 rod assembly cells.
Assume a stagnant slit region between assemblies (vertical direction).

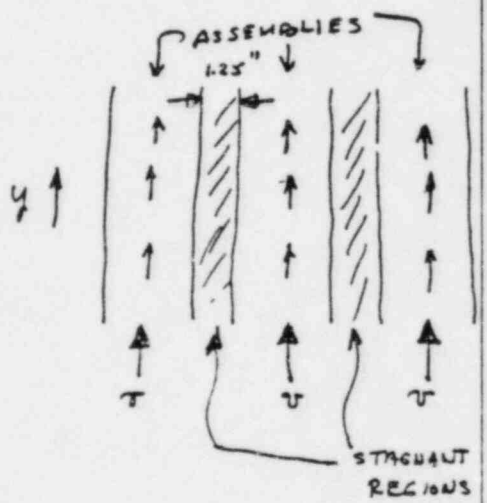

Rack F

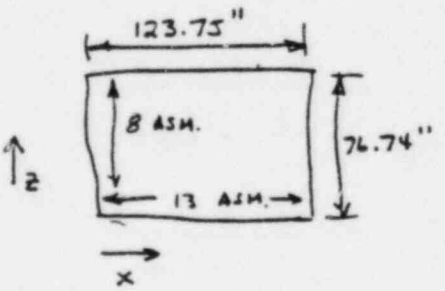

$\therefore \beta_z = (12_{gaps} * 1.25)/123.75 = .121$ $\qquad \beta_x = (7_{gaps} * 1.25)/76.74 = .114$

In the y-direction:

Flow Area = $104 * (23.44) = 2.438 * 10^3 \text{ in}^2$

(104 = # ASM., 23.44 = flow area)

Total y-area = $123.75 * 76.74 = 9496 * 10^3 \text{ in}^2$

$\therefore \beta_y = \frac{2438}{9496} = .257$

$$\beta_x = \beta_y = \frac{8 \text{ gaps} * 1.25}{82.25} = .122$$

y-direction

y-area = 6765 in^2

Flow area = $81 * 23.44 = 1899$ } $\beta_y = \frac{1899}{6765} = .281$

$$\beta \equiv \frac{\text{FLUID VOL.}}{\text{Total Vol}} = 1 - \frac{81 * 26.30 \cdot H}{6765 * H} = .685$$

where H = rack height

Open Racks

Rack - B

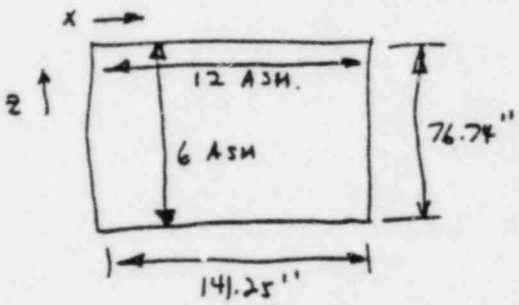

Assume open in x-z directions except for assembly cons.

$$\beta_z = \frac{141.25 - 12(7.25)}{141.25} = .384$$

$$\beta_x = \frac{76.74 - 6(7.25)}{76.74} = .433$$

y-direction

$A_{y\text{-total}} = 141.25 * 76.74 = 1.084 * 10^4 \text{ in}^2$

$A_{FLOW\text{-}y} = A_{TOT\text{-}y} - A_{ASH} + A_{rods} = 1.084 * 10^4 - 72(7.25)^2 + 72(23.44)$.

$\therefore \beta_y = \frac{A_{FLOW}}{A_{TOT}} = .807$

$$\beta \equiv 1 - \frac{72\{26.30 * H\}}{1.084 * 10^4 * H} = .825$$

For the volume β, we have

$$\beta = \frac{\text{FLUID VOLUME}}{\text{TOTAL VOLUME}} \simeq \frac{\text{TOTAL} - \text{Rod. Vol.} - \text{Ash. Vol.}}{\text{TOTAL}}$$

$$\beta = 1 - \frac{104\left\{121 * \pi(.446)^2/4 * H + (7.14)(.25)4H\right\}}{9496 * H}$$

or $\beta = .712$

Rack-D

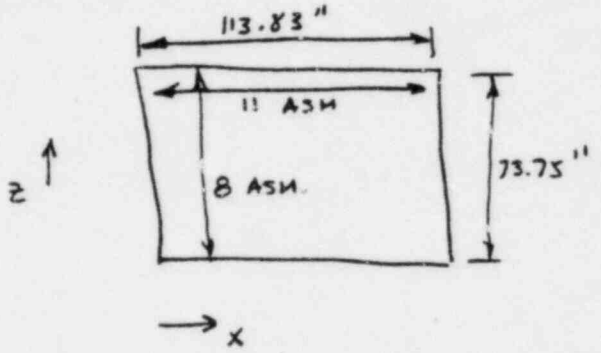

$$\beta_z = \frac{10 \text{ gaps} * 1.25}{113.83} = .110$$

$$\beta_x = \frac{7 \text{ gaps} * 1.25}{73.75} = .119$$

y-direction

Flow area $= 88 * 23.44 = 2063 \text{ in}^2$

Total Area $= 8395 \text{ in}^2$

$$\therefore \beta_y = \frac{2063}{8395} = .246$$

$$\beta \equiv \frac{\text{FLUID VOL.}}{\text{TOTAL VOL.}} \simeq 1 - \frac{88\{26.30\,H\}}{8395 * H} = 0.724$$

Rack-E

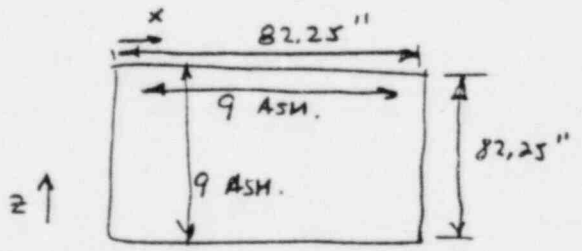

Rack A_1

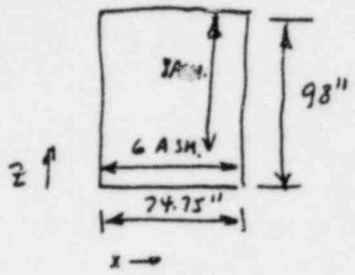

$$\beta_z = \frac{74.75 - 6(7.25)}{74.75} = .418$$

$$\beta_x = \frac{98 - 8(7.25)}{98} = .408$$

y-direction

$A_{y\text{-TOT}} = 7.326 * 10^3 \text{ in}^2$

Flow Areas = $\begin{cases} A_{rods} = 48 * 23.44 = 1125 \\ A_{SH.} = 48 * 7.25 = 2523 \\ A_{boxside} = A_{TOT} - A_{rod} - A_{ASH} = 7325 - 1125 - 2523 = \underline{3677} \end{cases}$

$$\beta_y = \frac{3677 + 1125}{7325} = .656$$

$$\beta \equiv 1 - \frac{48(26.30 \cdot H)}{7325 \cdot H} = .828$$

Rack A_2

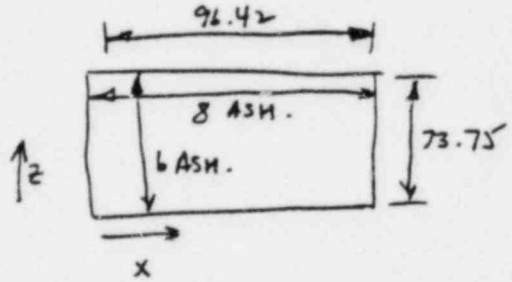

$$\beta_z = \frac{96.42 - 8(7.25)}{96.42} = .398$$

$$\beta_x = \frac{73.75 - 6(7.25)}{73.75} = .410$$

$A_{y\text{-TOTAL}} = 7111 \text{ in}^2$

$A_{rod\ flow} = 1125 \text{ in}^2$

$A_{ASH} = 2523 \text{ in}^2$

$A_{outside} = 7111 - 1125 - 2523 = \underline{3463 \text{ in}^2}$

$$\beta_y = \frac{3463 + 1125}{7111} = .645$$

$$\beta = 1 - \frac{48\{26.30\ H\}}{7111 \cdot H} = .822$$

APPENDIX D

EITACC-SFP GRAPHICAL OUTPUT

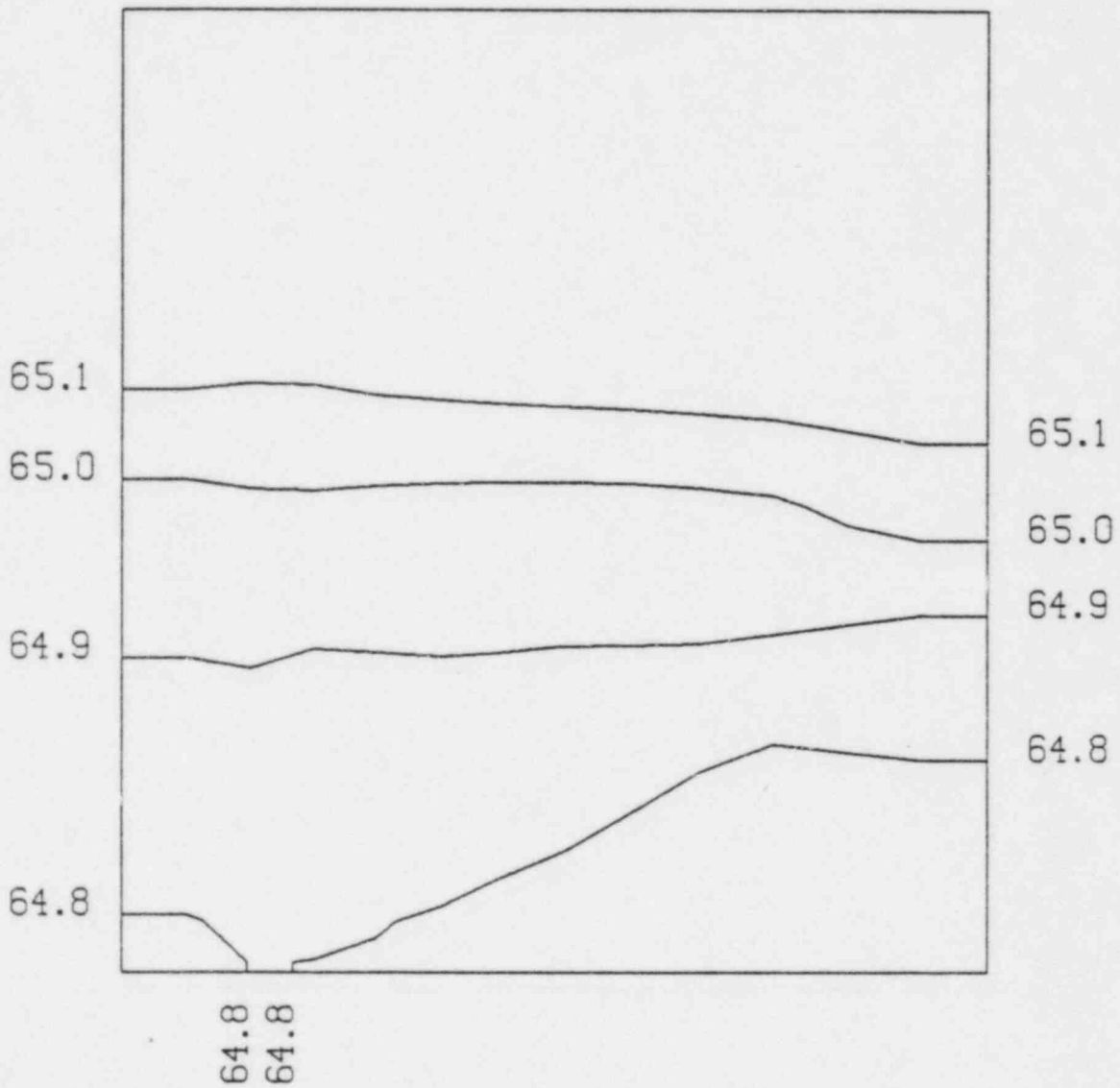

K - 2 TEMPERATURE CONTOURS AT TIME 1.55+003

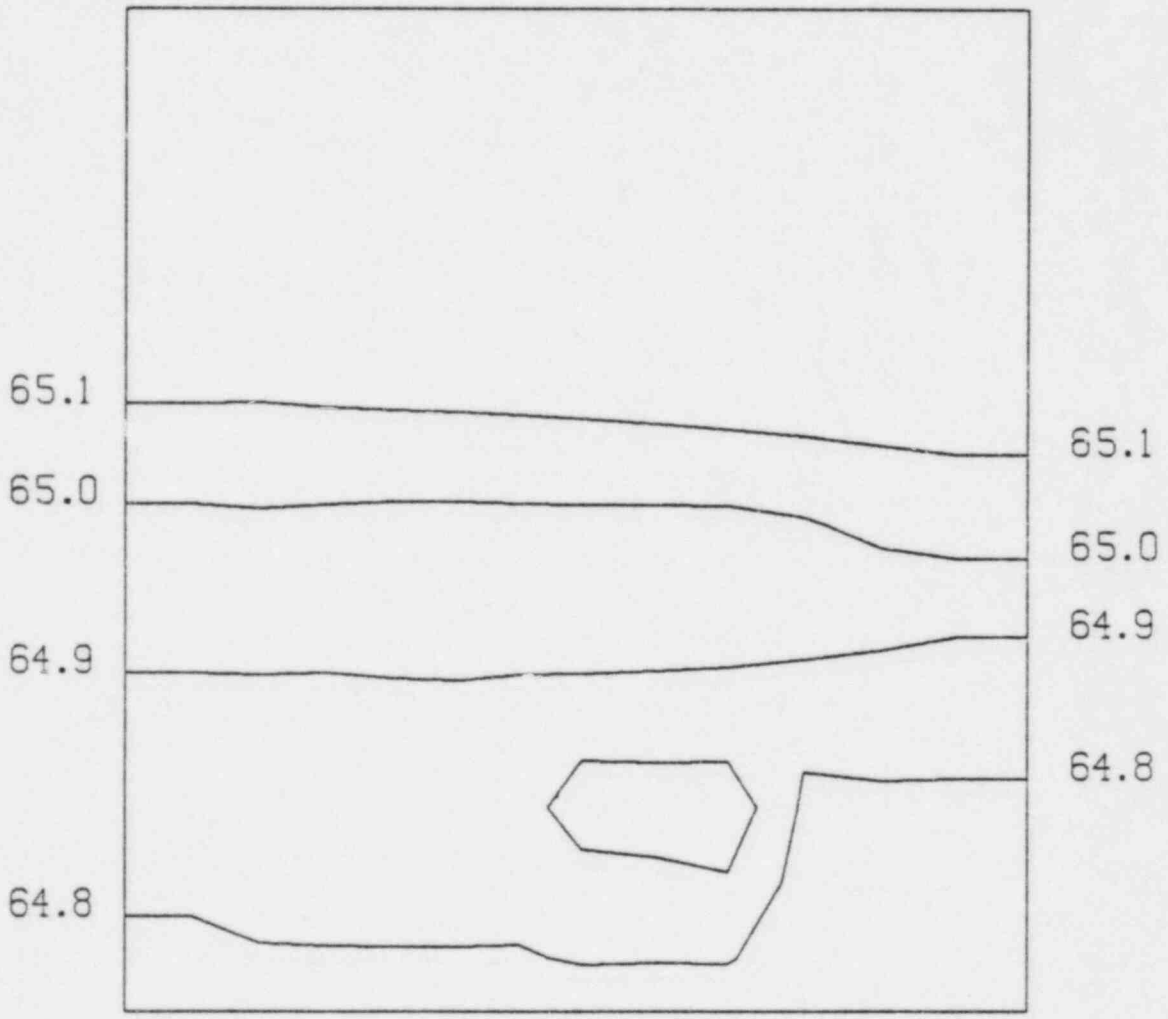

K - 3 TEMPERATURE CONTOURS AT TIME 1.55+003

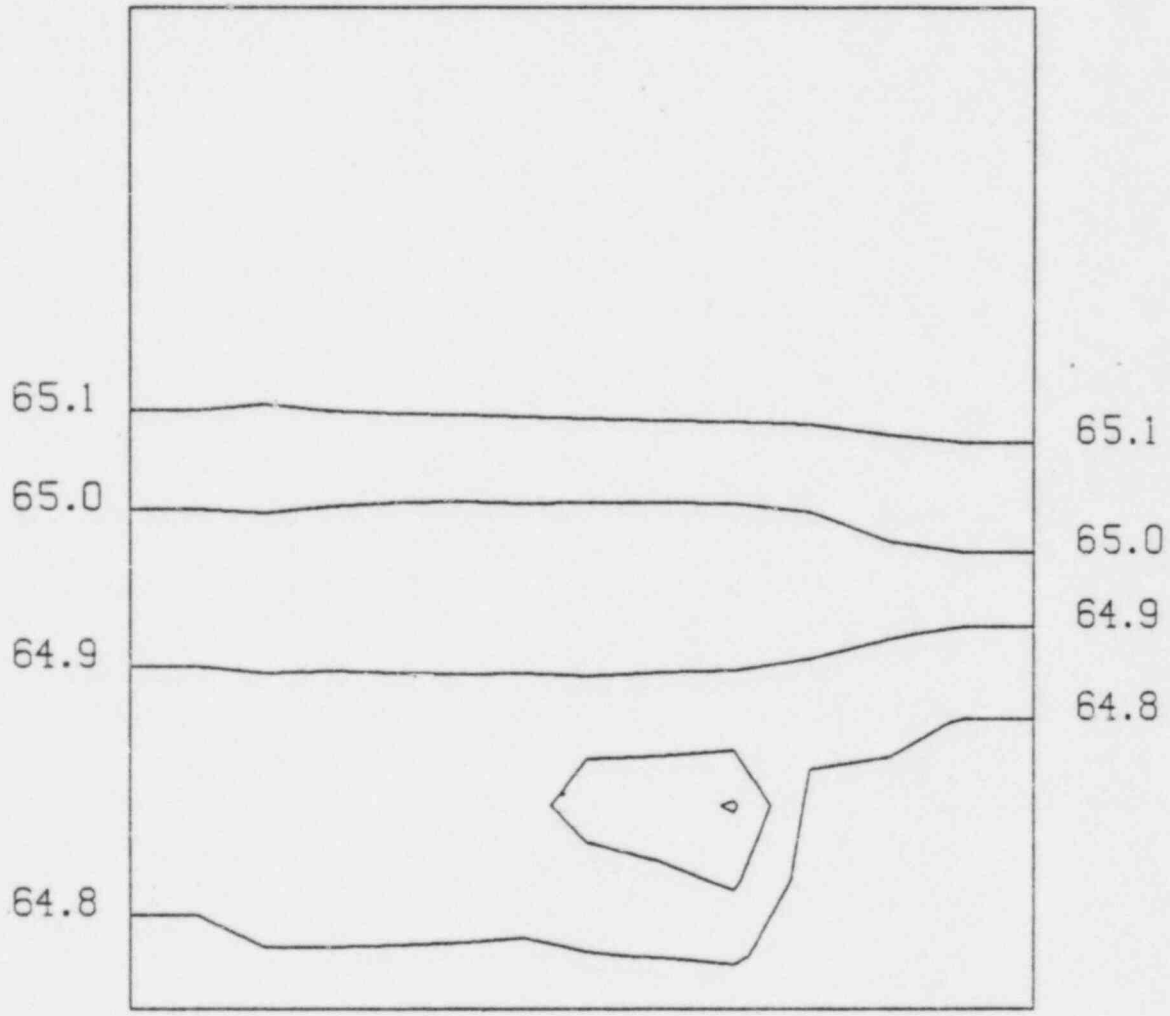

K = 4 TEMPERATURE CONTOURS AT TIME 1.55+003

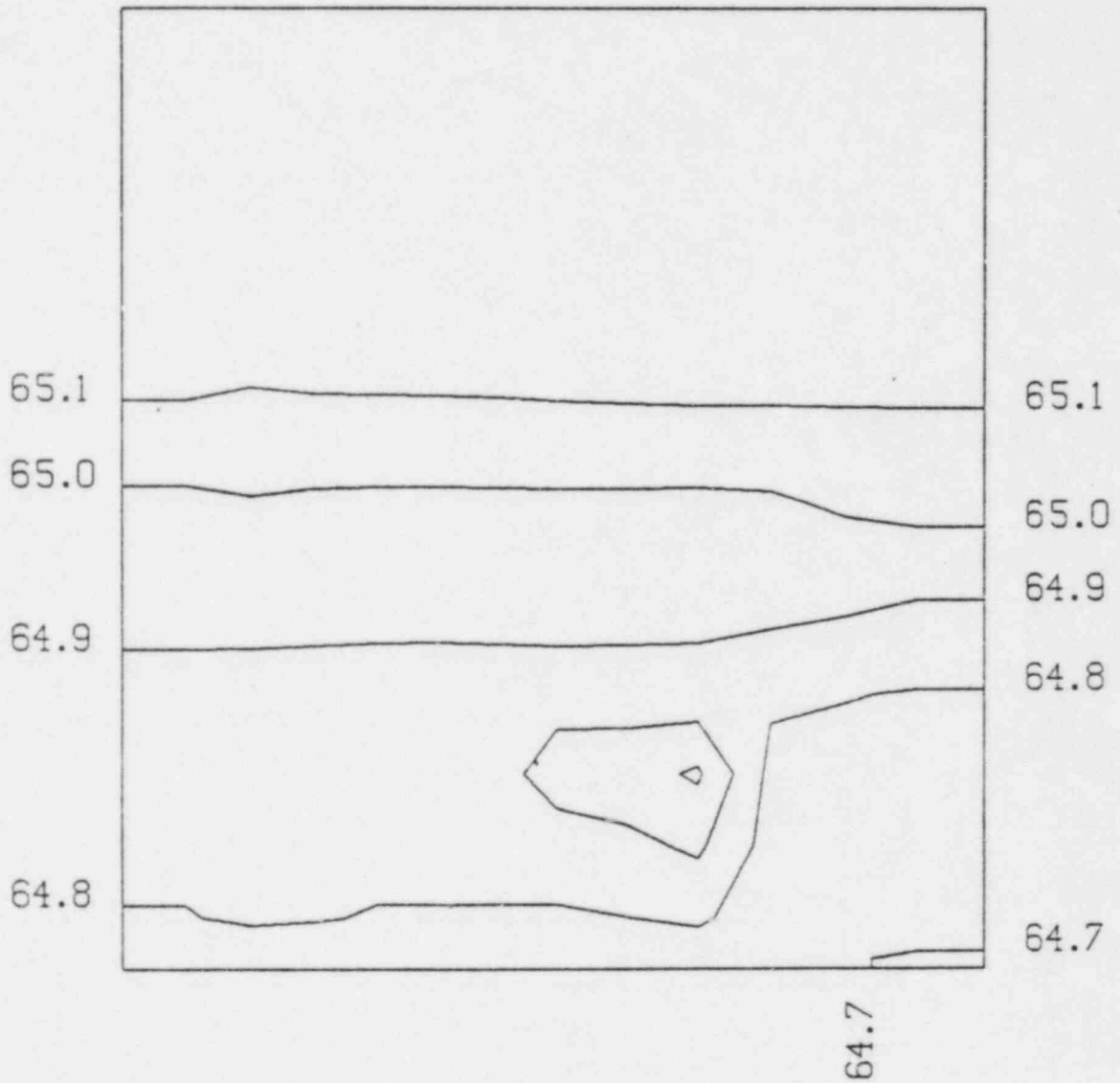

K = 5 TEMPERATURE CONTOURS AT TIME 1.55+003

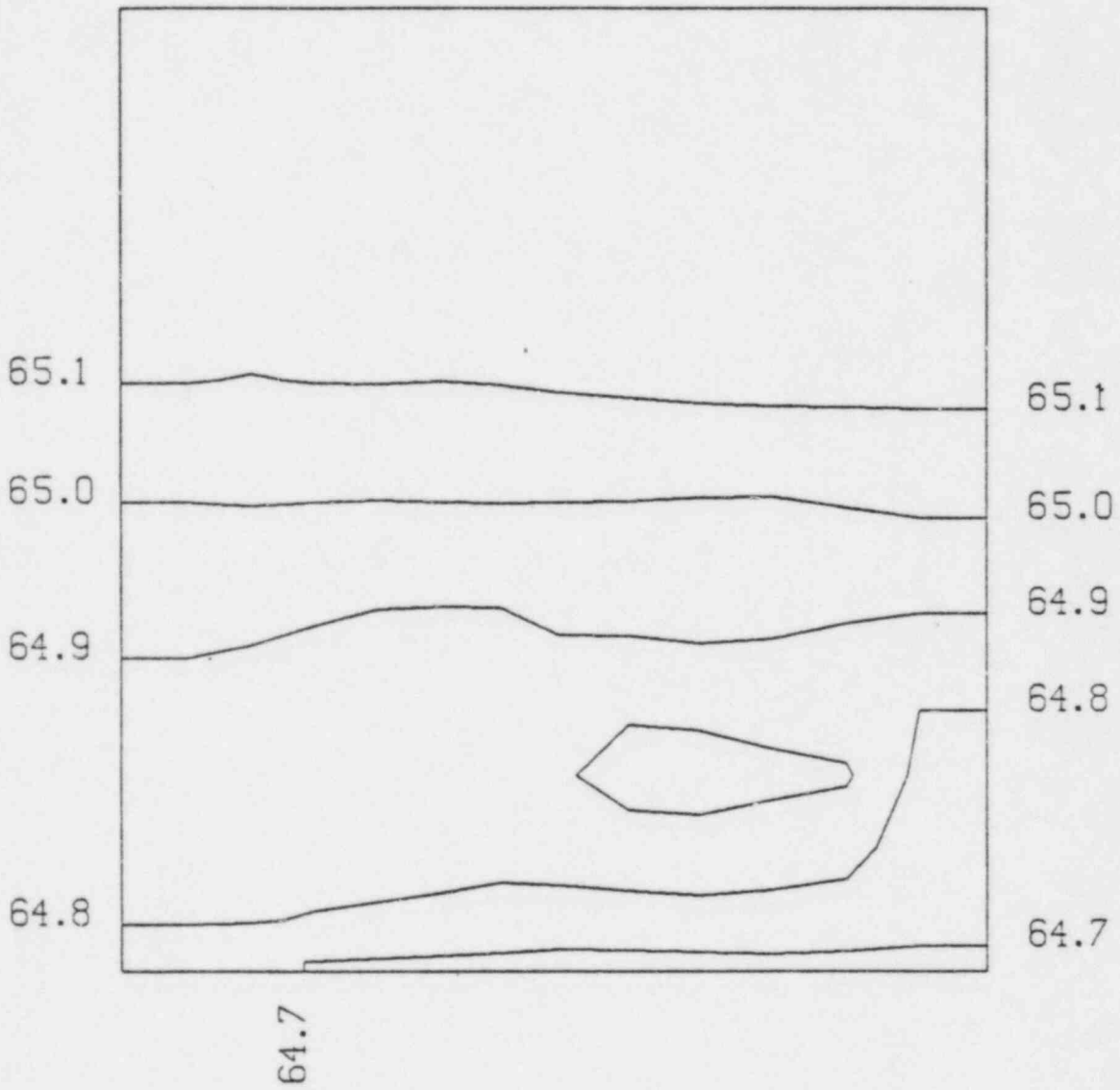

K - 6 TEMPERATURE CONTOURS AT TIME 1.55+003

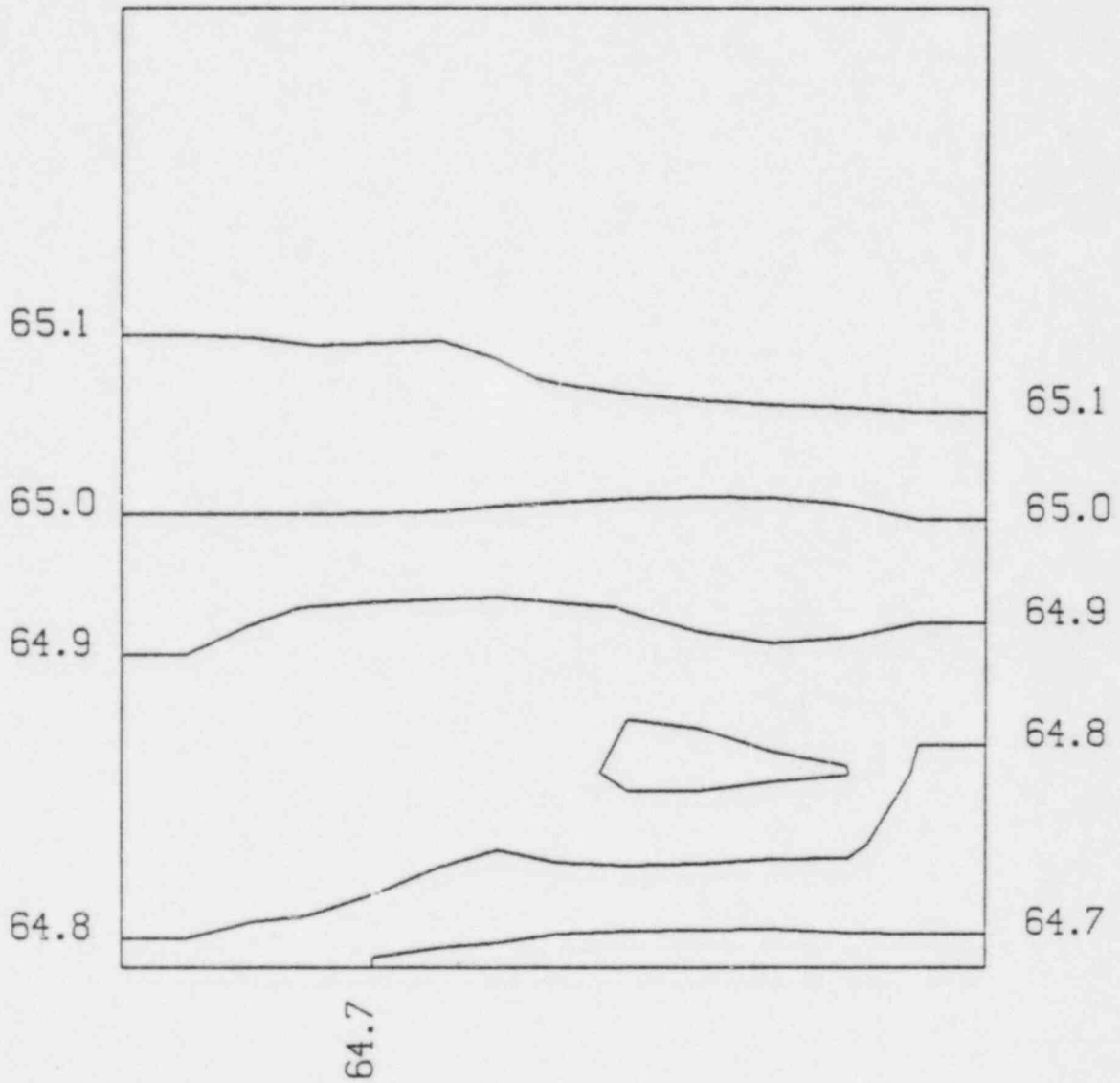

K - 7 TEMPERATURE CONTOURS AT TIME 1.55+003

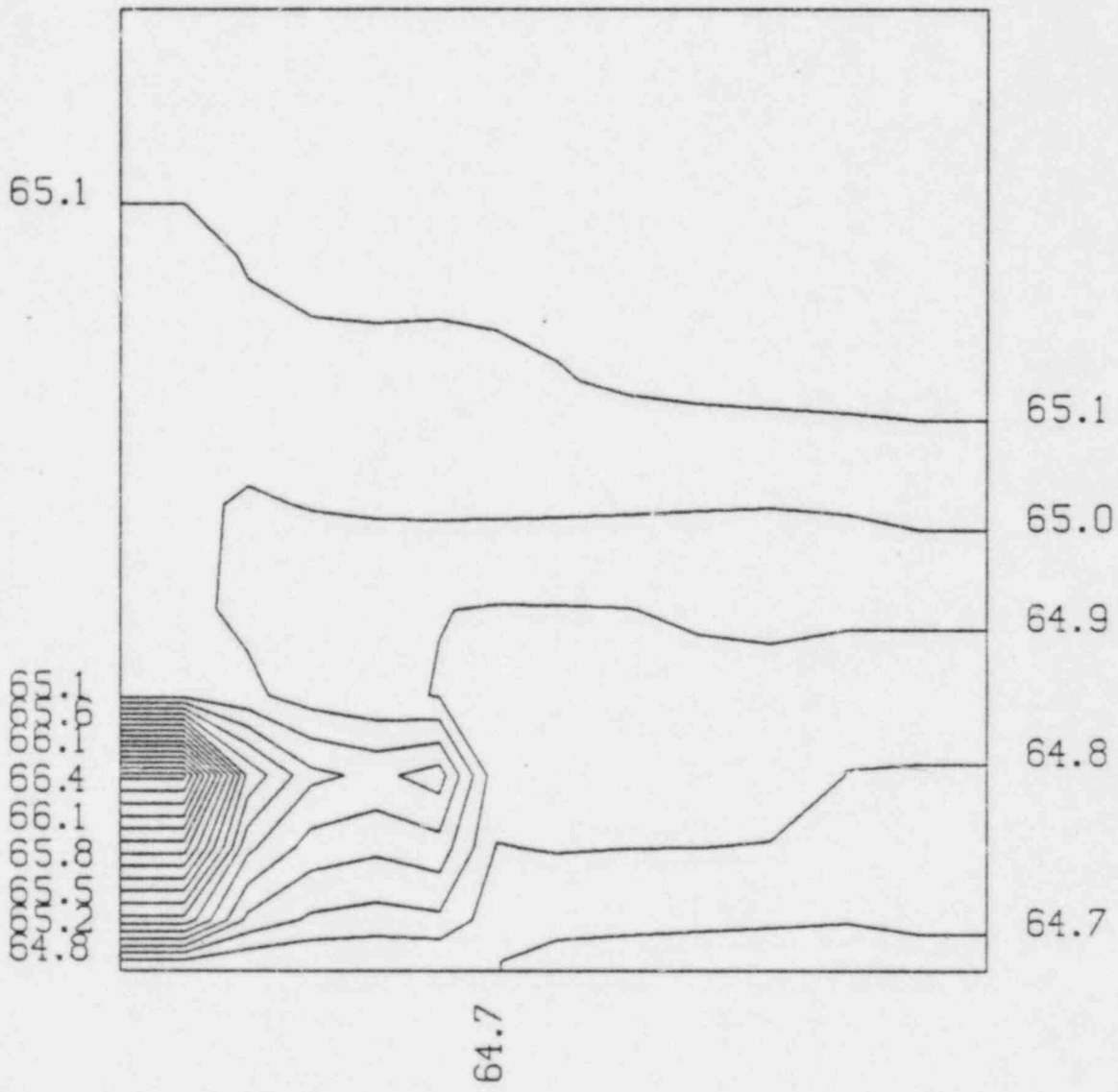

K = 8 TEMPERATURE CONTOURS AT TIME 1.55+003

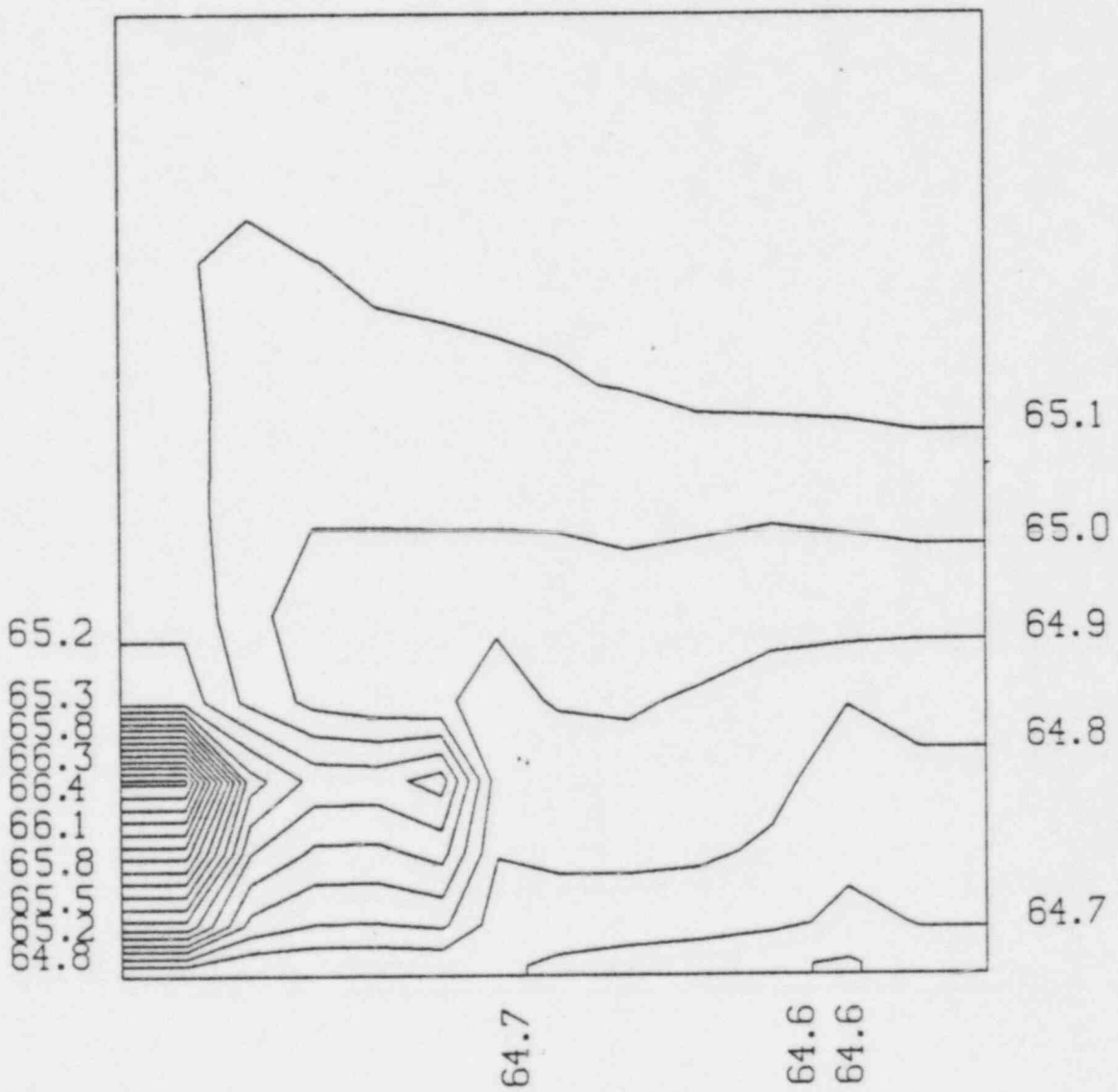

K = 9 TEMPERATURE CONTOURS AT TIME 1.55+003

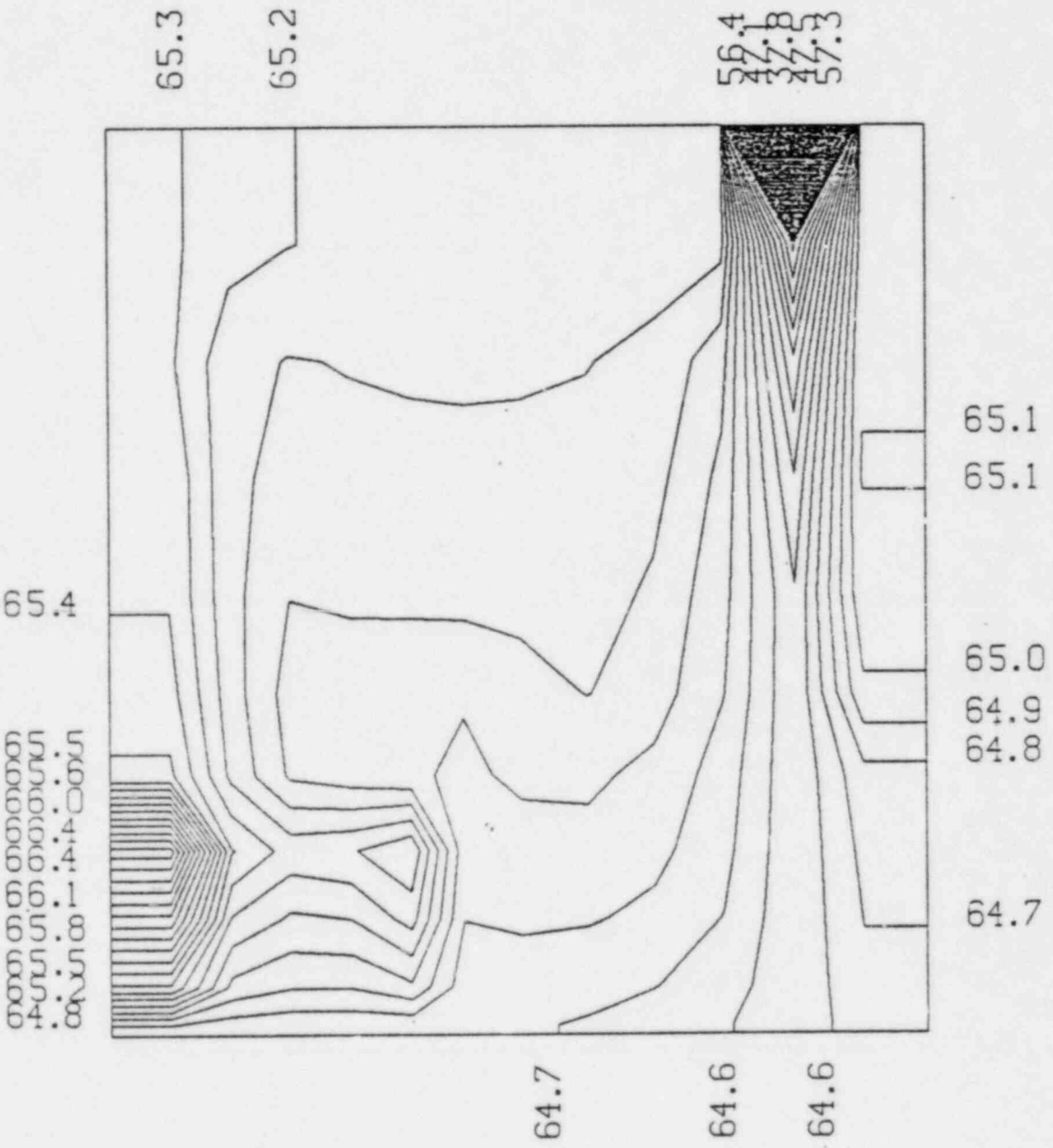

K = 10 TEMPERATURE CONTOURS AT TIME 1.55+003

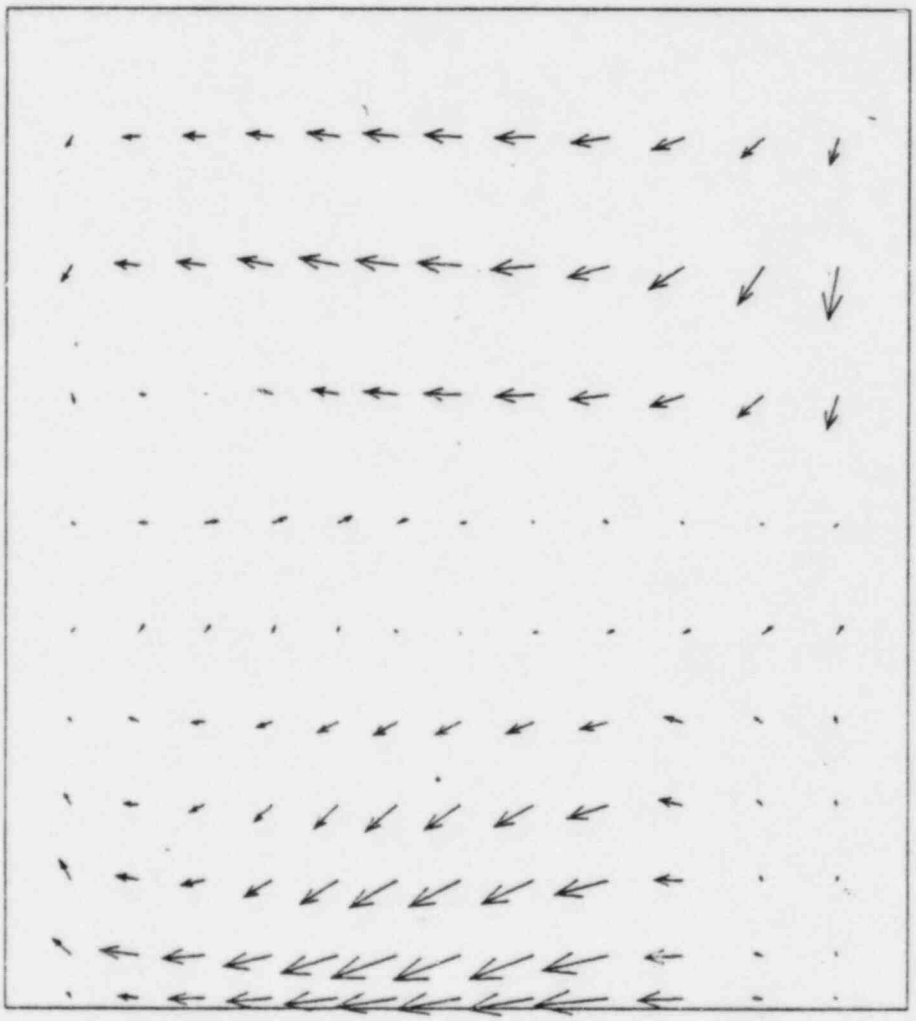

K = 2 VECTOR PLOTS AT TIME 1.55+003

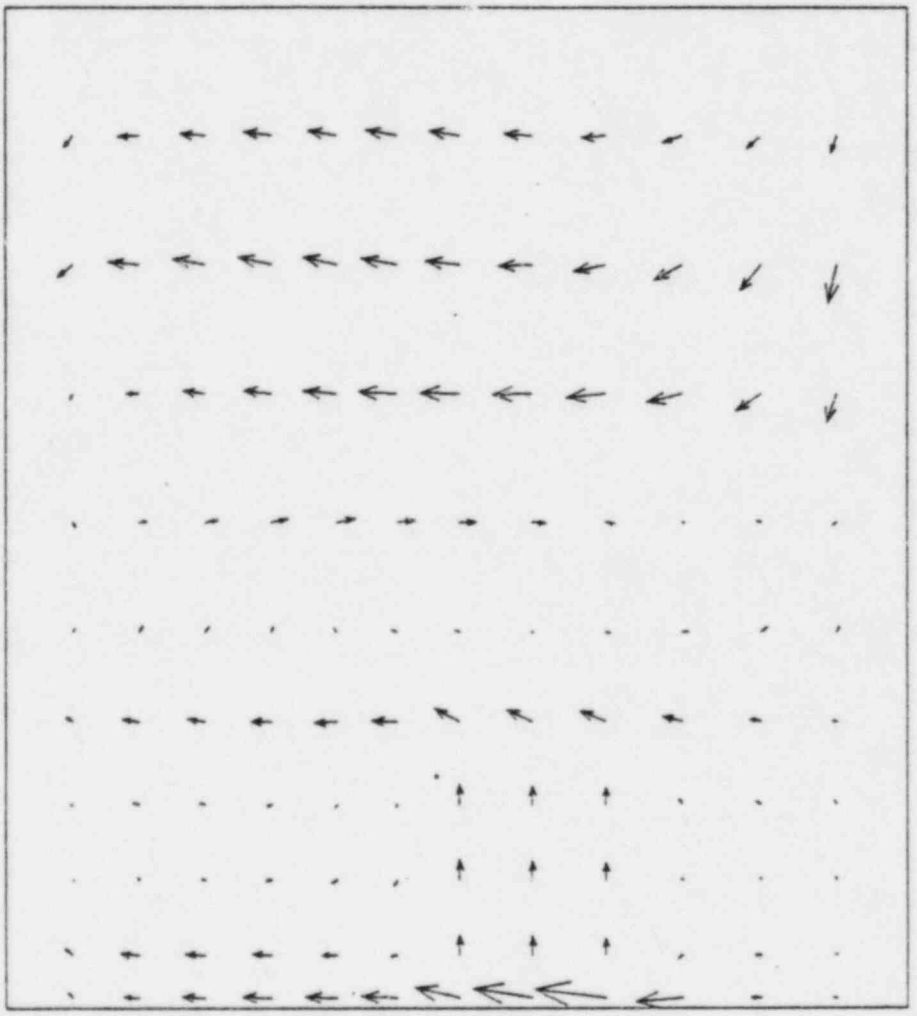

K = 3 VECTOR PLOTS AT TIME 1.55+003

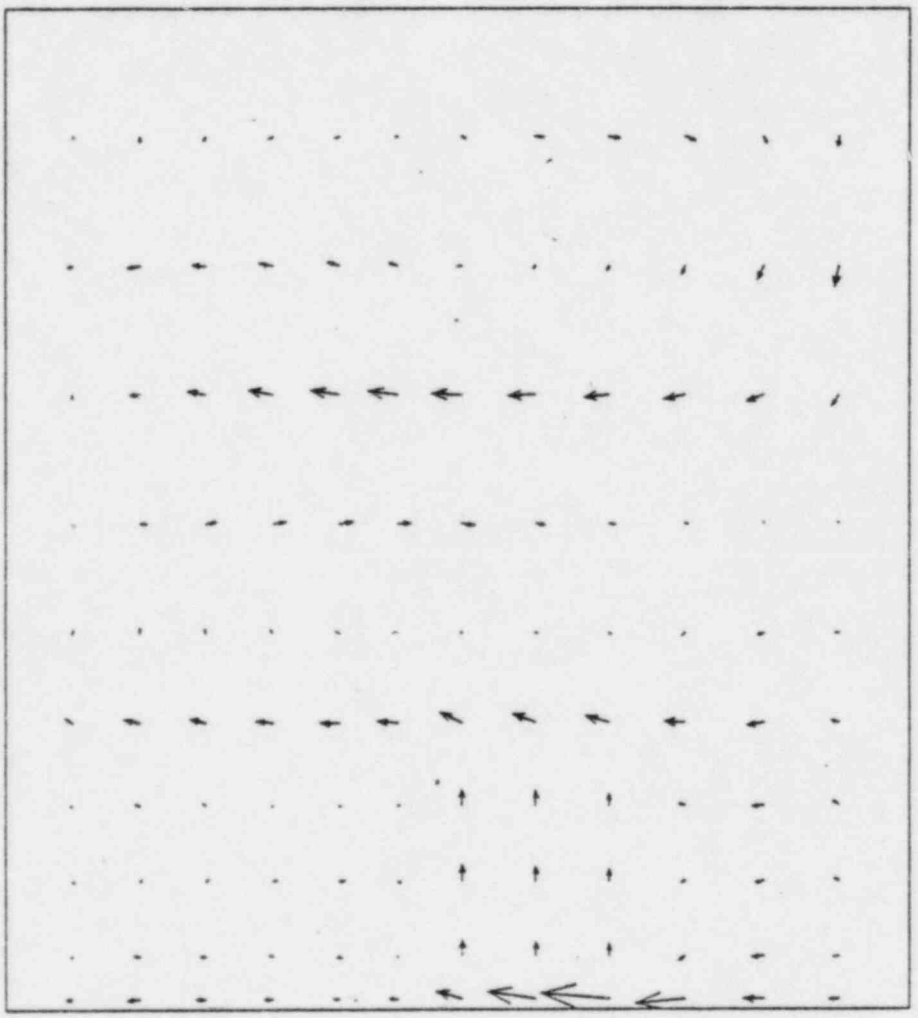

K = 4 VECTOR PLOTS AT TIME 1.55+003

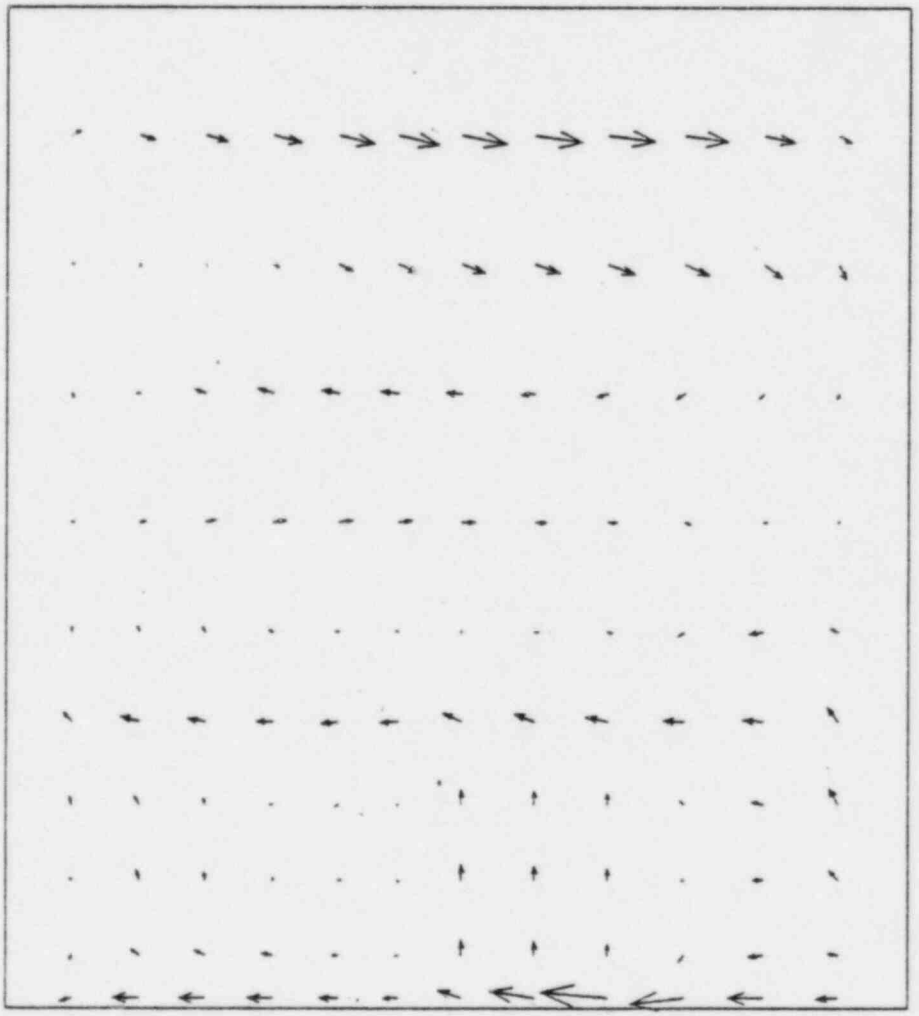

K = 5 VECTOR PLOTS AT TIME 1.55+003

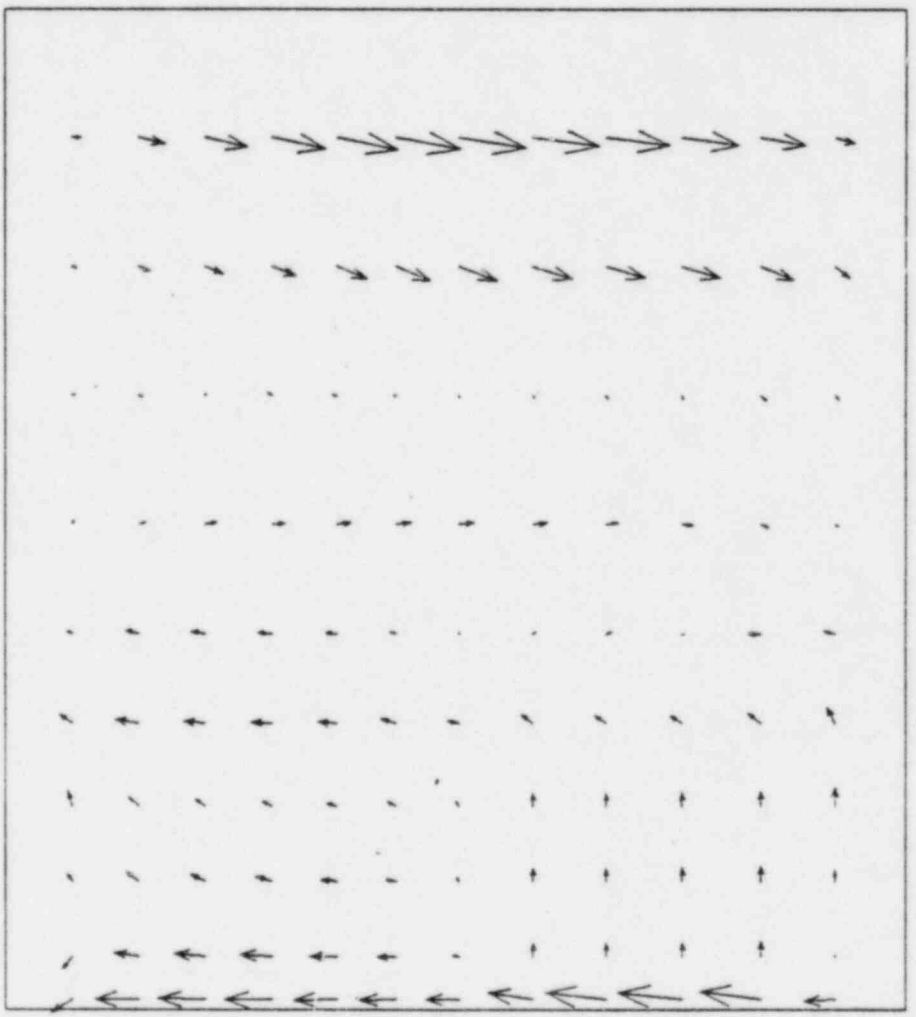

K = 6 VECTOR PLOTS AT TIME 1.55+003

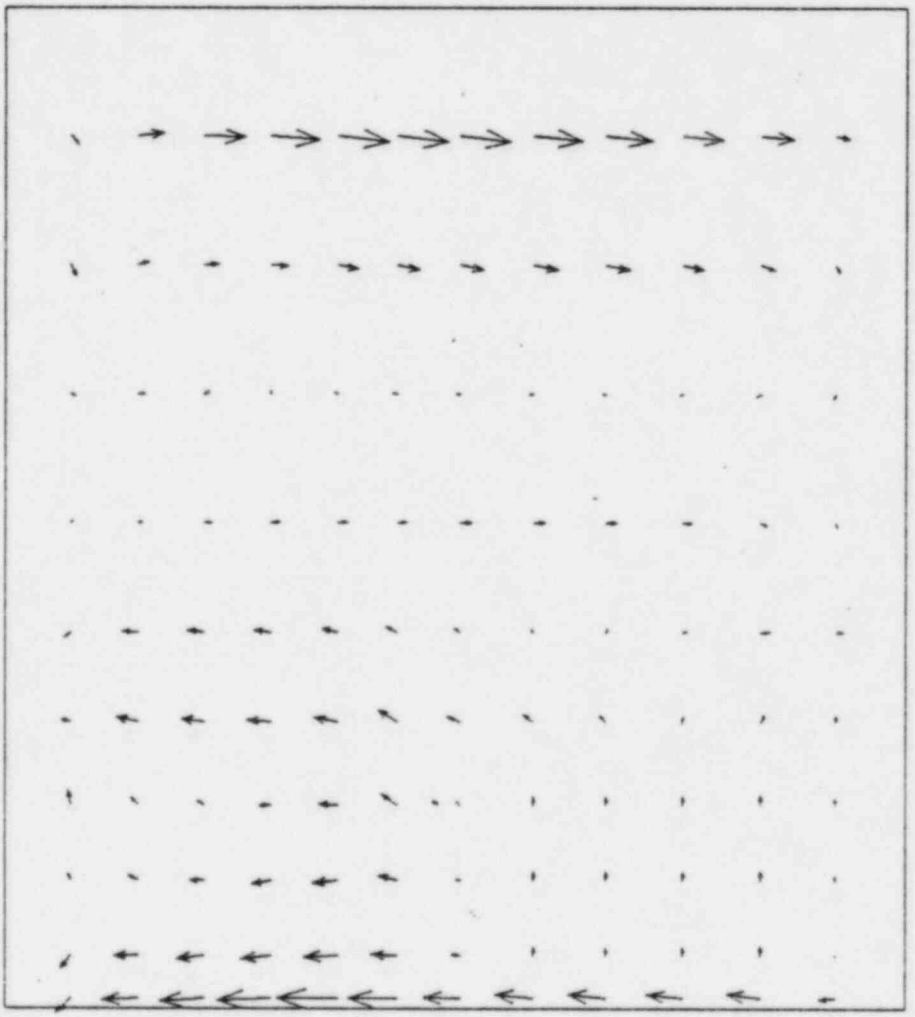

K = 7 VECTOR PLOTS AT TIME 1.55+003

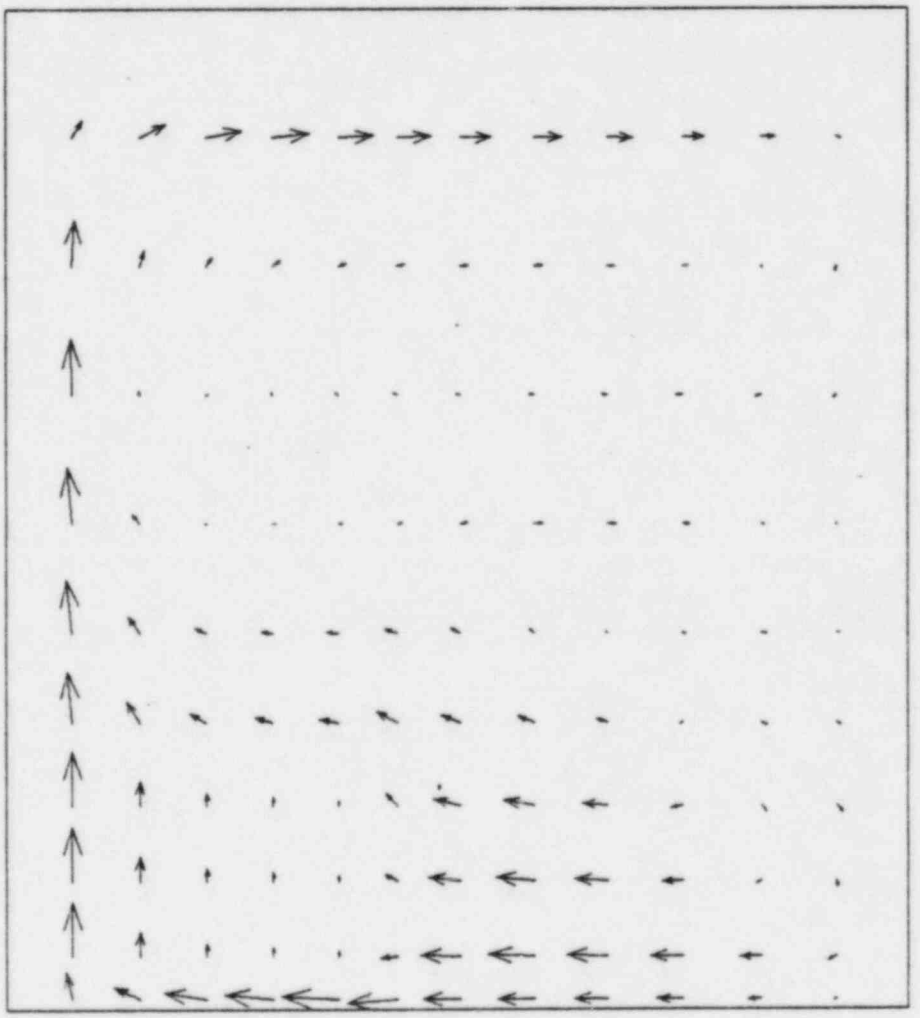

K = 8 VECTOR PLOTS AT TIME 1.55+003

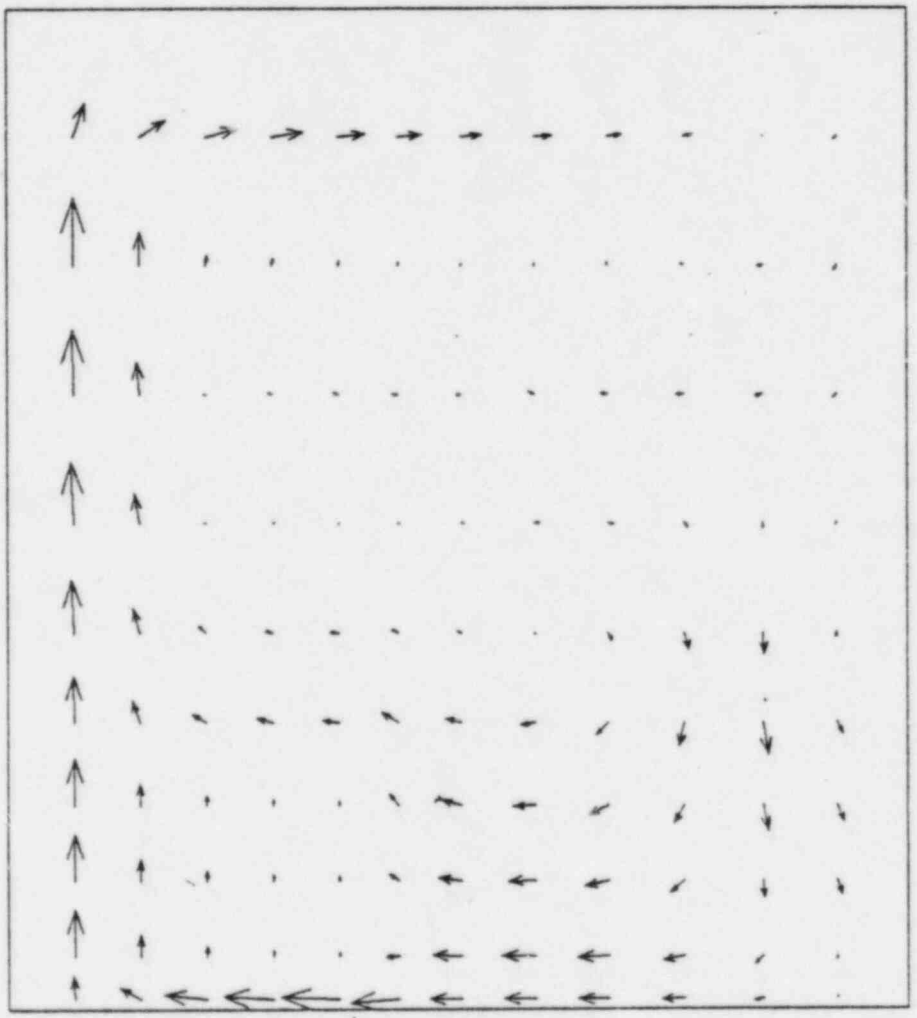

K - 9 VECTOR PLOTS AT TIME 1.55+003

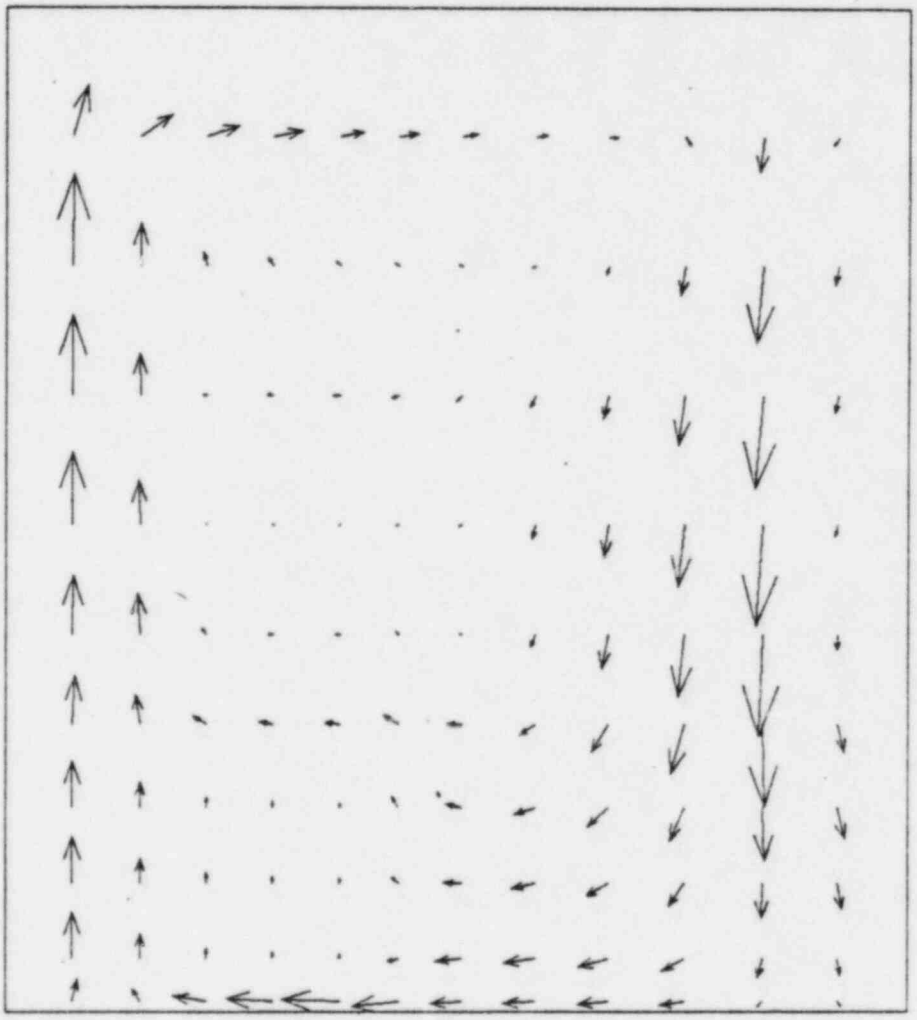

K = 10 VECTOR PLOTS AT TIME 1.55+003

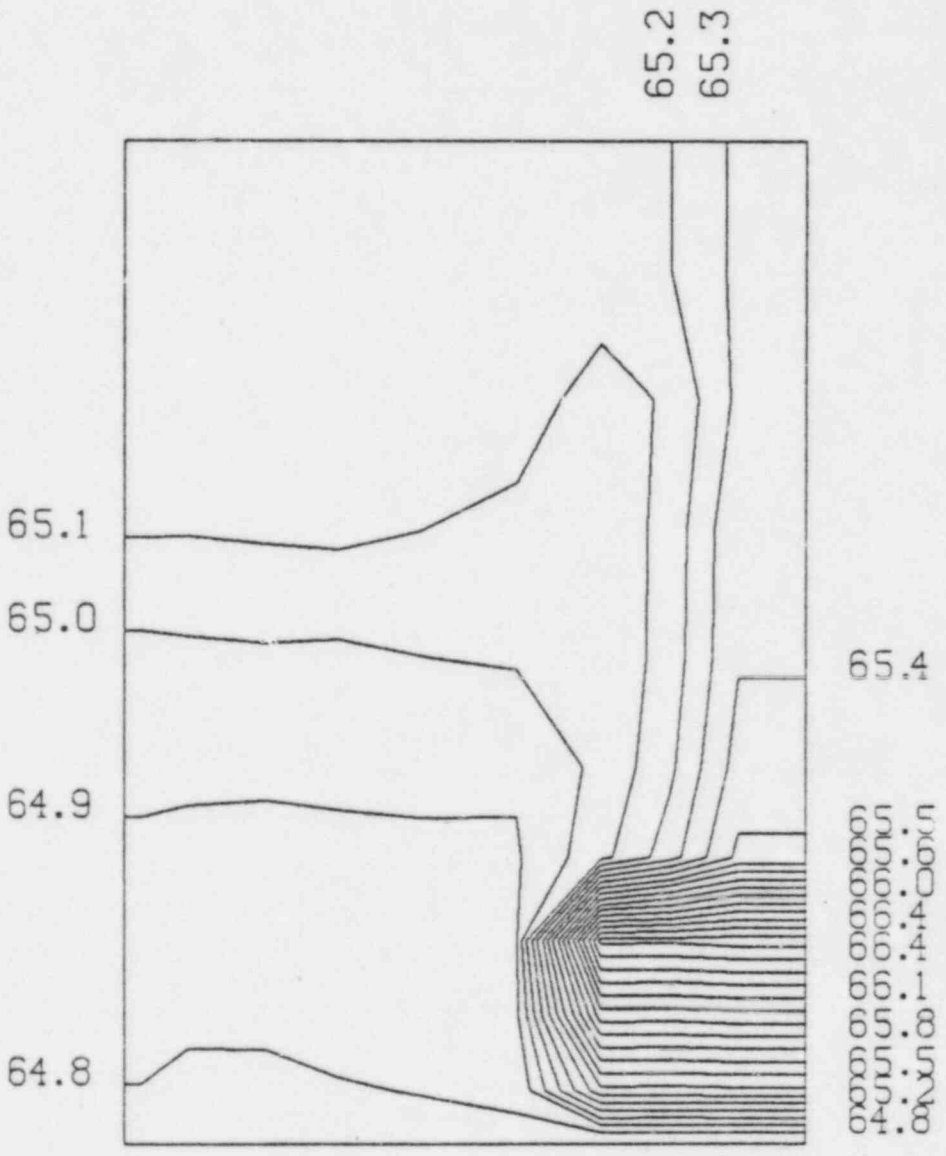

I - 2 TEMPERATURE CONTOURS AT TIME 1.55+003

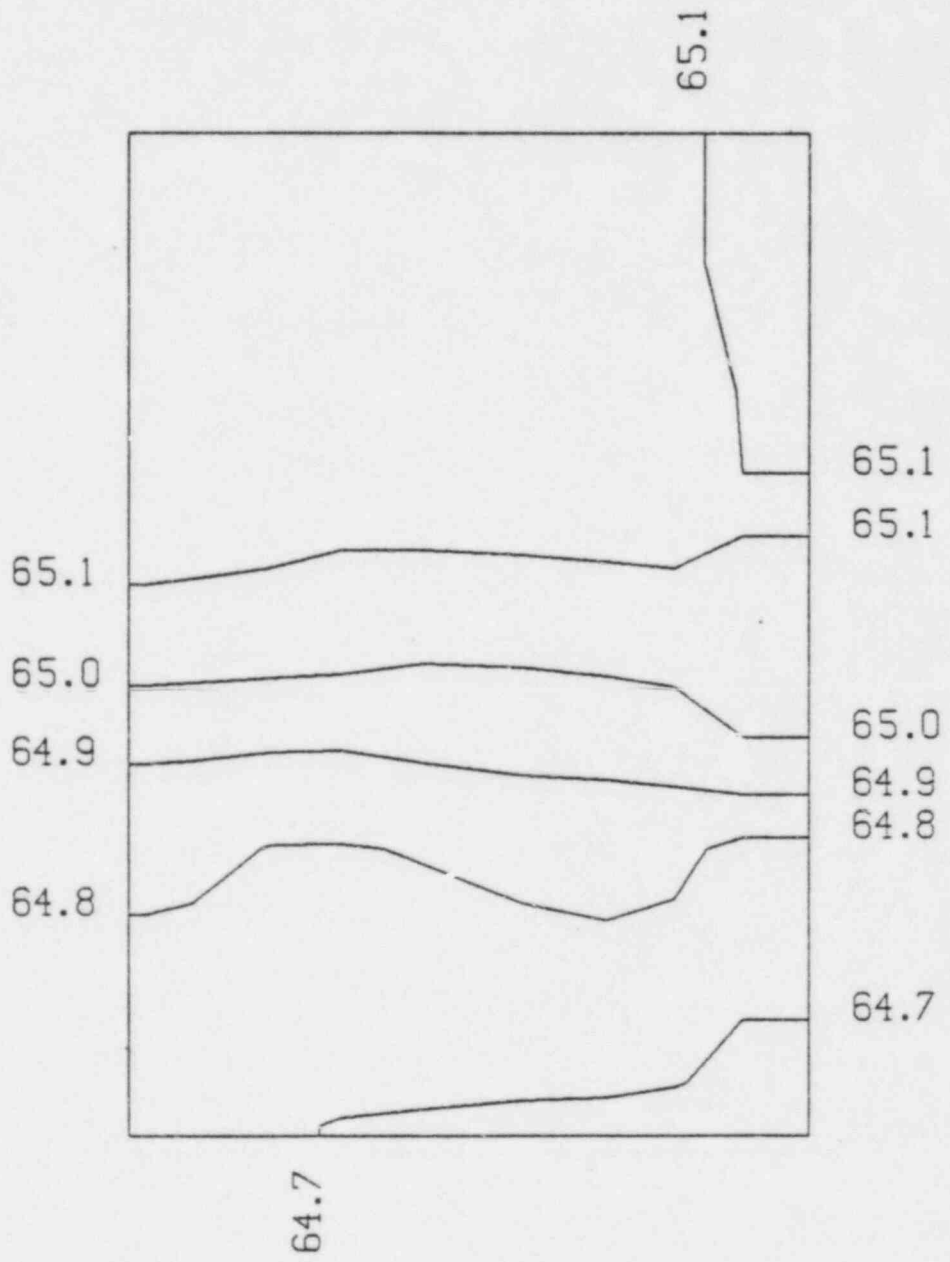

I - 13 TEMPERATURE CONTOURS AT TIME 1.55+003

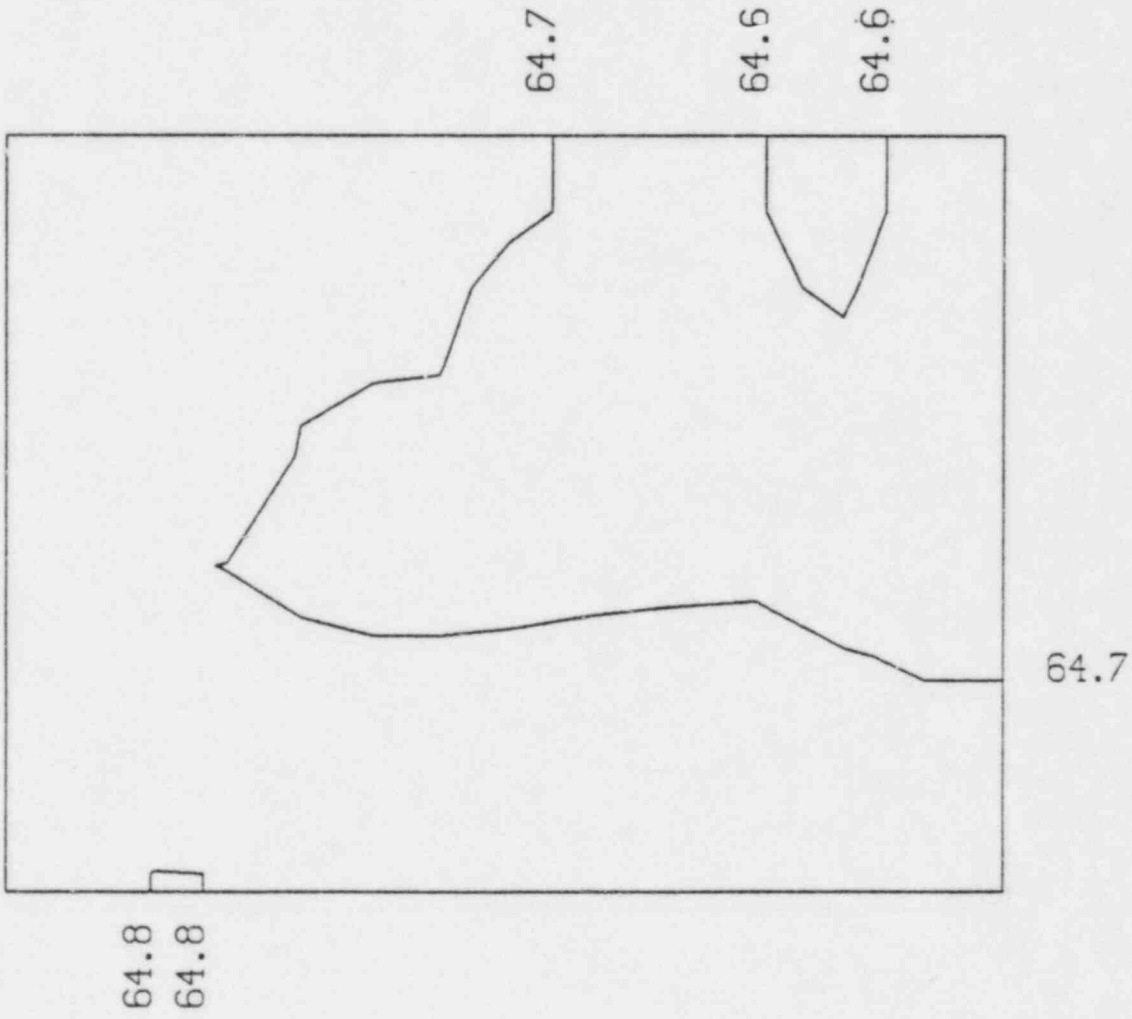

J = 2 TEMPERATURE CONTOURS AT TIME 1.55+003

J - 3 TEMPERATURE CONTOURS AT TIME 1.55+003

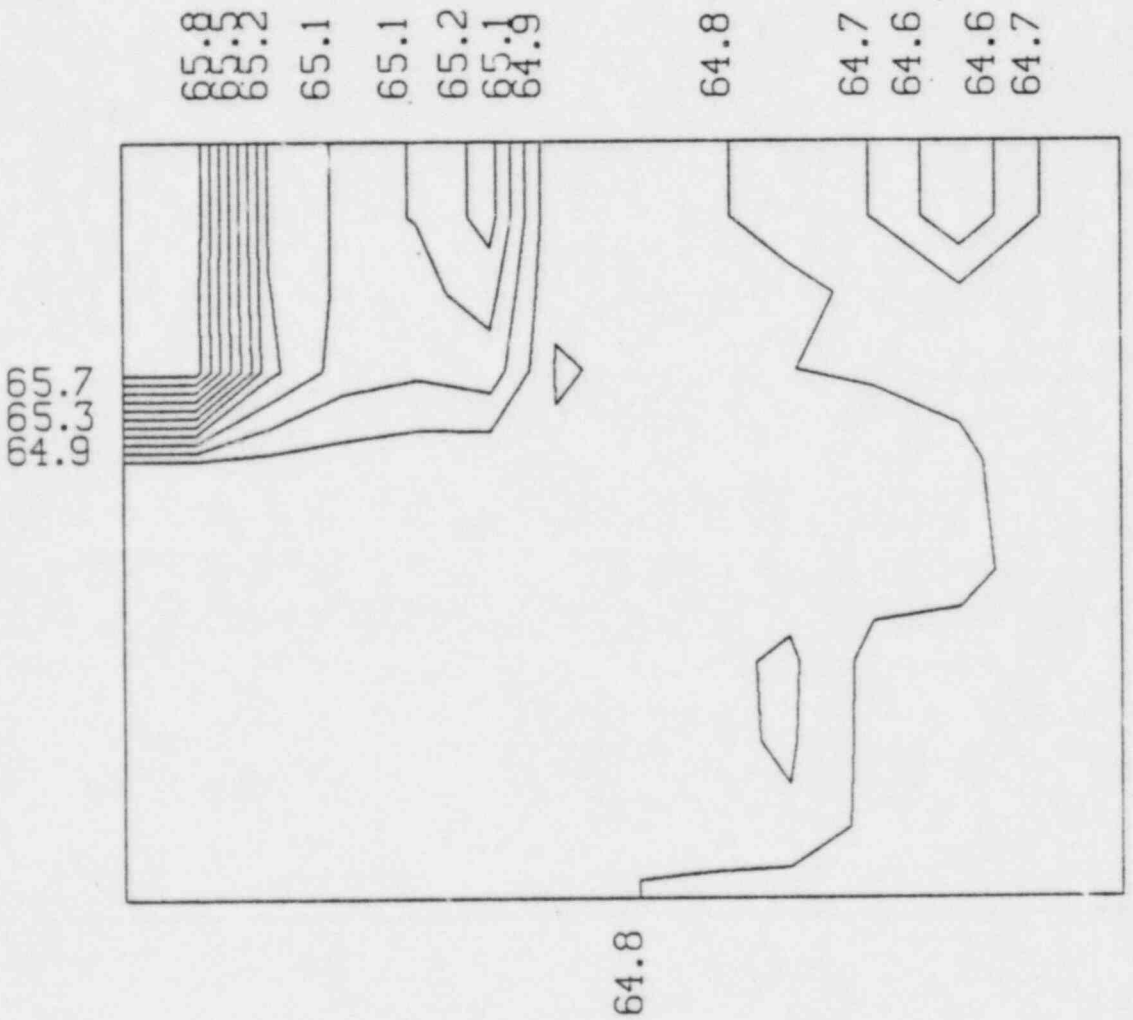

J = 4 TEMPERATURE CONTOURS AT TIME 1.55+003

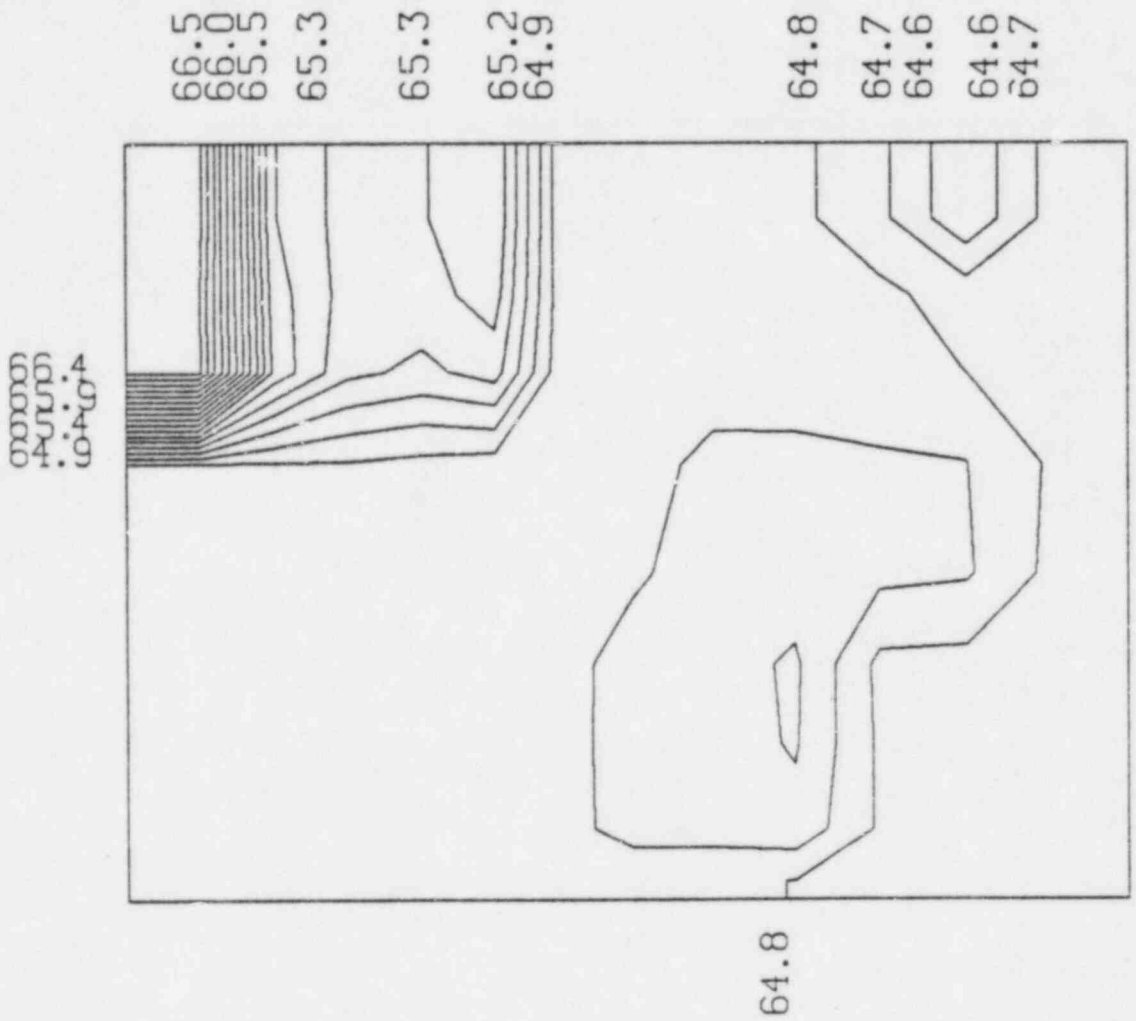

J = 5 TEMPERATURE CONTOURS AT TIME 1.55+003

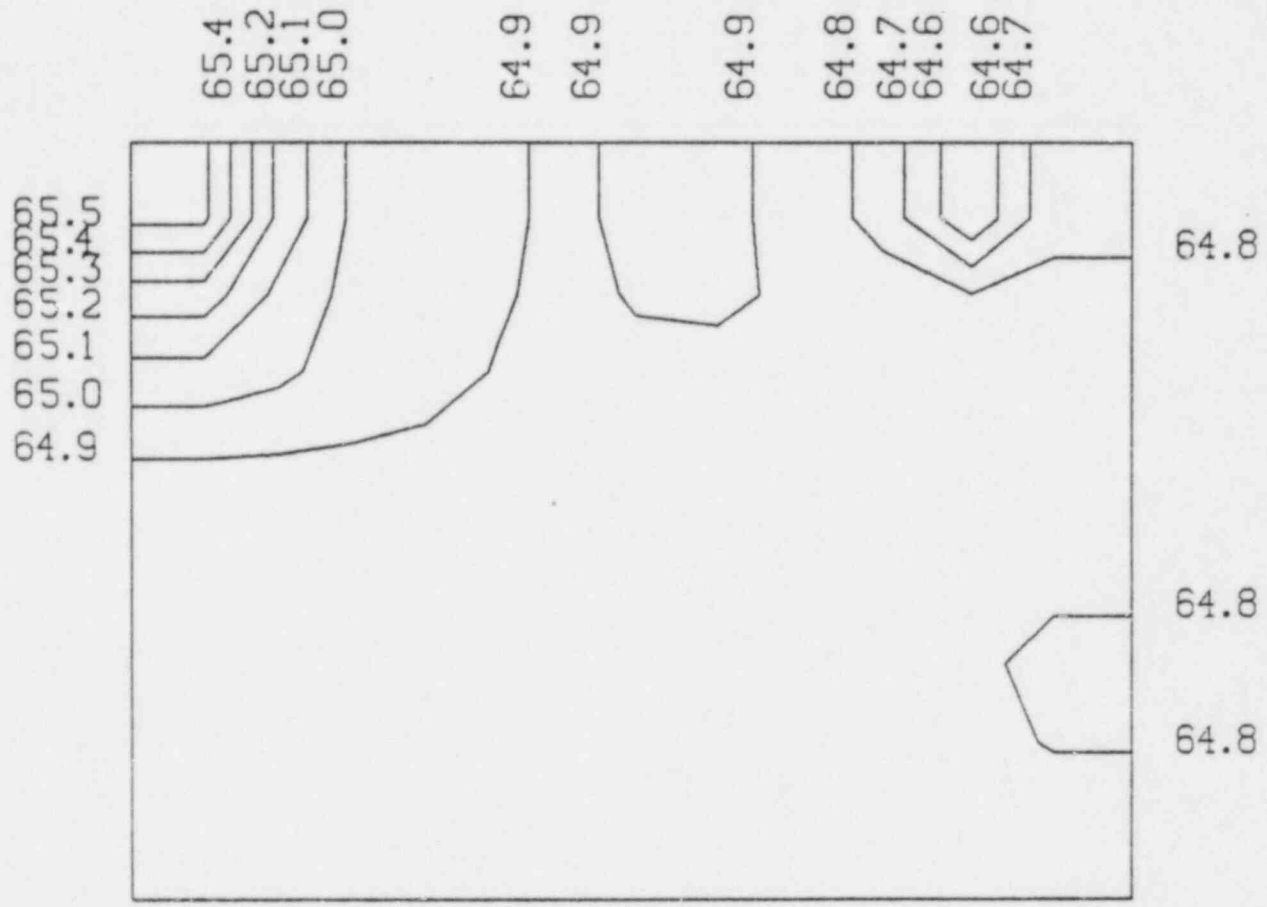

J - 6 TEMPERATURE CONTOURS AT TIME 1.55+003

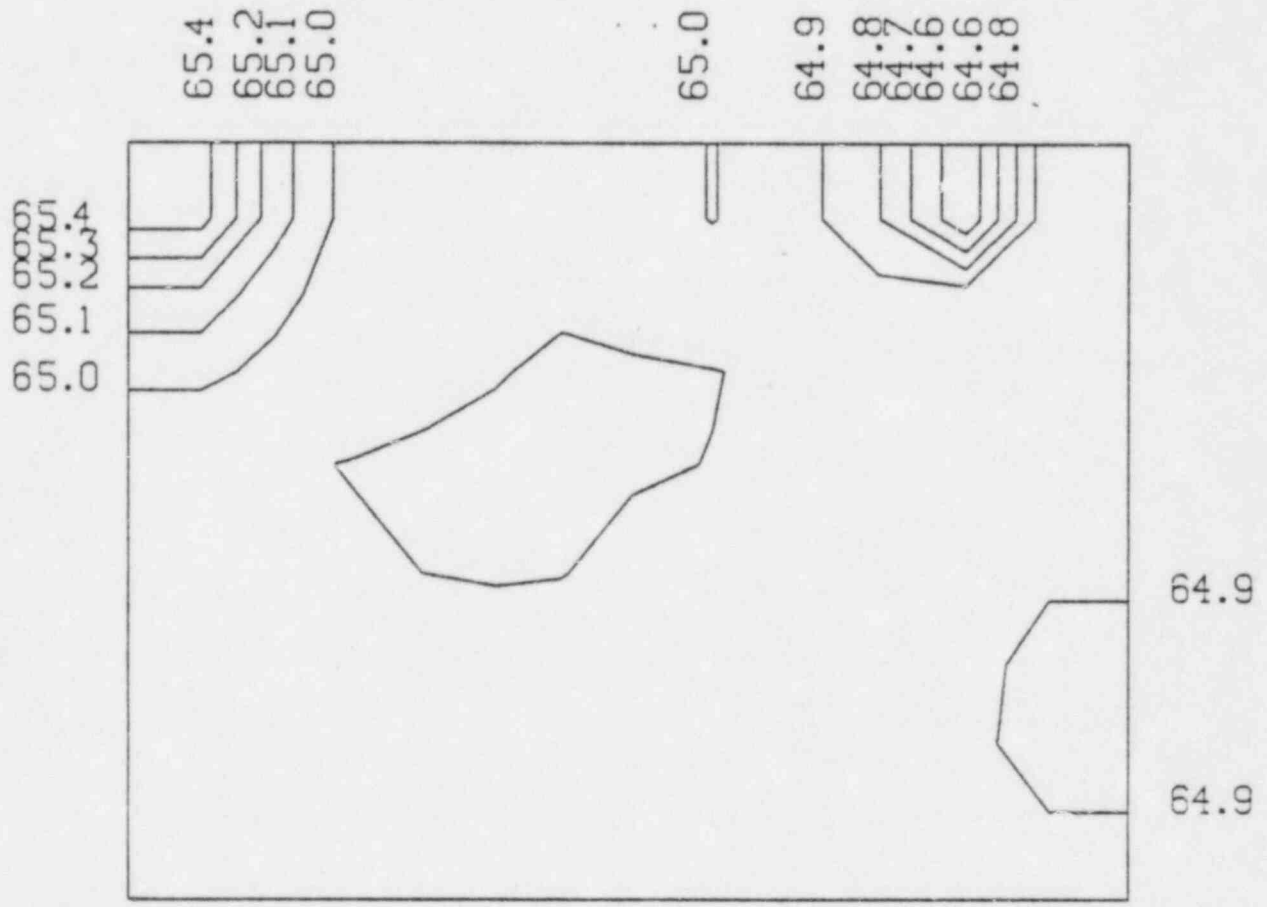

J = 7 TEMPERATURE CONTOURS AT TIME 1.55+003

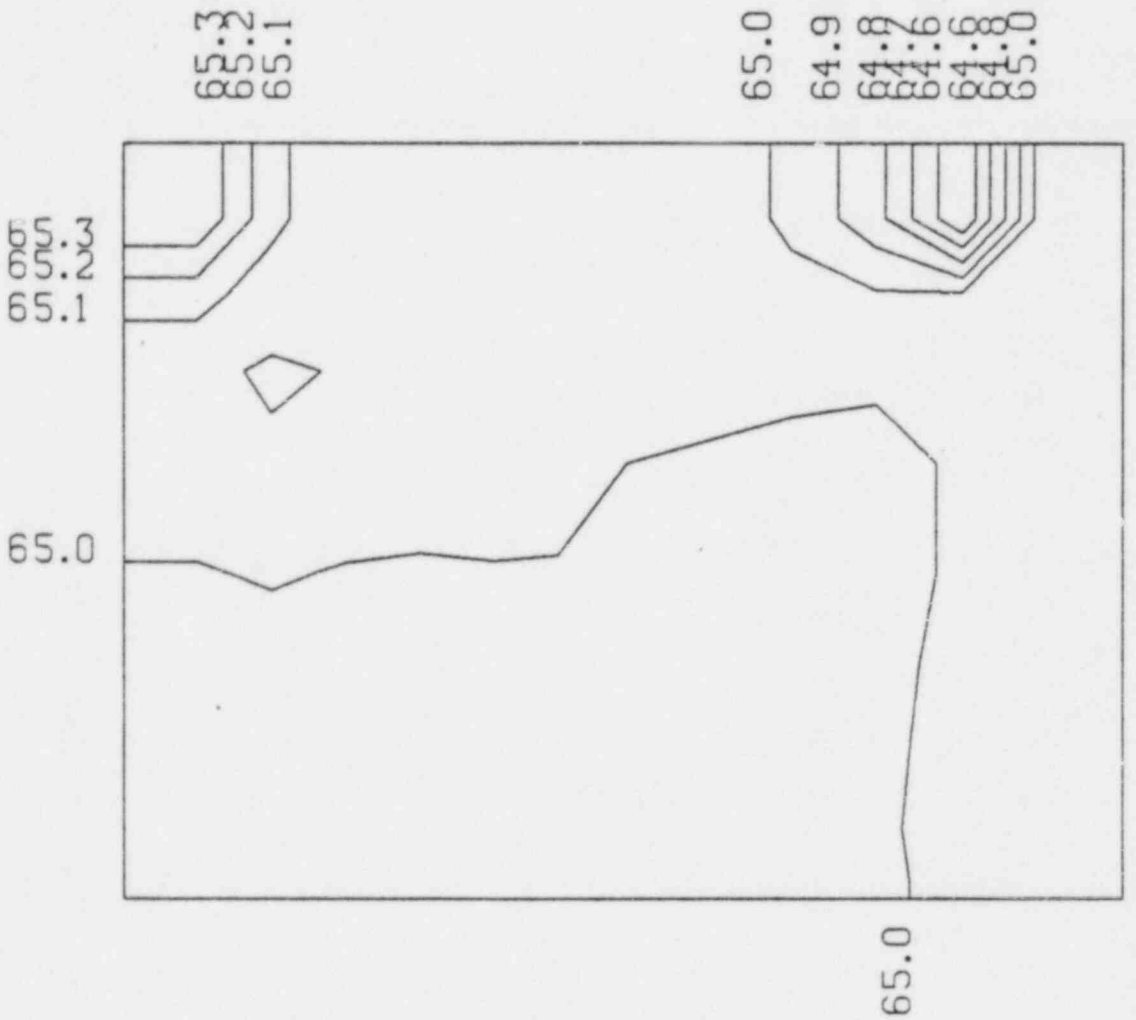

J = 8 TEMPERATURE CONTOURS AT TIME 1.55+003

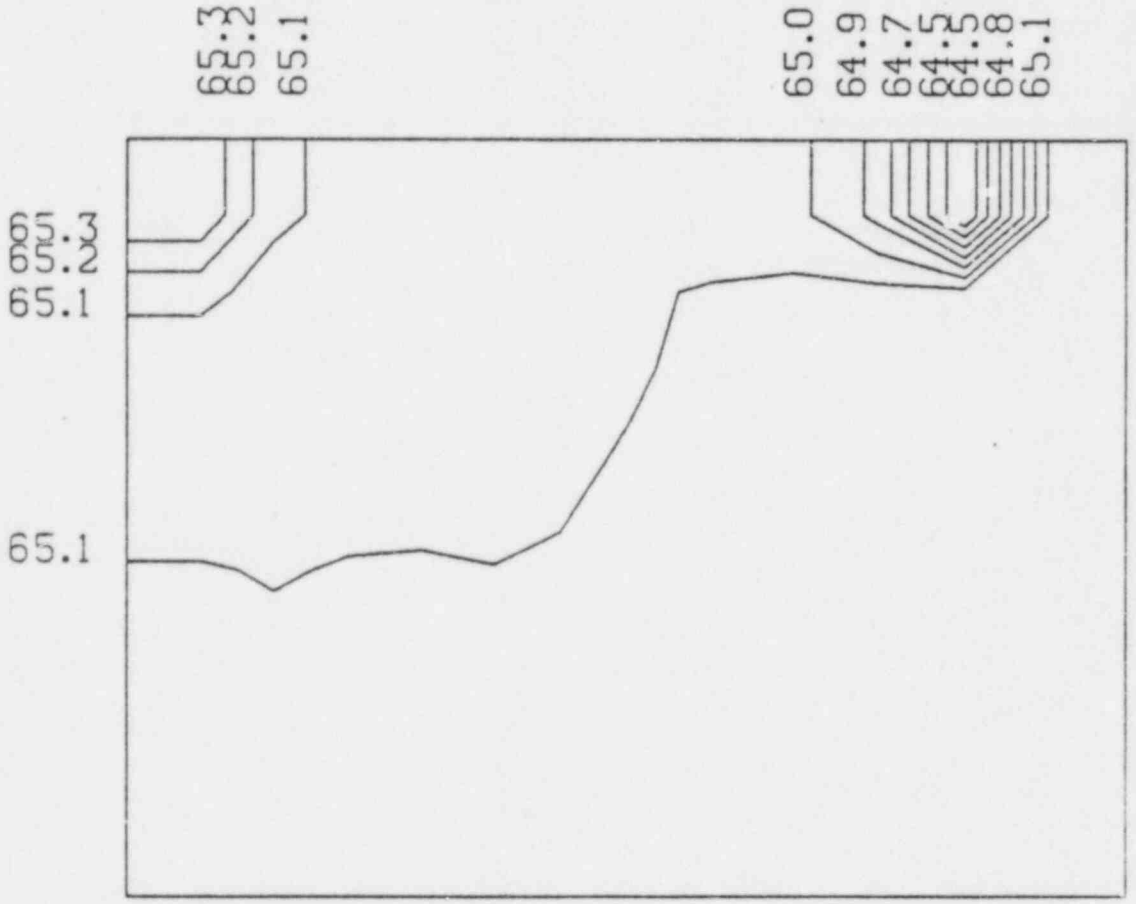

J = 9 TEMPERATURE CONTOURS AT TIME 1.55+003

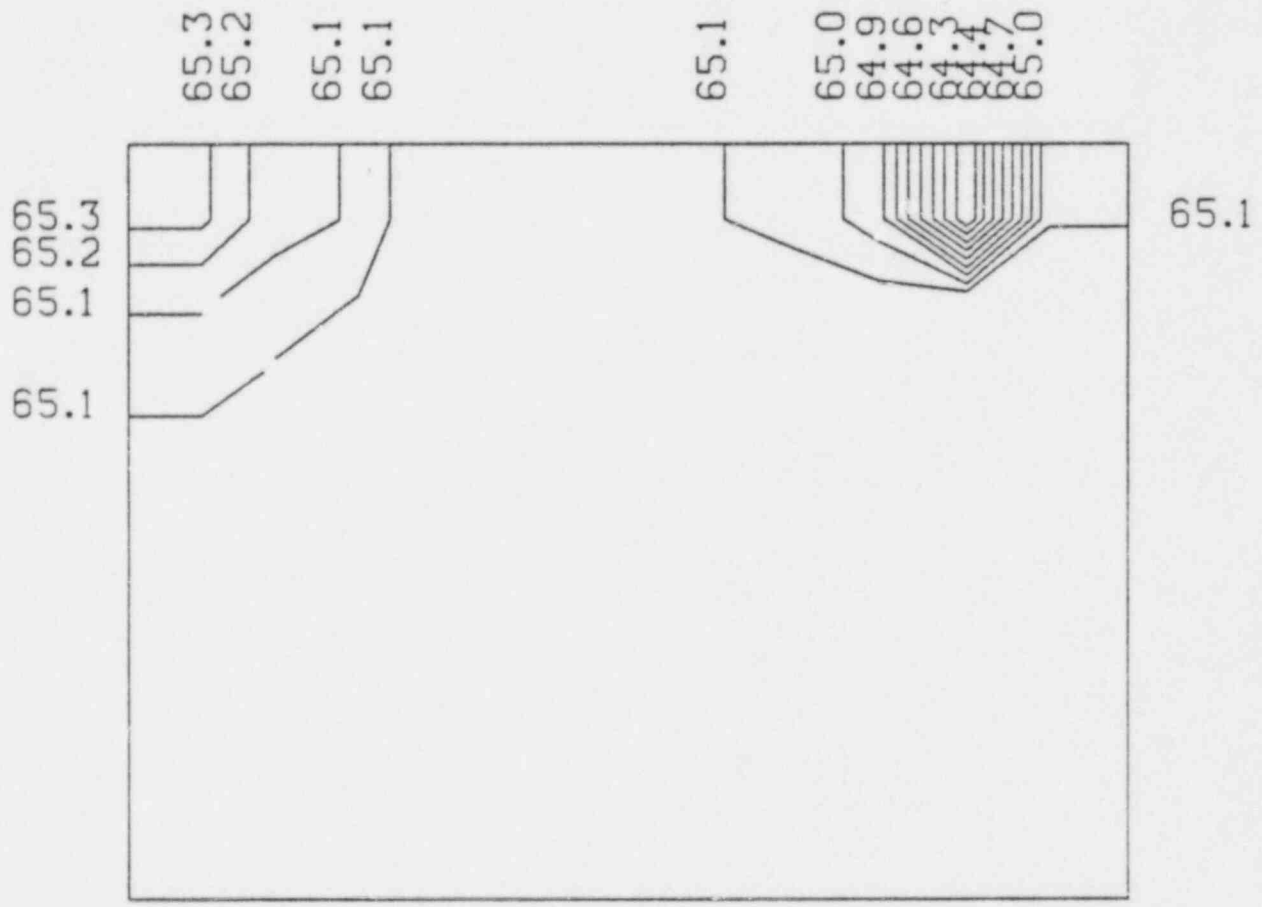

J = 10 TEMPERATURE CONTOURS AT TIME 1.55+003

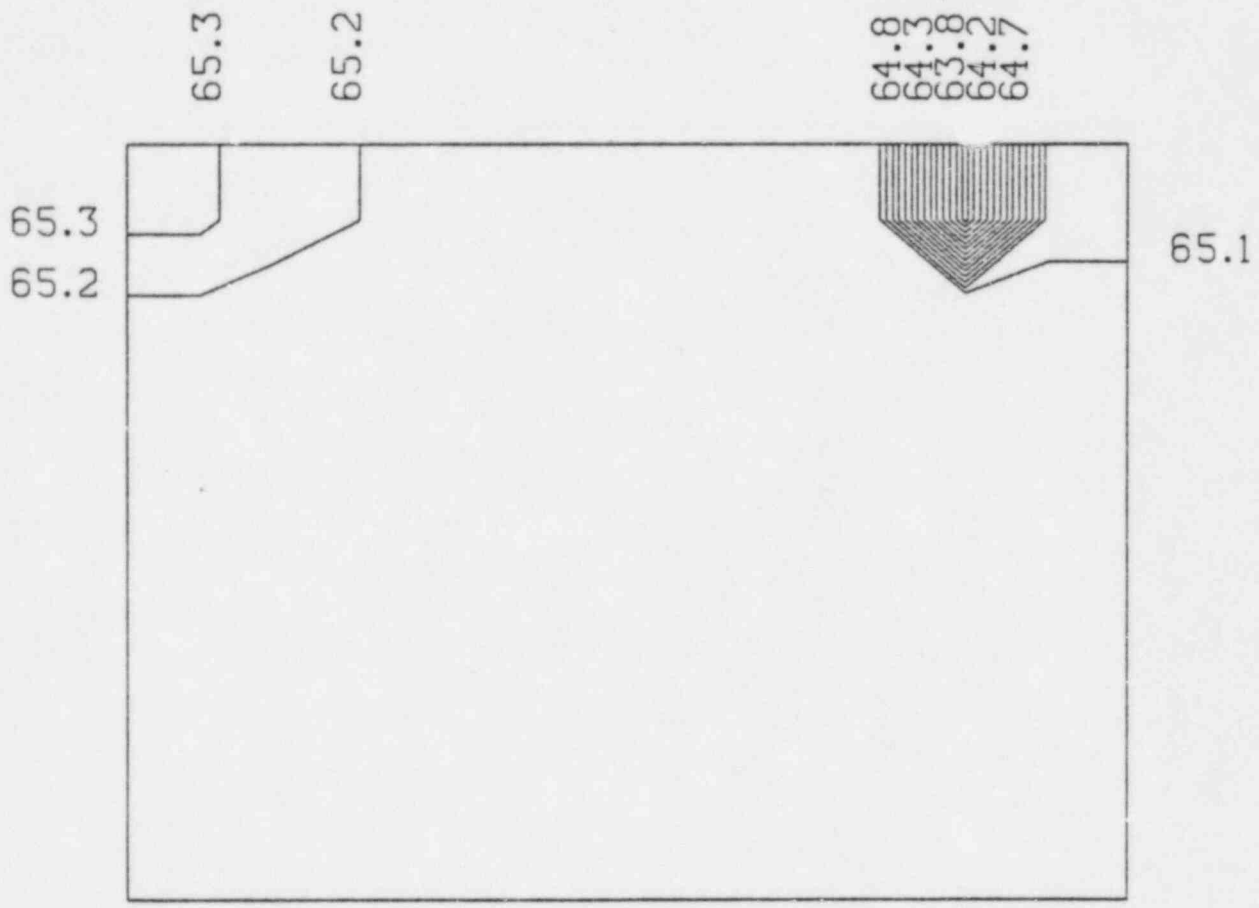

J - 11 TEMPERATURE CONTOURS AT TIME 1.55+003

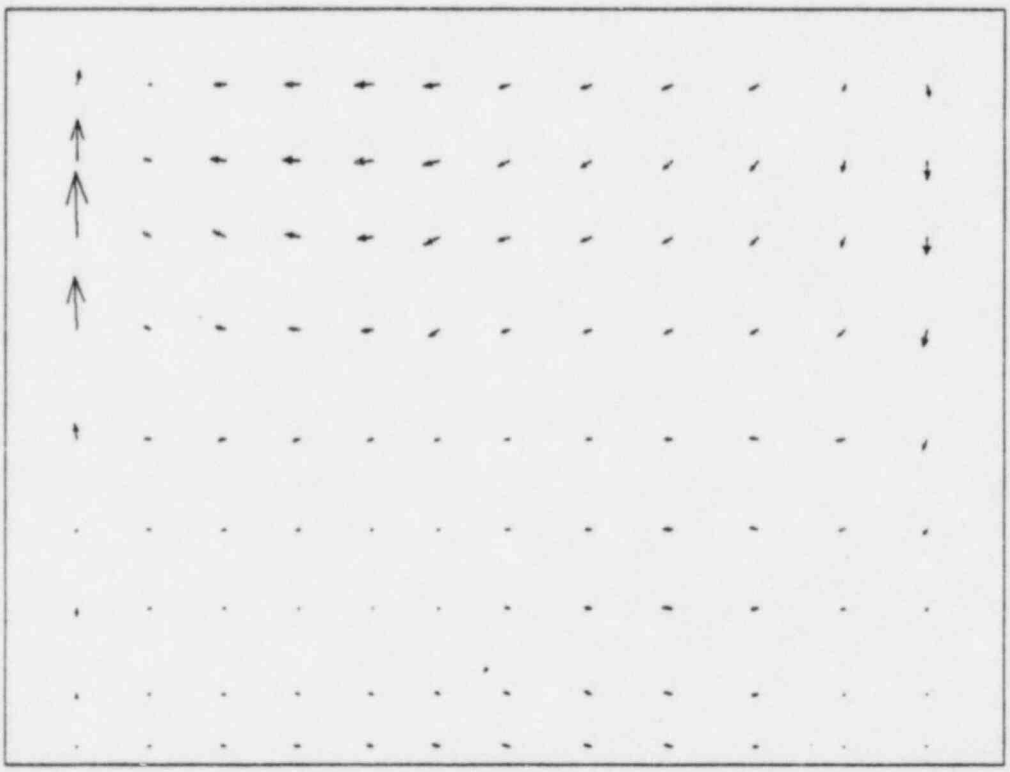

J = 2 VECTOR PLOTS AT TIME 1.55+003

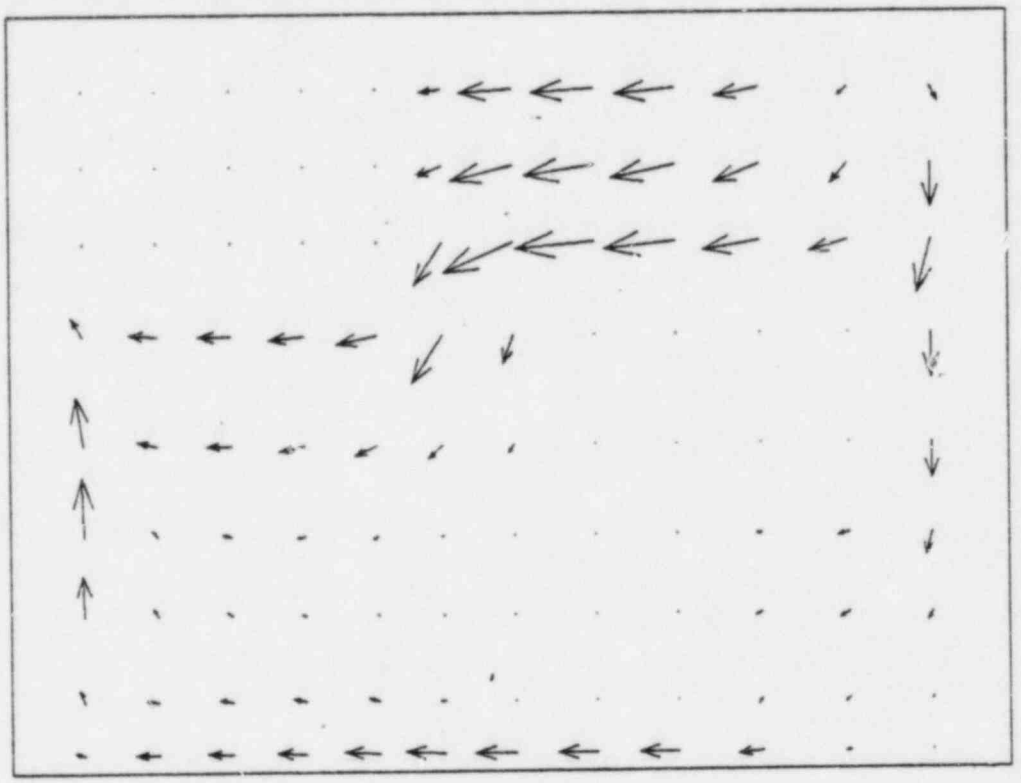

J - 3 VECTOR PLOTS AT TIME 1.55+003

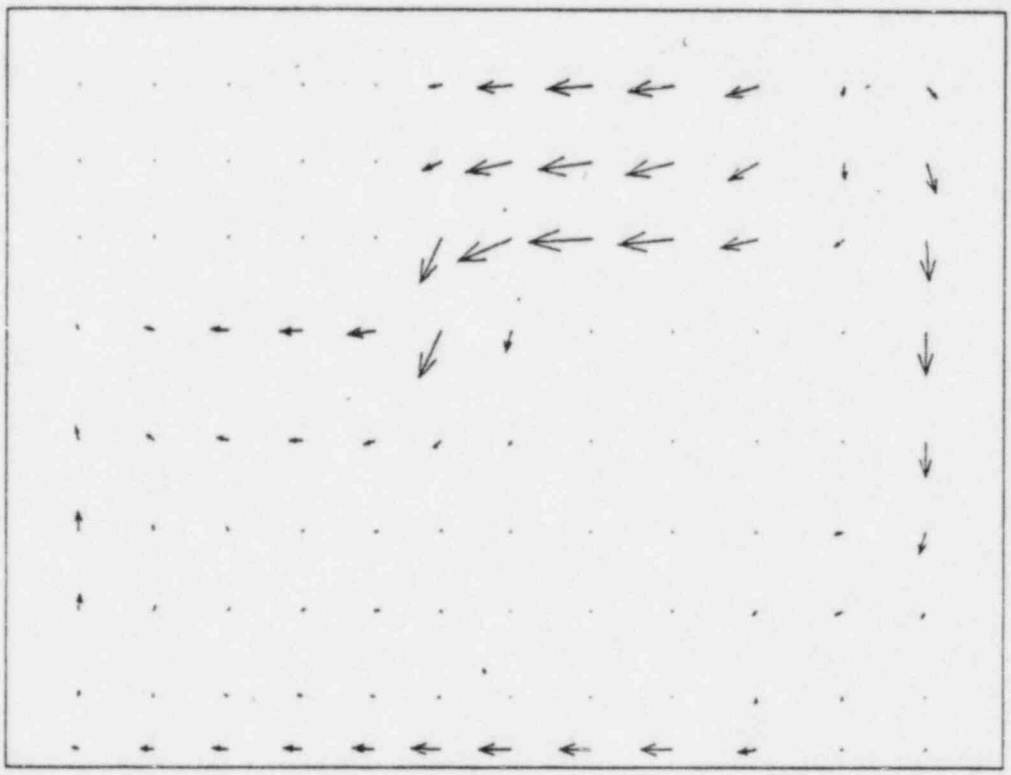

J = 4 VECTOR PLOTS AT TIME 1.55+003

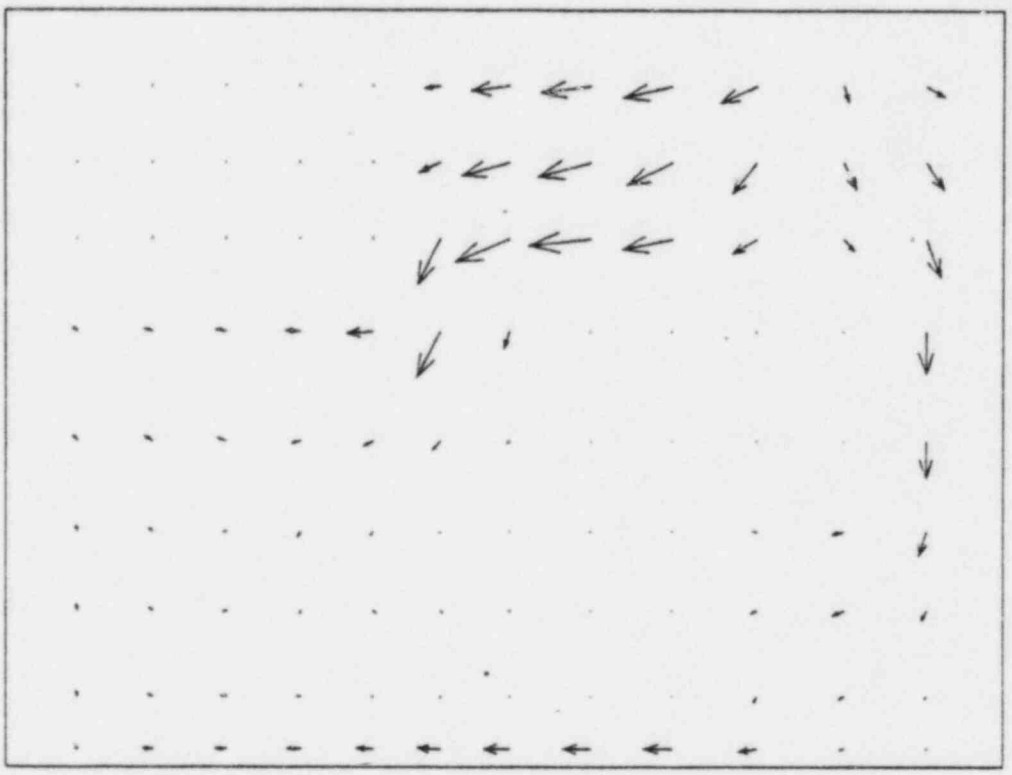

J = 5 VECTOR PLOTS AT TIME 1.55+003

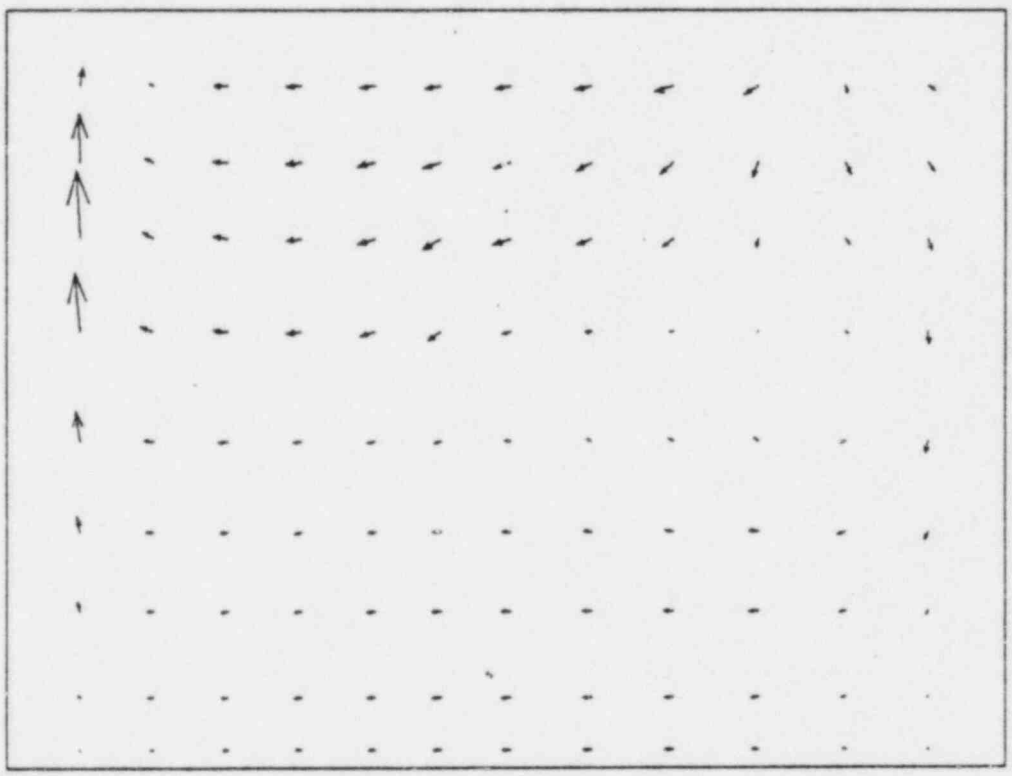

J = 6 VECTOR PLOTS AT TIME 1.55+003

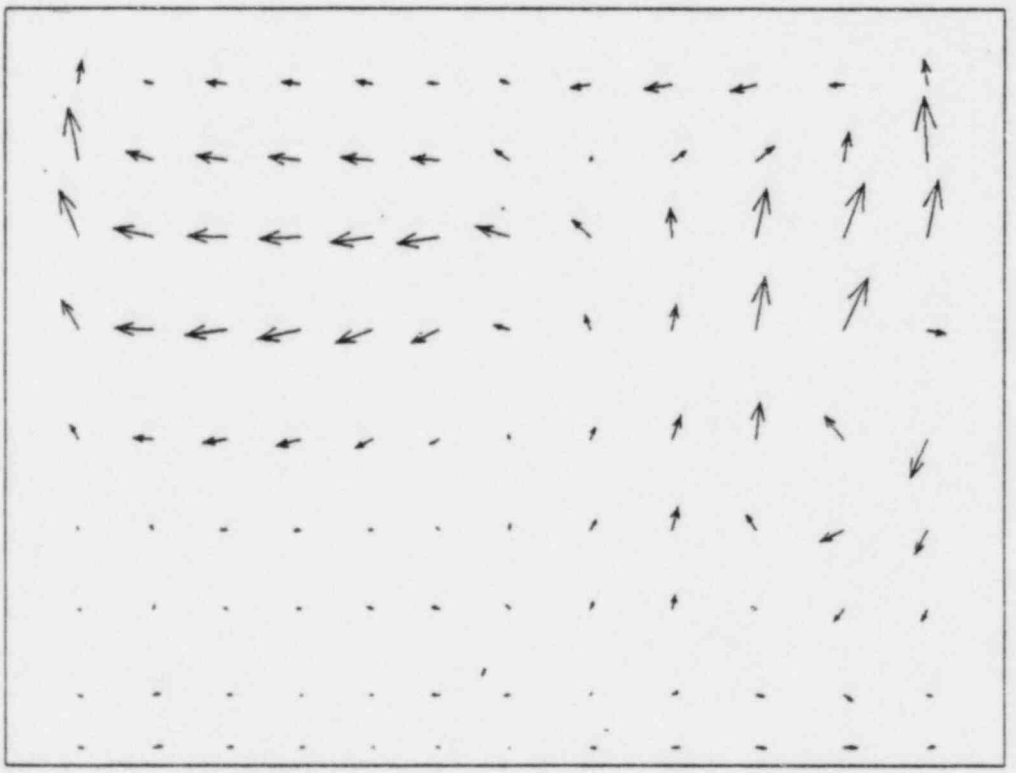

J = 7 VECTOR PLOTS AT TIME 1.55+003

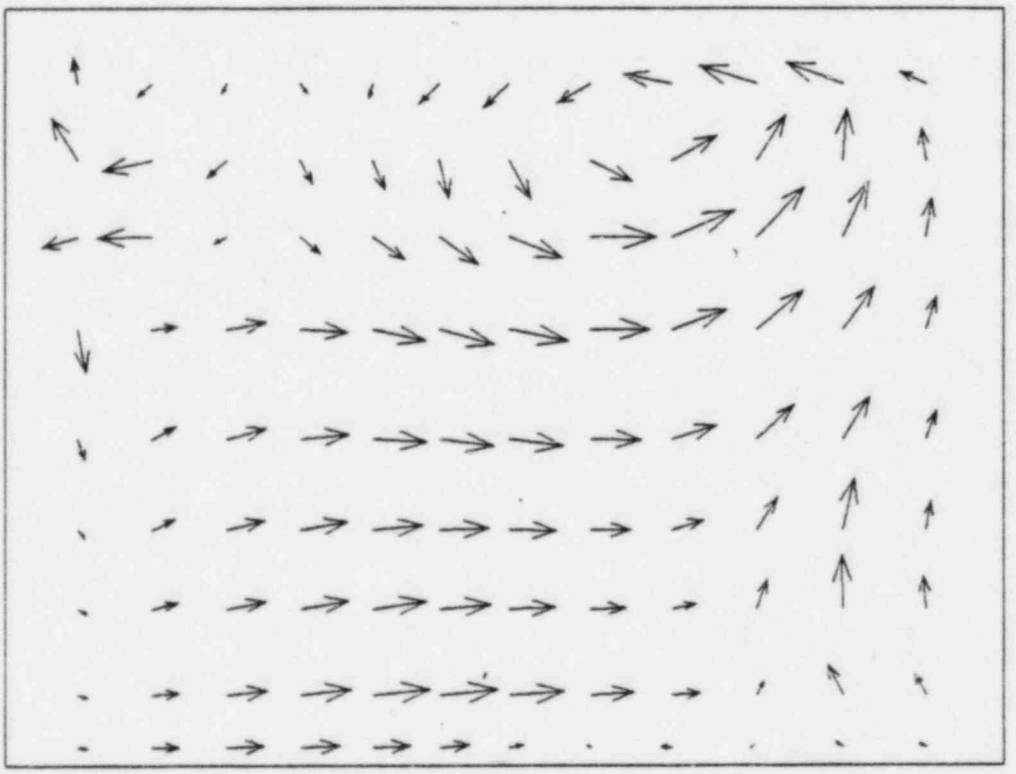

J = 8 VECTOR PLOTS AT TIME 1.55+003

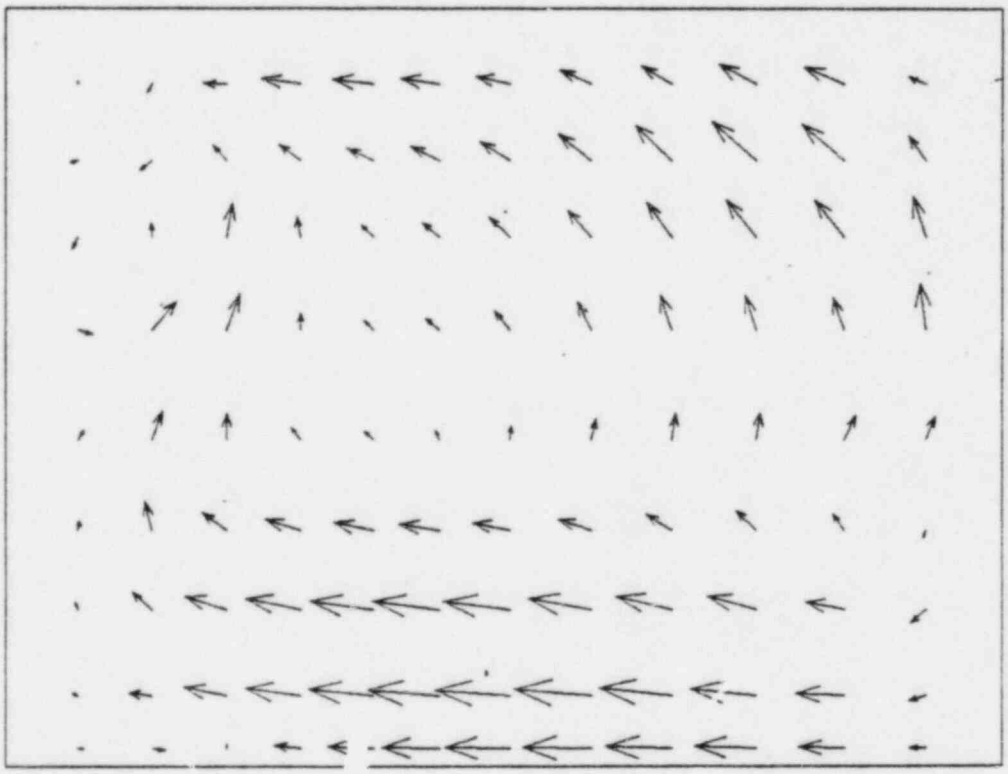

J = 9 VECTOR PLOTS AT TIME 1.55+003

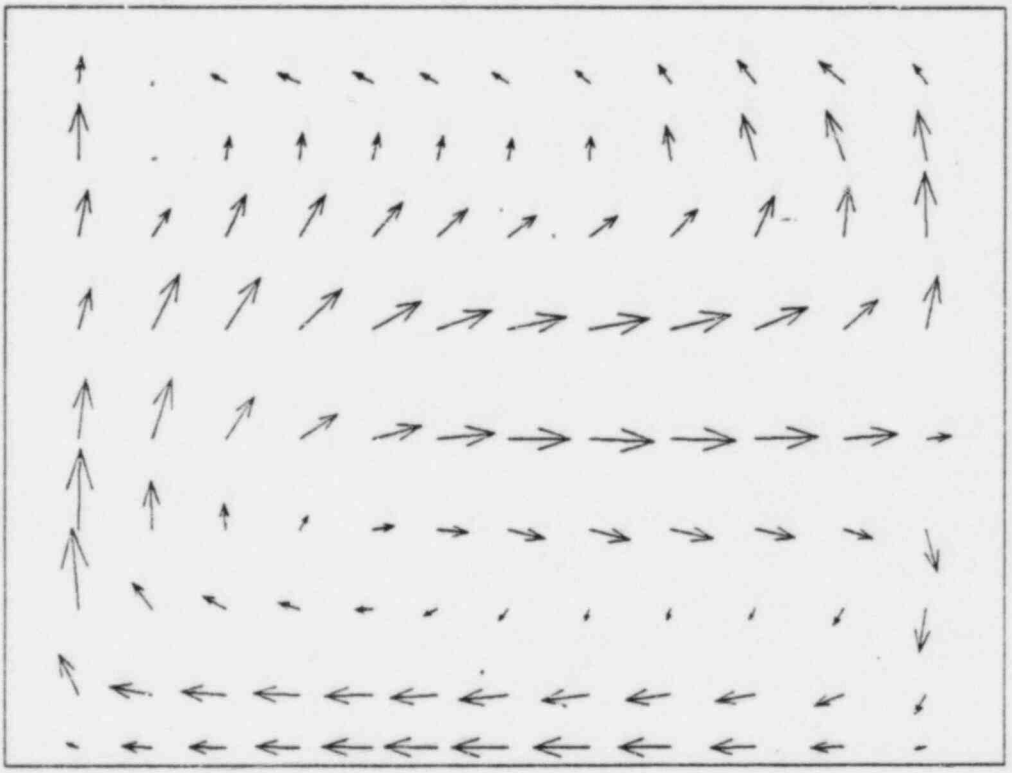

J = 10 VECTOR PLOTS AT TIME 1.55+003

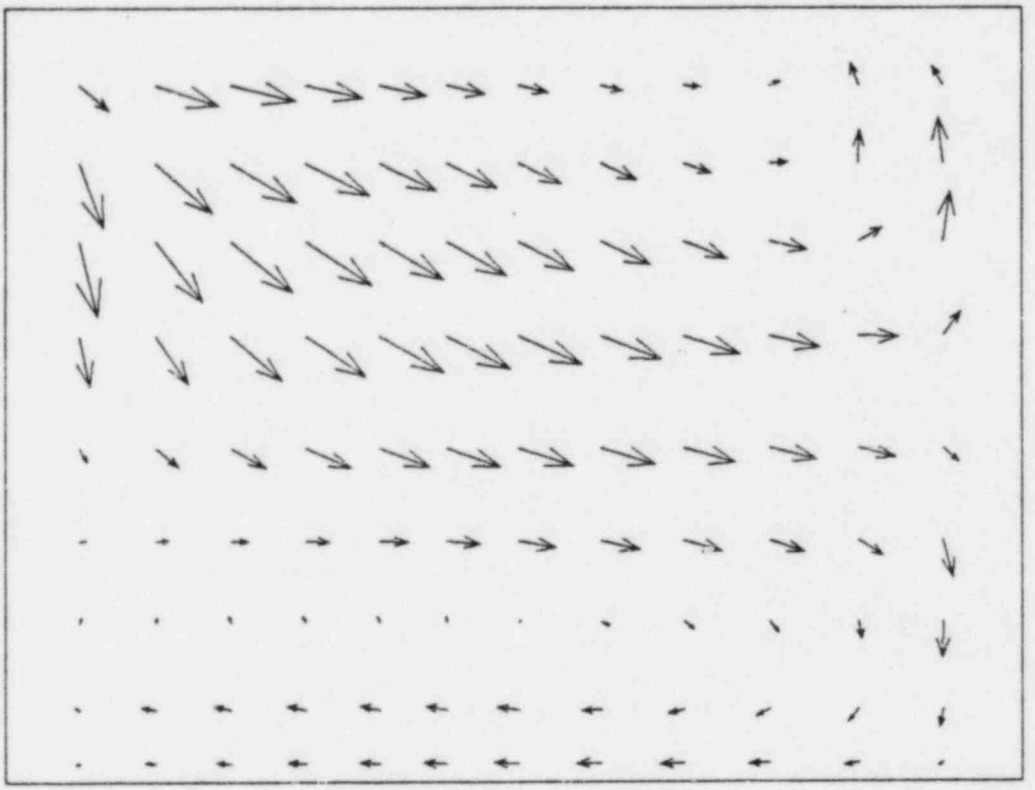

J = 11 VECTOR PLOTS AT TIME 1.55+003

REFERENCES

1. J. H. Stuhmiller and M. J. Vander Vorst, "The EITACC Program for Transient Fluid Dynamics Problems," Proceedings of the ANS/ENS International Topical Meeting on Advances in Mathematical Methods for Nuclear Engineering Problems, Munich, April 22-27, 1981.

2. M. J. Vander Vorst, J. H. Stuhmiller, and B. R. Sehgal, "Calculations of Heat Removal Due to Natural Convection in the TMI Core with Postulated Damage," ANS/ENS Meeting on Thermal Reactor Safety, Knoxville, Tennessee, April 1980.

3. M. J. Vander Vorst, J H. Stuhmiller, and D. A. Steininger, "Numerical Simulation of the Fluid Flow in a Centrifugal Steam Separator," Proceedings of the ANS/ENS International Topical Meeting on Advances in Mathematical Methods for Nuclear Engineering Problems, Munich, April 22-27, 1981.

4. I. E. Idel'Chik, Handbook of Hydraulic Resistance, U.S. A.E.C Translation, AEC-TR-6630 (1966).

5. Handbook of Heat Transfer, W. M. Rohsenow and J. P. Hartnett, eds., McGraw-Hill Book Company, New York, 19__.

6. Gary Pratt, Consumers Power Company, Jackson, Michigan, private communication.

7. S. Chandrasekhar, Hydrodynamic and Hydromagnetic Stability, Oxford University Press, London, 1961.